INFORMATION TO USERS

The most advanced technology has been used to photograph and reproduce this manuscript from the microfilm master. UMI films the text directly from the original or copy submitted. Thus, some thesis and dissertation copies are in typewriter face, while others may be from any type of computer printer.

The quality of this reproduction is dependent upon the quality of the copy submitted. Broken or indistinct print, colored or poor quality illustrations and photographs, print bleedthrough, substandard margins, and improper alignment can adversely affect reproduction.

In the unlikely event that the author did not send UMI a complete manuscript and there are missing pages, these will be noted. Also, if unauthorized copyright material had to be removed, a note will indicate the deletion.

Oversize materials (e.g., maps, drawings, charts) are reproduced by sectioning the original, beginning at the upper left-hand corner and continuing from left to right in equal sections with small overlaps. Each original is also photographed in one exposure and is included in reduced form at the back of the book.

Photographs included in the original manuscript have been reproduced xerographically in this copy. Higher quality 6" x 9" black and white photographic prints are available for any photographs or illustrations appearing in this copy for an additional charge. Contact UMI directly to order.

U·M·I

University Microfilms International
A Bell & Howell Information Company
300 North Zeeb Road, Ann Arbor, MI 48106-1346 USA
313/761-4700 800/521-0600

Order Number 9108196

Models for receptor-mediated LDL metabolism and arterial macromolecular transport

Yuan, Fan, Ph.D.

City University of New York, 1990

U·M·I
300 N. Zeeb Rd.
Ann Arbor, MI 48106

MODELS FOR RECEPTOR MEDIATED LDL METABOLISM AND ARTERIAL MACROMOLECULAR TRANSPORT

by

Fan Yuan

A dissertation submitted to the Graduate Faculty in Engineering in Partial Fulfillment of the Requirements for the degree of Doctor of Philosophy, The City University of New York

1990

This manuscript has been read and accepted for the Graduate Faculty in Engineering in satisfaction of the dissertation requirement for the degree of Doctor of Philosophy.

7/24/90
Date

Professor Sheldon Weinbaum
Chair of Examining Committee

7/26/90
Date

Professor Gerard G. Lowen
Executive Officer

Professor Shu Chien
(University of California)

Professor Peter Ganatos

Provost Robert Pfeffer

Professor David Rumschitzki

Professor Ira Tabas
(Columbia University, College of Physicians and Surgeons)

Professor Sheldon Weinbaum

Supervisory Committee

The City University of New York

Abstract

MODELS FOR ARTERIAL MACROMOLECULAR TRANSPORT AND THE LOW DENSITY LIPOPROTEIN METABOLISM

by

Fan Yuan

Advisors: Professor Sheldon Weinbaum

Professor Robert Pfeffer

In this thesis, three mathematical models are proposed. One attempts to study the receptor-mediated cellular regulation of the low density lipoprotein (LDL) metabolism in nonhepatic cells and the other two models greatly extend existing theoretical frameworks for modeling macromolecular transport in the artery wall.

The simplified model for the receptor-mediated LDL metabolism described in Chapter 2 is the first theoretical study to investigate the overall self-adaptive regulation of human fibroblasts and other cells with a native LDL receptor. The model also predicts the basic regulatory behavior of smooth muscle cells (SMCs), i.e., for a slowly increasing LDL concentration in the extracellular medium, the rate of intracellular degradation of LDL first increases and then becomes saturated.

In Chapter 3, an initial attempt is made to extend the leaky junction-cell turnover model proposed in Weinbaum et al. (1985) to include convective transport and a discrete IEL. The model is time-dependent and two dimensional but employs the simple one-dimensional

(1-D) continuity relation for the velocity in each wall layer. Unfortunately, this assumption of 1-D continuity relation for the velocity has led to physically spurious results for the subendothelial intima (SI) concentration. profiles and the total macromolecular flux entering the artery wall, because the major transport processes in the SI occur parallel rather than normal to the endothelial surface in the vicinity of the leaky cleft exit, due to the unique ultrastructure of the intima. A new view of convective-diffusive transport processes in the arterial intima is thus proposed in Chapter 4 and is described below.

The major conclusions of the new transport model in the intima proposed in Chapter 4 are: (1) it is impossible for the macromolecular concentrations in the SI to be higher than in the lumen unless a sieving structure exists in the intima; (2) 1-D convective-diffusive models can lead to the concentrations in the SI that are higher than in the lumen, and overestimate the macromolecular convective flux entering the artery wall by more than an order of magnitude; (3) the structure of the normal endothelial junction strand varies tremendously as one proceeds from the large arteries to capillaries; and (4) for rabbit aorta (200 μm wall thickness) the new model predicts, (i) 99 percent of the total arterial wall resistance to macromolecular transport resides in the endothelium, (ii) the macromolecular flux entering the artery wall is proportional to the frequency ϕ of the endothelial cells with leaky clefts when $\phi \leq 0.05$, and is proportional to the lumen pressure p_L when $p_L \geq 70$ mmHg, and (iii) the growth of the fluorescent leakage spot in the SI is confined to only several cell radii after 2 hrs. of labeling.

Acknowledgements

I would like to thank my mentor, Professor Sheldon Weinbaum, for his support and guidance throughout my graduate studies. He has shown me how to propose the mathematical model from a practical biological problem and to simplify it.

I would also like to thank Professor Shu Chien (University of California at San Diego), Professor Robert Pfeffer and Professor David Rumschitzki for their advice and many contributions in directing the research. I wish to thank Ms. Ruey-Yug Tsay, Dr. Yu Zeng and Mr. Nian-Zheng Cao for their valuable assistance and discussions.

I would also like to give special thanks to Associate Dean, Professor Gerard G. Lowen for his administrative help.

This research is supported by an NSF "Creativity Award" ENG 85-00301, NSF grant CBT-8803116 and NIH grant HL-19454.

Table of Contents

LIST OF TABLES

LIST OF FIGURES

Chapter 3

Chapter 4

INTRODUCTION

Atherosclerosis is the leading cause of death in the industrially developed nations. Although there is a vast literature in this field dating back to the last century, the mechanism for the initiation of arterial disease is still not clear. It is well recognized that the early stages of the atherosclerotic process (atherogenesis) are characterized by the lipid accumulation and the proliferation of SMCs in the intima. Based on the recent studies of Schwenke and Carew (1989b), the initial accumulation of lipid occurs prior to the proliferation of the SMCs, and it is a sufficient condition for the initiation of the atherogenic process. Many hypotheses (Haust, 1987; Steinberg, 1987; Weinbaum et al., 1988a; etc.) which focus on these two characteristics of atherogenesis have been proposed. The purpose of the present dissertation is to investigate the mechanisms that lead to the lipid accumulation in the artery wall.

The lipid accumulation in the artery wall is directly related to the macromolecular transport processes in the artery wall and the degradation of the lipid by cellular wall components (e.g. ECs, SMCs and monocyte-derived macrophages). To understand the underlying mechanisms for lipid accumulation, a mathematical model for the receptor-mediated LDL metabolism in the nonhepatic cells is proposed in Chapter 2, and new mathematical models for arterial macromolecular transport are proposed in Chapters 3 and 4 which emphasize the transport processes in the arterial intima.

The theoretical model proposed in Chapter 2 is the first mathematical model to study the self-adaptive regulative mechanism of

the receptor-mediated LDL pathway. The main purposes of the model are to determine how the free cholesterol level in non-hepatic cells is related to their external LDL concentration and to study the regulatory capacity of these cells to adapt to a changing LDL environment.

The mathematical model for arterial macromolecular transport proposed in Chapter 3 was an initial attempt to (i) study the role that the IEL plays in modulating the macromolecular transport in the artery wall, (ii) understand the limitations of one-dimensional (1-D) arterial macromolecular transport models and (iii) examine the effect of convection on the macromolecular transport. This model is time-dependent and two-dimensional (2-D) in which a simplified 1-D continuity equation for the velocity field is used to describe the convective transport across the artery wall. Unfortunately, this simplified 1-D model for the convective velocity has led to physically spurious results for the concentration distribution in the subendotheial intima (SI) and the total macromolecular flux entering the artery wall, because the major transport processes occur parallel rather than normal to the endothelial surface in the vicinity of the leaky cleft exit due to the unique ultrastructure of the intima. The modification of this model has led to a new conceptual model for convective-diffusive transport in the intima which is described in Chapter 4.

The new mathematical model proposed in Chapter 4 is also 2-D and time-dependent, in which special emphasis is placed on the modelling of the convective-diffusive transport processes in the SI and across the internal elastic lamina (IEL). This new model is an important extension of the leaky junction-cell turnover theory proposed in

Weinbaum et al (1985), and, we believe, sheds a new light on the role that the IEL plays in modulating both the subendothelial water and macromolecular fluxes in the artery wall and the structure of normal arterial interendothelial clefts. It will be shown that the convective transport through the leaky clefts surrounding the small population of endothelial cells in turnover and the subsequent interaction with the IEL are the dominant processes that determine the distribution of macromolecules in the SI in vivo.

CHAPTER 1

Biological background

1.1 Introduction

Atherosclerosis is the cause of half of all deaths in the U.S. and Western industrialized nations. Atherosclerosis is an arterial disease which is characterized by thickening and stenosis of the medium-sized and large arteries. Stenosis may block the blood flow and lead to myocardial and cerebral infactions in the heart and brain, respectively.

The well-established advanced atherosclerotic lesions are well documented. The major components of the advanced lesion regions are: (1) the accumulation of lipids, primarily cholesteryl esters, both intracellularly (in foam cells) and extracellularly; and (2) the proliferation of smooth muscle cells (SMCs) (Steinberg,1987). Current research has heavily focused on the early stages (atherogenesis) of lesion formation to investigate the factors that initiate the atherosclerotic process.

The four primary features of atherogenesis summarized in Ross (1986) and Haust (1987) are: (1) the grey gelatinous elevation (focal intimal edema), (2) the fatty spot or streak in the subendothelial intima, that is due to the lipid accumulation in both the extracellular and intracellular (monocyte and/or SMC) space in which monocyte-derived macrophages are the major constituent, (3) the proliferation of SMCs in the intima, and (4) a functionally changed endothelium, which may account for the surface adhesion of blood borne microthrombi and monocytes in the early foam cell lesion and platelets in more advanced lesions when the subendothelial matrix is

exposed. Advanced lesions will be capped with fibrous tissues or even calcified, in their later stages of development.

The most widely accepted Unified Hypothesis to explain the initiation of atherogenesis is summarized in (Steinberg, 1983). This hypothesis unifies the Lipid Infiltration and Endothelial Injury hypotheses, as shown in Fig.4 of Steinberg (1983).

According to the Lipid Infiltration hypothesis, the elevated LDL levels in the plasma will trigger the atherogenic process, because it causes the increase in the rate of LDL infiltration into the arterial wall and the cellular uptake and degradation of LDL. Cholesteryl ester will accumulate both intracellularly (EC, SMC and macrophage) and extracellularly in the subendothelial space, which eventually leads to atheroma. Proponents of the Endothelial Injury Hypothesis propose that the triggering event in atherogenesis is mechanical and chemical injury of the endothelium. In the original formulation of this hypothesis Ross and Glomset (1976), this injury causes platelet adherence and aggregation on the endothelial surface and the consequent release of PDGF or related growth factors which can cause proliferation of SMCs and the release of chemotactic agents that stimulate the migration of SMCs from the media into the intima. Based on these two hypotheses, the key points of this unified view are: (1) elevated plasma LDL levels or other toxic blood borne substances can damage the endothelium; (2) endothelial injury enhances lipoprotein infiltration and thus initiates both chains of events just described; and (3) if LDL or other lipoproteins cause platelet aggregation or directly stimulate cell growth, then hyperlipidemia can act to accelerate the same processes in the Endothelial Injury Hypothesis (Steinberg,1987). This unified approach suggests that there are many

factors that can initiate atherogenesis, and that the atherogenic process is not a simple causal chain.

Two other hypotheses for the initiation of the atherogenic process are often cited. The oldest theory for atherogenesis was proposed by von Rokitansky in 1852. This theory emphasized the adhesion of microthrombi to the arterial wall (thrombogenic theory). This theory was revised in the forties and expanded later by Canadian investigators [see summary in Haust (1987)]. Benditt and co-workers (1973) have proposed a monoclonal theory in which the proliferation of SMCs is stimulated by a clone of cellular elements derived from a single SMC that is transformed by viruses or chemical agents. In this dissertation, we shall adopt the unified view mentioned above and focus on the mechanisms responsible for the lipid accumulation in the subendothelial space, the most common feature of the early atherosclerotic lesion, the fatty streak.

1.2 Lipid accumulation in the subendothelial space

The lipid accumulation in the subendothelial space can be affected by many factors, such as the activities of ECs, SMCs and monocyte-derived macrophages, the macromolecular transport properties of arterial wall (e.g. the diffusion coefficients, the structure of the wall, and the pressure gradient across the wall, etc.), the cellular degradation of LDL and the binding of LDL to cell membrane and extracellular tissue matrix.

1.2.1 The endothelial barrier

The endothelium is the major barrier for macromolecular entrance into the arterial wall. Scanning electron microscopy (SEM) studies, in both normal and hyperlipidemic animals, have shown a continuous layer of endothelial cells covering the surface, with no evidence of

denudation until after lesion formation [see summary in Schwartz,S.M. et al.,(1983) and Ross (1986)].

More recent electron microscopic studies, using ultrathin serial sectioning techniques, indicate the existence of short discontinuous gaps of 10 to 30 nm width (length of break) and 4 to 6 nm gap height in the junctional complexes of arterial capillaries (Bundgaard,1984). If one assumes that the structure of capillary and arterial endothelial clefts are similar, these short gaps are the most likely structural correlate for the small pore through which water and small proteins cross the endothelium. All these SEM studies indicate that the normal endothelium is impermeable to macromolecules. Therefore, the fundamental question that needs to be answered is where is the large pore through which macromolecules cross the endothelium?

(A) <u>The search for large pore</u>

The search for the structural correlate of the large hydrophilic pores via which macromolecules such as LDL cross the endothelium, has been the subject of numerous studies since the 1950's [see summary in Weinbaum et al. (1988a)].

The transendothelial vesicular transport hypothesis was originally proposed by Palade (1960). For the next two decades vesicular transport, or fused open vesicle channels were generally thought to be the most likely structural correlate of the large 10 nm radius cylindrical pores via which macromolecules entered the subendothelial tissue. This hypothsis was critically re-evaluated around 1980 in light of the experimental studies by Bundgaard et al. (1979) & (1983) and Chien et al. (1982), which showed that cytoplasmic vesicles thought to be free were actually attached to the plasmalemma in a different plane of section through invaginating

elements. The failure of vesicle hypothesis led Weinbaum and co-workers (1985) to propose the leaky junction-cell turnover hypothesis. They believed that the large pore in the large arteries might be part of a statistically infrequent normal dynamic process that occurred on the endothelial surface. One possible process of this nature is the formation of transient open junctions during cell turnover. The mathematical model based on this hypothesis (Weinbaum et al., 1985) predicted that the measured local increases (typically 50 to 100 percent) in macromolecular transport in regions with focal intimal staining of Evans blue albumin (EBA) (Packham et al.,1967 and Bell et al.,1974a & 1974b) could be quantitatively accounted for by an increase in permeability through leaky junctions involving only a few cells per thousand. The en face area of the leaky junctions could occupy as little as 10^{-6} of the total endothelial surface.

The first observation indicating localized macromolecular leaks was reported by Stemerman et al. (1986) in their short time en face studies of HRP in rabbit aorta. These investigators concentrated on widely scattered foci of brown reaction product to HRP of approximately 200 μm diameter, and also measured the concentration of LDL in these regions. They found that the concentration of LDL was up to 47 times greater than that in surrounding regions not showing increased permeability to HRP. However, the area of these foci were far too large for the structure of the leaky sites to be identified at the cellular level.

An important break-through in the search for the large endothelial pore was achieved in the experiments by Lin et al. (1988) & (1989). Guided by the leaky junction-cell turnover hypothesis (Weinbaum,1985) and the time-dependent models in Weinbaum et al.

(1988b) and Wen et al. (1988), these investigators performed experiments in which the entire aorta of a rat was scanned using hematoxylin to identify cells in mitosis and fluorescent tracer molecules to identify leakage sites. It was found that nearly 99 percent of all cells in M phase had junctions which were leaky to EBA and 80 percent of all cells in M phase were leaky to the much larger molecule Lucifer yellow-LDL (LY-LDL). Furthermore, it was reported in the same experiments that the leaky cells in M phase accounted for roughly 30 percent of the total leakage sites for EBA and 45 percent of the total leakage sites for LY-LDL. Studies using IgG as marker for cells death (Lin, 1989) showed that a large fraction of the unidentified leakage sites could be accounted for by cells in the process of dying and/or sloughing. The combined frequency of leakage sites for EBA was approximately 5 cells in ten thousand. In addition, the distribution of the ECs in turnover is not random along the aorta. The cell turnover as indicated by ^{3}H-thymidine (Lin, 1989) was roughly twice the normal background level in the regions surrounding the branch orifices of the rat aorta. The permeability to ^{131}I-LDL in these regions of the rabbit abdominal aorta has been shown to be 3- to 5-fold higher than in adjacent uniform abdominal aorta (Schwenke and Carew, 1989b). Based on this evidence, one can conclude that the early injury of endothelium occurs in a more subtle form than overt denudation, and that the large endothelial pores via which macromolecules cross the endothelium are principally the leaky junctions of the cells in turnover (dying cells or mitotic cells).

(B) Factors injurious to endothelium

The factors injurious to the arterial wall and specifically to the endothelium may be derive from three main sources: (1) the blood

constituents, (2) hemodynamic forces, and (3) the arterial wall itself. Elevated LDL levels can damage the EC; strong evidence that this can occur comes from patients with familiar hypercholesterolemia (Steinberg,1983); other chemicals and toxins can also damage the endothelium. In the regions of low shear stress and flow reversal, e.g. in the aortic arch and downstream side of the branch orifices, the endothelial cells have a polygonal as opposed to an elongated shape and endothelial cell turnover is increased (Caplan et al.,1973; Nerem et al.,1981; and Ku et al.,1985). The third source is related to the abnormal "make up" of the artery wall (Haust,1987). The first two sources are the most important ones for normal individuals, and it is due to these factors that the endothelial damage is usually located at some specific regions of the aorta. It has long been known that atherosclerosis generally occurs in the large systemic arteries and sites of arterial branching.

1.2.2 The roles of ECs, SMCs and monocytes in atherogenesis

There are three major cell types which are observed to be involved in the development of atherogenesis. They are the EC, the SMC and the monocyte-derived macrophage.

(A) Foam cells in the lesion

Foam cells filled with droplets of fat are the most prevalent cell type in early atherogenic lesions (fatty streak). However, this cell type is usually a relatively minor cell component in advanced fibrous plaques (Wissler,1987). As reviewed in Fowler et al. (1985), the foam cells can originate from both monocyte-derived macrophages and SMCs. However, what percentage of advanced lesions are occupied by macrophages and what percentage by SMC is still not clear (Ross,1986). The most common current view is that initially foam

cells are largely monocyte-derived macrophages, but that as the lesion progresses the proliferation of SMCs contributes an increasing fraction of the lesion and in later stages becomes the principal cellular component.

(B) Chemotactic factors for monocytes

The elevated LDL level in the plasma (hyperlipidemia) is one of the sufficient conditions for the attachment of monocytes to the surface of the endothelium. Circulating monocytes migrate along chemotactic gradients in the plasma. It was found that ECs, SMCs and macrophages can produce factors that are chemotactic to monocytes (Bevilacqua et al., 1985; Martin et al., 1984; Berliner et al., 1986; Jauchem et al., 1982). LDL that has been oxidatively modified by ECs is also chemotactic for monocytes (Quinn et al.,1987). In addition, the monocyte recruitment into the artery wall depends on the stimulation of the circulating monocyte by some factors present in the hypercholesterolemic plasma (Gerrity, 1985).

It is hypothesized by Weinbaum et al. (1988a) that when the monocytes receive activation signals, they will migrate via chemotactic gradients to the endothelial surface where they first attach to the plasmalemma. These cells then alter the cell junctions so that they can enter the subendothelial space where they are subsequently converted to macrophages in the intima. Little is known concerning in vivo mechanisms controlling the migration of monocytes into the vessel wall.

(C) Degradation of LDL in the arterial wall

The formation of the foam cell lesion is more complicated than lipid entry alone since the well known experiments of Minick et al. (1977) have shown that in lipid fed rabbits early lesions form under

the leading edge of a healing endothelial injury where endothelial cells have regrown rather than the central region of the injury where reendothelialization has not yet occured. This result suggests that the EC plays a very important role in the localization of the early lesions. A possible explanation from Weinbaum et al. (1988a) is given below.

Since monocytes have very few native LDL receptors (Steinberg,1983), further modification of the LDL must first occur before the monocytes can act as macrophages. The tissue culture experiments of Henriksen (1983) and Quinn (1987) suggest that proliferating endothelial cells are capable of significantly modifying LDL and that the oxidatively EC-modified LDL is readily taken up by the macrophages, at least in cell culture, without regulation. It was reported by Carew et al. (1987) that the rate of degradation of LDL in the macrophage-rich fatty-streak lesions of the LDL receptor-deficient rabbit treated with probucol (an effective antioxidant) is reduced to about one-half of that in the lesions of the same kind rabbit not given probucol; this was the first in vivo evidence to suggest that the absence of oxidation can significantly reduces the rate of development of fatty-streak lesions. If the endothelium is removed in a certain region, the chemotactic gradient produced by ECs in this region will disappear, and the native LDL will not be modified. Since there are few SMCs in the normal intima, the native LDL can neither be degraded by macrophages nor by ECs. Thus LDL can not accumulate in the intima in a region denuded of its endothelium. However, in the region where the endothelial cells are replicating, all the necessary conditions for lipid accumulation are

provided, and the early foam cell lesion is able to form under the leading edge of the healing endothelial injury.

Carew et al. (1989b) have demonstrated in their lipid feeding experiments that accumulation of lipid occurs prior to the adhesion and penetration of monocytes into the intima. This accumulated lipid is in the forms of intact LDL and degraded LDL (free cholesterol and cholesteryl esters). Forty percent of the total degradation in the rabbit aorta takes place in the intima, which represents less than 5 percent of the total wall thickness. The remaining 60 percent occurs in the media, where there is little doubt that the cellular degradation of the LDL is due to SMCs, since there are no other cellular components. However, the cellular origin of the LDL degradation that occurs in the intima (ECs and/or SMCs) before the recruitment of monocytes is still unknown and the high level of degradation is very puzzling. In the normal intima there are only a few SMCs, and rate of native LDL receptor-mediated degradation by down-regulated confluent ECs is only 0.5 percent of that by SMCs (Fielding et al.,1979). For cationized LDL, the lysosomal degradation by confluent ECs is comparable to that by SMCs (Fielding et al.,1979). It was shown by Baker et al. (1984) that aortic ECs possess the native LDL receptor, the scavenger receptor for modified LDL and the β-VLDL receptor. Thus if the LDL in the intima is degraded by ECs, it may be through the scavenger receptor-mediated pathway.

(D) Growth factors

The migration of SMCs and their subsequent proliferation in the intima is a common feature of the atherogenic process. The mechanism of SMC proliferation is still not clear. Many factors released from

platelets, ECs and stimulated macrophages can stimulate the proliferation and migration of SMCs (Ross et al, 1974; DiCorleto et al., 1983; Ross, 1986).

1.2.3 Metabolism of LDL and cholesterol transport

The cholesterol in atherosclerotic plaques is primarily derived from low density lipoproteins (LDL), which are synthesized de novo in the liver (Goldstein and Brown, 1977). The LDL molecule transports esterified cholesterol manufactured in the liver to the non-hepatic cells in the body which need the cholesterol in hydrolyzed form for membrane synthesis and in some special organs for hormone synthesis. The non-hepatic tissues have no machinery for storing cholesterol; therefore, the extra load of cholesterol must somehow be transported back to the liver for excretion. This reverse transport is conducted by another plasma lipoprotein - high density lipoprotein (HDL).

(A) LDL pathway

The sequence by which cells take up cholesterol from native LDL is called the LDL pathway. Brown and Goldstein first discovered the LDL receptor on the membranes of fibroblasts in 1973. Their pioneering series of experiments has provided invaluable insight into the nature of the high affinity, native LDL receptor-mediated pathway.

The LDL receptor-mediated pathway has three characteristics (Goldstein et al.,1977): (1) the LDL receptor is a highly specific, this receptor will bind only to apoprotein B and apoprotein E; (2) it is high affinity, which means that the binding can take place at very low LDL concentrations ($<10^{-9}$ molar); and (3) the number of receptors can be regulated up and down by the cell itself. This enables the cells to take up enough cholesterol from the outside for their

utilization and at the same time prevent the overaccumulation of cholesterol. Because of all these features, the LDL receptor-mediated pathway is called the high-affinity pathway or specific pathway. Correspondingly, the non-receptor pathway is called the low affinity pathway or non-specific pathway. The latter include pinocytosis and adsorptive endocytosis.

Before the discovery of the LDL receptor, LDL was believed to enter the artery wall only via a low affinity, non-specific pathway such as vesicular transport. It is now realized that about one half of total body LDL degradation occurs by way of the LDL receptors in the intact animal (Steinberg,1983). Experiments with cultured fibroblasts, however, show that this distribution of uptake and degradation between low and high affinity pathways is dependent on the concentration of LDL in the medium (Goldstein and Brown, 1974). When the extracellular concentration of LDL is low, most of the LDL degradation is via the receptor-mediated pathway. As the LDL concentration in the external medium is increased, the percentage of LDL degradation via the low-affinity pathway will increase, because the receptor-mediated LDL degradation in the cell's lysosomes will be saturated. The saturation value for the high affinity pathway is less than 50 μg LDL protein/ml (Brown and Goldstein, 1979). This is far less than the normal LDL level in the blood serum [the mean value for humans is about 1200 μg LDL protein/ml (Goldstein and Brown, 1977)]. The uptake of LDL via the low affinity pathway, on the other hand, increases almost linearly with the concentration of LDL in the medium. However, the latter pathway does not contribute to the regulation of the intracellular lipid metabolism (Goldstein and Brown, 1977). It only affects the clearance of LDL from the

interstitium of the arterial wall. Thus, it will contribute to the lipid clearance in the subendothelial space.

When LDL is taken up by a non-specific pathway, it reaches the lysosome where its protein and cholesterol ester are hydrolyzed in a manner similar to that which occurs during the receptor-mediated uptake process. However, the free cholesterol released from LDL via the low affinity pathway does not contribute to the intracellular cholesterol pool, since it is excreted into the extracellular medium (Brown and Goldstein, 1976). Attie et al. (1982) have shown that the degradation of apo B internalized by non-receptor-mediated endocytosis in cultured hepatocytes is not sensitive to chloroquine or leupeptin treatment of the cells. This treatment prevents the lysosomal hydrolysis of LDL via the high-affinity pathway suggesting that the hydrolysis of LDL taken up through the low-affinity pathway is part of a different mechanism.

The receptor-mediated pathway by which LDL is metabolized in cultured human fibroblasts is shown in Fig.1 of chapter 2. Under conditions of cholesterol deprivation, such as the incubation of the cells in lipoprotein-deficient serum, these cells are capable of increasing the synthesis of the native LDL receptor by more than an order of magnitude (Goldstein and Brown, 1977). Newly formed receptors are randomly inserted into the surface membrane of the cell. The receptors then migrate into coated pit regions (an indented structure on the membrane in which more that 70% of LDL receptor sites are concentrated; these microdomains which constitute less than 2% of the total surface membrane are coated with clathrin). The coated pit then invaginates into the cell to form coated vesicles. The entire sequence mentioned above proceeds

continuously in fibroblasts no matter whether the LDL is present in the medium (Brown and Goldstein, 1979). When the LDL is added to the medium, the initial event of the LDL metabolism is the binding of LDL to its receptor, and together with the receptors, LDL is internalized when the coated pit pinches off to form coated vesicles. These vesicles will move to the lysosome (a digestive organ in the cell). Before the vesicles fuse with lysosomes, most of the receptors dissociate from the vesicles and are returned to the cell membrane in a "short time" recycling that takes a few minutes. Within the lysosome LDL and a few LDL receptors are catabolized. The protein component of LDL is rapidly degraded to free amino acids, which are then released into the culture medium. The cholesteryl ester component of LDL is hydrolyzed by a lysosomal acid lipase, and the resultant free cholesterol is transferred to the cellular compartment where it is found largely associated with cell membrane (Brown and Goldstein, 1976).

Free cholesterol has different utilizations depending on cell type; for example, it is used in steroid hormone synthesis in endocrine glands, bile acid formation in the liver and membrane synthesis in most kinds of the cells, especially during cell division. Some of the free cholesterol in the nonhepatic cells is transported back to the medium because of the chemical potential gradient (effective concentration difference between the membrane and the medium). This kind of efflux of free cholesterol is maintained by a chemical reaction, the esterification of cholesterol by lecithin:cholesterol acyltransferase (LCAT) in the medium (Fielding,C.J. and Fielding,P.E., 1985). The esterified cholesterol is taken up by HDL and transported back to the liver as mentioned

before. Any cholesterol that accumulates over the amount that can be either utilized or transported to the external medium is esterified with a long chain fatty acid and stored within the cell as a liquid crystal of cholesteryl ester. The esterifioation process is promoted by an enzyme called Acyl-CoA: cholesterol acyltransferase (ACAT).

In the LDL receptor-mediated pathway, there are three important regulation processes. We have already mentioned the reesterification process. The other two regulation processes are the regulation of cholesterol synthesis de novo promoted by HMG-CoA reductase and the regulation of receptor number on the cell membrane through receptor synthesis initiated by the release of mRNA.

In the usual steady state when the non-hepatic cell are growing in a medium containing whole serum, there is enough cholesterol entering the cell through the LDL pathway. The activity of HMG-CoA reductase is suppressed and the cells preferentially take up and utilize the LDL-derived cholesterol. It's only under extreme conditions, when the cells are deprived of LDL or lack the LDL receptor, that they increase their ability to synthesize cholesterol (Brown and Goldstein, 1976).

In general, the number of functional LDL receptors is less than 10% of the maximal number that the cells are capable of synthesizing in a lipid depleted environment (Goldstein and Brown, 1977). The synthesis of receptors is determined by the rate at which the gene is transcribed. This transcription results in an mRNA species that encodes the complete sequence of amino acids required to form receptor protein. An excess of cellular free cholesterol reduces the transcription of the LDL receptor gene into mRNA. There is some evidence which suggests that the LDL-mediated suppression of LDL

receptor activity is due to an inhibition of synthesis of the LDL receptor (Goldstein and Brown, 1977). Compared with the "short time" recycling of receptors in endocytosis, receptor regulation is a "long time" recycling. A small fraction of the membrane receptors internalized in the coated vesicles are hydrolyzed in the lysosomes and discharged to the extracellular environment. The new receptors are synthesized on the endoplasmic reticulum and Golgi apparatus, then inserted into the membrane. The half-life of the receptor is about 15~20 hours. A maximum number of LDL receptors is reached after actively growing fibroblasts have been incubated for 48~72 hours in the absence of LDL.

Under normal conditions, although the concentration of LDL in the medium may fluctuate with time, the cellular content of free cholesterol is kept nearly the constant by the LDL receptor-mediated pathway, in which the influx just balances the efflux at steady state. This self-adaptive system will allow the non-hepatic cells to take up enough cholesterol for their utilization (e.g. membrane synthesis, etc.), and yet avoid excessive accumulation of cholesterol in the cells.

(B) The functions of HDL

HDL is secreted by the liver and intestine and also by the contributions of chylomicrons and VLDL (Steinberg,1987). A high plasma concentration of HDL cholesterol is associated with a lower risk of coronary heart disease (Barr et al.,1951).

The Reverse Cholesterol Transport Hypothesis proposed by Glomset (1968) suggested that the function of HDL is to remove excess cholesterol from peripheral tissues and carry it back to the liver for elimination; and that lecithin-cholesterol acyltransferase (LCAT)

is involved in cholesterol transport between the cell membrane and HDL particles by promoting the cholesterol esterification.

The mechanism for cholesterol efflux remains uncertain. The studies for cultured rat Fu5AH hepatoma cells and GM 3468 human fibroblasts (Karlin et al.,1987) suggested that cholesterol efflux is not facilitated by the specific cell-surface binding of HDL to cell membrane, but involves the diffusion of cholesterol in the aqueous phase between cell membrane and the acceptor HDL. The transfer of cholesterol from membrane to HDL appears to be passive, since no metabolic energy is detected during this process [see summary in Bruckdorfer and Graham (1976)].

1.3 Initiation of atherogenesis

Athough there are multiple causes that could initiate the atherogenic process, only some of them are examined in this dissertation. Based on the discussion in this chapter, the initiation of atherogenesis can be summarized as follows.

The mechanical and/or chemical (hyperlipidemia or toxins, etc) factors can lead to subtle non-denuding injury of the endothelium. These injuries occur more frequently in the lesion-susceptible regions (e.g. the branch areas in the aorta), and involve an increase in the rate of EC turnover instead of overt endothelial denudation. The endothelial permeability to macromolecules is increased due to the transient open junctions (large pores) associated with the cell turnover. Thus, more LDL molecules enter the arterial wall, especially when blood plasma LDL levels are high. When subendothelial LDL levels are low and there is no recruitment of monocytes, the degradation of LDL in the intima is due primarily to ECs, while LDL in the media is degraded by SMCs.

According to the hypothesis proposed by Weinbaum et al. (1988a), the sequential events occurred after injury of the endothelium are described below. Increases in LDL concentration in the intima can saturate the LDL receptor-mediated pathway on the abluminal side of the ECs. In response, the ECs will release a chemotactic signal for monocytes recruitment and a PDGF-like growth factor for proliferation and migration of SMCs. The ECs can also oxidatively modified the native LDL, to activate its uptake by scavenger cells (macrophages, etc.), which also release chemotactic agents for monocytes. Having received the chemotactic signals, the monocytes will migrate along the chemotactic gradient and finally attach to the endothelium in low shear areas with flow separation and re-attachment. Through some unknown mechanism, monocytes cross the endothelium and are thereafter converted to macrophages, which take up the modified LDL to restore the LDL level in the interstitium of the intima. If the LDL concentration in the lumen is decreased sufficiently, the above process could be reversed and the monocyte-macrophages re-enter the blood. Otherwise, the unregulated scavenger receptor-mediated pathway will convert the macrophages to lipid-filled foam cells. Macrophages can also secrete several growth factors for SMC proliferation and migration. In addition to proliferation and migration, SMCs will secrete a large amount of extracellular matrix (EM) macromolecules (Robert,1987) and accumulate lipid. The chemotactic factors released by SMCs might also help the penetration of monocytes into the subendothelial space.

There are two lipid pools: an extracellular pool of primarily native LDL and an intracellular pool of degraded LDL, that is stored

in the cell primarily as cholesteryl ester. The major intracellular lipid pool is probably the macrophages.

The lipid accumulation and SMC proliferation in the intima form the early fatty streaks in the atherogenic process. These streaks become enlarged by the continued migration of monocytes and SMCs into the intima, where initially the monocyte-derived macrophages are the major cellular constituent. This growth is also accompanied by the secretion of EM macromolecules by SMCs and ECs (Robert,1987).

CHAPTER 2

A Mathematical Model for the Receptor-Mediated Cellular Regulation of the Low Density Lipoprotein Metabolism

2.1 Introduction

It has been more than ten years since the pioneering experimental studies on the low density lipoprotein (LDL) metabolism of human fibroblasts by Brown and Goldstein were performed (Goldstein and Brown, 1977). These studies have led to the discovery of the native LDL receptor and an in-depth understanding of the LDL pathway in cells and the intracellular regulation of cholesterol content. While several kinetic models have been proposed for different aspects of the LDL receptor-mediated pathway (Keizer et al., 1985; Peacock-Lopez and Ramirez, 1986; Truskey et al., 1984; Phillips et al., 1987), there is, to our knowledge, no overall mathematical model for the intracellular regulation of the LDL pathway. A statistical theory of non-equilibrium thermodynamics was developed to describe the random re-insertion of LDL receptors and coated pits into the cell membrane, the diffusion and binding of the LDL receptors on the cell membrane to coated pits and the formation of coated pit vesicles (Keizer et al., 1985; Peacock-Lopez and Ramirez, 1986). This model led to an equation that relates receptor diffusion to receptor binding in coated pit regions. The kinetic analysis of receptor-mediated endocytosis and lysosomal degradation of LDL molecules in cultured cells was conducted by Truskey et al. (1984), and the rate constants for these processes were obtained by comparison with experiments. Investigations involving the cholesterol and phospholipid exchange and transfer are reviewed by Phillips et al. (1987). In this latter study various mechanisms and kinetic models

for the cholesterol efflux from cells to high density lipoproteins (HDL) are examined. At present, there is no mathematical model for the regulation of LDL receptor number, the de novo synthesis of free cholesterol, and the storage of cholesteryl esters. These models are required for studying quantitatively the cholesterol homeostasis in the cells. In this chapter, theoretical models are proposed for these processes and an overall quantitative framework is developed to explore the LDL receptor-mediated pathway.

One of the earliest features of atherogenesis in cholesterol fed rabbits, prior to the subendothelial penetration of blood-borne monocytes and their conversion to foam cells, is the lipid accumulation in the subendothelial space in the arterial wall (Schwenke and Carew, 1989b). This depends not only on the convective-diffusion of LDL, but also on the binding of LDL to extracellular tissues and the degradation of LDL by endothelial cells (ECs) and smooth muscle cells (SMCs). Therefore, it is important to quantitatively investigate the lipid metabolism of ECs and SMCs before the monocytes have entered the intima. Since sufficient data does not exist for various processes that enter into the regulation of the LDL receptor-mediated pathway in these cell types, we shall resort to a mathematical model that uses partial experimental data derived from fibroblasts. The use of this data in a first approximate quantitative model can be justified in that: (1) fibroblasts behave in a manner that is representative of most non-hepatic body cells, including ECs and SMCs, which prefer to obtain their cholesterol from plasma lipoproteins secreted by the liver (Gold Brown, 1977); and (2) the data for human fibroblasts are the most complete of any cell type and have been systematically presented in a series

of papers by Brown and Goldstein, which were reviewed by Brown and Goldstein (1979).

It is now realized that about one half of total body LDL degradation occurs by way of the LDL receptor-mediated pathway in vivo (Steinberg, 1983). The LDL degradation of the remaining 50 percent can occur by either the non-receptor mediated pathway or by a high affinity modified LDL receptor-mediated pathway (Steinberg, 1983). In the later pathway, LDL molecules are first modified and then recognized by receptors for apoproteins other than apoprotein B-100, the native LDL recognition protein. The uptake of LDL via the low affinity non-receptor mediated pathway increases almost linearly with the concentration of LDL in the external medium. The experiments in Attie et al. (1983) suggest that the hydrolysis of LDL taken up through the low affinity non-receptor mediated pathway is part of a different mechanism that does not involve the regulation of the native LDL receptor (Goldstein and Brown, 1977). Therefore, the non-receptor mediated pathway is not considered in our present model which reflects only the regulatory aspects of the native LDL pathway. However, the non-receptor mediated pathway can have significant effect on the interstitial concentration of LDL, when we investigate the LDL transport across the arterial wall.

The present model is based largely on the experiments of Brown and Goldstein with human fibroblasts (Goldstein and Brown, 1977; Brown and Goldstein, 1979). It attempts to predict the time dependent changes of the free cholesterol in the cell, for given initial conditions and a specified concentration of LDL in the surrounding medium. The time scale for the regulation of the cellular free cholesterol content in the model is typically half a day or longer,

since this is the known characteristic time of the receptor regulation process. Processes which occur on a significantly shorter time scale will be considered to be instantaneous and thus be treated as if they were time-independent.

2.2 Mathematical model

Under normal conditions, although the concentration of LDL in the medium may fluctuate with time, the cellular content of free cholesterol is kept nearly constant by a complicated system of intracellular regulation, which in our proposed mathematical model includes six important processes, as schematically shown and numbered in Fig.1. These processes are: (1A,B) the hydrolysis and synthesis of LDL receptors in the cell, (2) the binding and the internali- zation of LDL by its receptors on the cell membrane, (3) the hydrolysis of LDL in the lysosome of the cell, (4) the storage of cholesteryl esters, (5) the regulation of de novo synthesis of cholesterol, and (6) the efflux of free cholesterol to the external medium.

2.2.1 Regulation of LDL receptor number

Before the internalized coated vesicle fuses with the lysosome, most of the receptors are separated from the LDL molecules and recycled to the cell membrane as shown in Fig.1. Only a small fraction of the LDL receptors are hydrolyzed with LDL in the lysosome (Brown and Goldstein, 1979), process (1A) in Fig.1. Meanwhile, the cell will also synthesize new receptors, process (1B), which are inserted randomly into the cell membrane. Therefore, the rate of the change of total receptor number comes from the difference between the rate of synthesis and the rate of hydrolysis, that is

$$\frac{dR}{dt} = V_s - V_H \qquad (1)$$

where R is the total receptor number, V_s is the rate of receptor synthesis and V_H is the rate of lysosomal receptor hydrolysis.

(A) Hydrolysis of LDL receptor in the lysosome

We assume that the rate of receptor hydrolysis is proportional to the total number of receptors,

$$V_H = K_0 R \tag{2}$$

where K_0 is a rate constant.

(B) Synthesis of LDL receptor

The synthesis of the LDL receptor is a complicated process that involves several steps. When the cell needs to synthesize LDL receptors, the transcription of the structural gene for the LDL receptor starts in the nucleus. This transcription leads to the export from the nucleus of a mRNA species that encodes the complete sequence of amino acids required to form the receptor protein on the ribosome of the endoplasmic reticulum. The rate at which new mRNA is transcribed is the main basis for the up- or down- regulation of the native LDL receptor number. A simplified model for this process is,

$$A_p + A_t \xrightarrow[tRNA]{k_1} A_{Rt} \xrightarrow{k_2} R + A_t$$

where A_p, A_t, A_{Rt} and R represent the amino acids pool, the template composed of the mRNA and the ribosomes for receptor synthesis in the cell, the template-bound LDL receptor and the produced LDL receptors, in that order. This is a typical Michaelis-Menten type reaction (Bray and White, 1966). The kinetic equation is

$$\frac{d[A_{Rt}]}{dt} = k_1[A_p][A_t] - k_2[A_{Rt}] \tag{3}$$

and the rate of receptor production can be expressed as

$$V_s = k_2[A_{Rt}] \tag{4}$$

where $[\cdot]$ represents the concentration of the corresponding substances in the cells and k_1 and k_2 are constants.

Substituting (4) into (3), we have

$$\frac{dV_s}{dt} = K_1(A - V_s) \tag{5}$$

where $K_1 = k_1[A_p] + k_2$ is the rate constant, $A = k_1k_2[A_p][A_t]_t/K_1$ and $[A_t]_t = [A_t]+[A_{Rt}]$ is the total template in the cells.

Differentiating (1), and using (1), (2) and (5) to eliminate V_H and V_s, one obtains

$$\frac{d^2R}{dt^2} + (K_0 + K_1)\frac{dR}{dt} + K_0K_1(R - R_i) = 0 \tag{6}$$

where $R_i = A/K_0$ is the value of R in the steady state. This is a second order system in which K_0 and K_1 characterize the time scales of the hydrolysis and synthesis of LDL receptors. The initial conditions for an experiment are,

$$R(0) = R_0 \tag{7}$$

$$\frac{dR(0)}{dt} = \dot{R}_0 \tag{8}$$

where R_0 can be obtained from the initial data of the experiment and $\dot{R}_0$ is determined from the initial slope of the experimental results.

It was also assumed that there is an over abundance of amino acids for the synthesis of new receptors, so that during synthesis, the change of the amino acid pool is negligible, i.e. K_1 is a constant. The solution of (6) can be obtained analytically. This

expression for receptor number R can be used to determine the rate constants K_0 and K_1 by curve fitting the experimental data by the method of least squares. The solutions for K_0 and K_1 are symmetric and non-unique. However, we found that there always exists a solution with $K_0 = K_1$, and the sum of the squares of the residuals is less than the solution with $K_0 \neq K_1$. Therefore, we assumed that $K_0 = K_1$ and they are denoted by K. The solution of (6) with initial conditions (7) and (8) is thus obtained

$$R = R_i + (R_0 - R_i)(1+Kt)\exp(-Kt) + \dot{R}_0 t \exp(-Kt) \qquad (9)$$

The receptor number in the steady state R_i is proportional to the total template $[A_t]_t$ for LDL receptor synthesis in the cells, which, in turn, depends on the cholesterol level in the cell. The experiments in Goldstein and Brown (1977) and Brown and Goldstein (1975) show, however, that the up- or down-regulation of LDL receptors in the normal cells can also be directly related to the concentration of LDL in the medium. In the steady state, the number of LDL receptors is completely determined by this external LDL concentration. Therefore, we can simplify the model by assuming that the total amount of the template only depends on the concentration of LDL (L_e) in the extracellular medium. Thus, R_i is only a function of L_e. The experiments of Brown and Goldstein (Brown and Goldstein, 1975 and 1979; Goldstein and Brown, 1977) show that the relation between R_i and L_e can be approximated by the expression

$$R_i = a_i \exp(-b_i L_e) + c_i \qquad (10)$$

where a_i, b_i and c_i are constants determined by curve fitting the experimental data.

Since the recycling time of the coated vesicles (approximately 10 minutes) is very short compared to the receptor synthesis process (Goldstein and Brown, 1977), the number of LDL receptors on the cell membrane is proportional to the total number of LDL receptors recycling within the cells. Since equations (6) through (8) for R are homogeneous, this proportionality constant cancels out and equation (9) will still be valid if R represents the number of LDL receptors on the cell membrane. The later representation of R will be used in the following studies.

2.2.2 Binding of LDL to its receptors

The initial event in the LDL pathway is the binding of LDL to its receptors on the cell membrane, process (2) in Fig.1. The amount of binding depends on the difference between the rate of association of the LDL molecule to its receptor and the rate of dissociation. Usually the rate of spontaneous dissociation of ^{125}I-LDL from the receptor is very small (Goldstein and Brown, 1977).

The time scale for the regulation of a system depends generally on its slowest process. The slowest process in the entire LDL pathway is the regulation of LDL receptor number, which has a characteristic time of about one day. Experiments in Goldstein and Brown (1974) indicate that the amount of ^{125}I bound to the cells reaches a maximum after 2 hours and remains constant for the next 28 hours. Therefore, for times greater than 2 hr, the amount of binding is approximately time-invariant and depends only on the concentration of LDL in the medium. In normal cells, as the concentration of ^{125}I-LDL in the medium is increased, the amount of LDL bound to the receptor

increases exponentially until all of the sites become occupied (Brown and Goldstein, 1979). Based on these observations, we assume that the amount of LDL bound to its receptors on the cell membrane can be expressed as

$$B = R\,[1 - \exp(-\alpha L_e)] \tag{11}$$

where B is the amount of bound LDL, R is the number of LDL receptors on the cell membrane (R is equal to the amount of binding when every receptor recognition site is filled by an LDL molecule) and α is a constant which reflects the affinity of binding. If $\alpha L_e \ll 1$, the binding is low-affinity, and the amount of binding is proportional to the LDL concentration in the extracellular medium, whereas if $\alpha L_e \geq 1$, the binding is high-affinity.

2.2.3 Hydrolysis of LDL in the lysosome

The hydrolysis of LDL occurs in the lysosomes, process (3) in Fig.1. It depends on the amount of LDL internalized, which, in turn, is proportional to the amount of binding. Thus we assume the rate of LDL hydrolysis R_H is proportional to the amount of binding.

$$R_H = K_2 B \tag{12}$$

where K_2 is a constant. However, it will be discussed later that the value of K_2 may depend on the degree of the confluency of cell monolayers, which is the case for ECs (Fielding et al., 1979).

2.2.4 Storage of cholesteryl ester in the cells

(A) Reesterification of free cholesterol

The reesterification of free cholesterol derived from the hydrolysis of LDL is catalyzed by a microsomal enzyme ACAT (Goldstein and Brown, 1977), process (4) in Fig.1. When normal fibroblasts are

deprived of cholesterol by growth in the absence of LDL or other sources of exogenous cholesterol and then incubated with [^{14}C]oleate, no detectable incorporation of ^{14}C-radioactivity into cellular cholesteryl ester occurs (Goldstein and Brown, 1977), although in this case the rate of cholesterol synthesis in the normal cells reaches its maximum value. When the LDL is added to these cholesterol-deprived fibroblasts, the rate of [^{14}C]oleate incorporation into cellular cholesteryl [^{14}C] esters increases more than 500-fold within 6 hours (Goldstein et al., 1974). These results suggest that the cholesterol reesterified in the fibroblasts originates from the hydrolysis of LDL via the receptor-mediated pathway. Our simplified kinetic model for the reesterification process is

$$E + C_H \underset{k_{-1}}{\overset{k_1}{\rightleftharpoons}} EC_H \xrightarrow{k_2} CE + E$$

where E, C_H, EC_H and CE represent ACAT, the free cholesterol in the cytoplasm derived from the high-affinity pathway, ACAT-bound cholesteryl ester and the produced cholesteryl ester, respectively. Again, this is a Michaelis-Menten type reaction. The kinetic equation for this reaction is

$$\frac{d[EC_H]}{dt} = k_1[E][C_H] - (k_{-1}+k_2)[EC_H] \qquad (13)$$

where [•] represents the concentration of the corresponding substances in the cells and k_1, k_{-1} and k_2 are constants.

The rate of reesterification U_e is

$$U_e = k_2[EC_H] \qquad (14)$$

The reesterification process is also a fast process compared with the regulation of LDL receptors (Goldstein et al., 1974). Therefore the reesterification is assumed to be a quasisteady equilibrium process, in which the rate of reesterification does not explicitly depend on the time, but can change with the amount of free cholesterol hydrolyzed from LDL. Combination of equations (13) and (14) with $d[EC_H]/dt = 0$ gives

$$U_e = \frac{k_2[E]_t[C_H]}{[C_H] + K_S} \tag{15}$$

where $K_s = (k_{-1} + k_2) / k_1$ is the equilibrium constant, and $[E]_t = [E]+[EC_H]$ is the total amount of ACAT in the cells.

The experiments by Goldstein and Brown (1977) indicate that the regulation of free cholesterol reesterification does not appear to involve changes in enzyme synthesis, whereas the activity of ACAT will depend on the cellular content of free cholesterol. However, there is presently inadequate experimental data to determine the relationship between the activity of ACAT and the intracellular content of free cholesterol. Thus we assume that the total amount of the activited ACAT enzyme $[E]_t$ to be a constant. This assumption may need to be modified in the future studies.

After cholesterol enters the cell through the LDL receptor-mediated pathway, it will either stay in the cytoplasm, be reesterified to cholesteryl ester, become part of the lipid component of the cell membrane, or be excreted to the extracellular medium. Unless the rate of LDL hydrolysis R_H is very low, most of free cholesterol hydrolyzed from LDL will stay in the cytoplasm, because

the rates of reesterification, membrane incorporation and efflux are rather limited. It is thus reasonable to assume that the free cholesterol in the cytoplasm C_H derived from the hydrolysis of LDL via the high-affinity pathway is proportional to the rate of LDL hydrolysis R_H. Thus (15) can also be written as

$$U_e = \frac{a_1 R_H}{b_1 + R_H} \tag{16}$$

where a_1 and b_1 are constants.

(B) Nonlysosomal hydrolysis of cholesteryl ester

Fibroblasts are not observed to store large amounts of cholesteryl esters under normal conditions. Therefore, when there is too much cholesteryl ester stored in the cell, it will be hydrolyzed. This process is promoted by neutral, nonlysosomal cholesterol esterase (Fielding and Fielding, 1985). The hydrolysis, similar to the reesterification process, is also a rate-limiting process. Thus, the rate of hydrolysis U_H of stored cholesteryl ester is determined by a derivation similar to equation (16) and is given by

$$U_H = \frac{a_2(Q_e - Q_{eo})}{b_2 + (Q_e - Q_{eo})} \tag{17}$$

where Q_e is the cellular content of cholesteryl ester, Q_{eo} is the minimum value of cellular cholesteryl ester which is not involved in the regulation process, and a_2 and b_2 are constants.

The rate R_e of the change of stored cholesteryl ester in the cells is the difference between the rate of reesterification (16) and the rate of hydrolysis (17).

$$R_e = U_e - U_H \qquad (18)$$

or

$$\frac{dQ_e}{dt} = \frac{a_1 R_H}{b_1 + R_H} - \frac{a_2 (Q_e - Q_{eo})}{b_2 + (Q_e - Q_{eo})} \qquad (19)$$

2.2.5 Synthesis of cholesterol

The synthesis of cholesterol in the cell, symbolized by process (5) in Fig.1, involves more than 30 chemical reactions, in which the rate-determining step is the reaction catalyzed by HMG-CoA reductase. The suppression of the activity of HMG-CoA reductase or the synthesis of cholesterol in the cells is possibly due to the presence of several oxysterols in the cells, which originate exogenously or endogenously (Kandutsch, 1986; Gupta et al., 1986). The LDL-dependent inhibition of cholesterogenesis is the result of the oxidation of cholesterol derived from the receptor-mediated endocytosis of LDL, or the oxysterol contained in the LDL molecule. It does not appear to be the result of the excessive accumulation of free cholesterol in the cell, since purified cholesterol does not affect the activity of HMG-CoA reductase in several cell lines (Breslow et al., 1975; Kandutsch and Chen, 1977; Chen et al., 1979).

In our model we assume, based on the experimental results of Gupta et al. (1986), that the oxysterol that can inhibit the activity of HMG-CoA reductase is derived entirely from the LDL receptor-mediated pathway. Therefore, the rate of cholesterol synthesis in the cells will depend on the amount of LDL internalized, which in turn, depends on the number of LDL receptors and the concentration of LDL in the external medium. Because the mechanism for the regulation of cholesterol synthesis is still unknown, we can not derive the

relationship between the rate of cholesterol synthesis and the amount of LDL internalized. This missing relationship will be replaced by an assumed function form for R_s, the rate of cholesterol synthesis, that is obtained from experiments of Brown and Goldstein (1979) and Goldstein et al. (1976b),

$$R_s = K_3 R \left[\exp(-a_s L_e) + b_s\right] \tag{20}$$

where K_3, a_s and b_s are constants that will be determined by curve fitting the experimental data.

2.2.6 Efflux of cholesterol

Aside from reesterification, the removal of free intracellular cholesterol arises from another source, the efflux of cholesterol to the external medium, process (6) in Fig.1. The mechanism for cholesterol efflux remains uncertain. The studies for cultured rat Fu5AH hepatoma cells and GM 3468 human fibroblasts (Karlin et al., 1987) suggests that cholesterol efflux is not facilitated by the specific cell-surface binding of HDL to cell membrane, but involves the desorption of free cholesterol from cells membrane and the diffusion of cholesterol in the aqueous phase between cell membrane and the acceptor HDL molecules. Desorption of cholesterol from the cell membrane is rate-limiting for efflux and the rate of this step is influenced by the interaction of free cholesterol molecules with neighboring phospholipid molecules in the membrane (Phillips et al., 1987). Therefore, the rate of efflux is equal to the rate of cholesterol desorption. Several kinetic models reviewed by Phillips et al. (1987) have been proposed for efflux. In this chapter, the aqueous diffusion model was adopted, and this desorption process is further simplified by neglecting the concentration of free

cholesterol in the extracellular medium, because the water solubility of cholesterol is very low. Thus the rate of efflux (or desorption) R_x is proportional to the cholesterol concentration associated with the cell's plasmalemma membrane.

$$R_x = K_4 C \tag{21}$$

Here C is defined as the amount of cholesterol associated with the membrane per mg cell protein and K_4 is a rate constant. The value of K_4 will depend on the interaction of cholesterol molecules with neighboring phospholipid molecules in the plasmalemma membrane and also acceptor molecules (e.g. HDL) in the external medium (Phillips et al., 1987).

2.2.7 Balance of intracellular cholesterol

All the processes discussed above have the common purpose of letting the cell take up enough cholesterol from the external medium and yet avoiding the excessive accumulation of cholesterol in the cells. Finally, we can write an overall balance equation for the intracellular content of free cholesterol,

$$\frac{dC}{dt} = R_H + R_s - R_e - R_x \tag{22}$$

The uptake of LDL via the non-receptor mediated pathway is not involved in the balance equation (22) for the reasons discussed in the Introduction of this chapter.

In the steady state, C and Q_e are constant, so that the rates of hydrolysis of LDL, synthesis of cholesterol and efflux of free cholesterol must be in balance.

2.3 Determination of constants

The determination of the various constants in the expressions for R, B, R_H, R_e, R_s and R_x will now be described. These constants will differ depending on the cell type and the state of the cells. The procedure for obtaining these constants from available data is illustrated below for human fibroblasts. Some of the constants for SMCs are also obtained.

2.3.1 Binding affinity

Equation (11) can be rewritten as

$$\ell n\left(1 - \frac{B}{R} \right) = -\alpha L_e \qquad (23)$$

As discussed before, the time scale for receptor regulation is much longer than that of the binding experiments in (Brown and Goldstein, 1979), so that the number of receptors R can be treated as a constant equal to the saturation value for binding. For a given concentration of LDL in the medium, B is obtained by measuring the heparin-releasable LDL bound to the cells (Goldstein et al., 1976a). Then using a least square curve fit for the data in Fig.4 of Brown and Goldstein (1979), one obtains for the binding affinity constant α in (23)

$$\alpha = 0.048 \text{ ml}/\mu\text{g LDL protein}$$

The results of this curve fitting is shown in Fig.2, where the curve given by equation (11) is compared with the experimental data of Brown and Goldstein (1979).

The relationship between the concentration of LDL in the external medium and the amount of LDL bound to its receptor for SMCs is similar to that for fibroblasts (Chait et al., 1980). By using the

experimental data of Chait et al. (1980), one finds that the binding affinity α for SMCs is

$$\alpha = 0.041 \text{ ml}/\mu\text{g LDL protein}$$

which is close to the value of α for fibroblasts.

2.3.2 Receptor regulation

The number of LDL receptors on the cell membrane can be estimated indirectly by using the model for binding obtained from equation (11)

$$R = \frac{B}{1 - \exp(-\alpha L_e)} \tag{24}$$

If L_e is fixed, as described in the protocol for the experiments shown in Fig.2a of Goldstein and Brown (1977), where L_e=10 μg LDL protein/ml, K in equation (9) can be obtained by a nonlinear curve fitting technique. This technique requires that δ_R, which is defined by

$$\delta_R = \sum_j [R_j - R(t_j,K)]^2 \tag{25}$$

have a minimum value at the solution for K. In (25) R_j is the experimental data at time t_j from Fig.2a of Goldstein and Brown (1977) and $R(t_j,K)$ is the corresponding theoretical result from (9). The initial conditions are that R_0= 184 ng/mg and $\dot{R}_0$= 0. Here $\dot{R}_0$= 0 is assumed, because the cells had been incubated in the lipoprotein-deficient serum (LPDS) for 3 days, the cells had reached the steady state before the start of the experiment. At the beginning of the experiments, the extracellular concentration of LDL is a heavy side function with respect to the time t, therefore the derivative of R is

continuous at t=0. Following this procedure, one finds that δ_R has a minimum when

$$K = 2.4 \text{ day}^{-1}$$

The results of this curve fitting for the time-dependent binding using the above value of K is shown by the curve labeled by L_e=10 μg/ml in Fig.3. The curve for L_e=50 μg/ml will be discussed later. The experimental data are from Fig.2 of Goldstein and Brown (1977).

If the cells have been incubated in an invariant serum for more than two days, they will approach nearly the steady state behavior. This steady state behavior, which is described in the three experiments (Goldstein and Brown, 1977; Brown and Goldstein, 1975 and 1979), can be used to determine the three constants which appear in (10) for the steady state expression for the number of LDL receptors on the cell membrane of the fibroblasts:

a_i = 205 ng LDL protein/mg cell protein

b_i = 0.39 ml/μg LDL protein

c_i = 4.2 ng LDL protein/mg cell protein

The relationship between the concentration of LDL in the external medium and the number of LDL receptors on the cell membrane at the steady state for SMCs (Floren et al., 1981) is similar to that for fibroblasts. These constants for SMCs were evaluated from the experimental results of Floren et al. (1981):

a_i = 118.5 ng LDL protein/mg cell protein

b_i = 0.30 ml/μg LDL protein

c_i = 52.8 ng LDL protein/mg cell protein

where the protein/cholesterol ratio in normal human LDL molecules is 0.60 (Goldstein et al., 1974). This ratio will also be used in the following derivations.

2.3.3 Lysosomal hydrolysis of LDL

Experimentally, the amount of ^{125}I-labeled trichloroacetic acid-soluble material hydrolyzed from ^{125}I-LDL and the ^{125}I-LDL bound to its receptors on the cell membrane can be measured simultaneously. Therefore, K_2 in equation (12) for fibroblasts is obtained by using the data of binding and degradation of Brown and Goldstein (1976),

$$K_2 = 0.20\ \mu g \text{ cholesterol/ng LDL protein/day}$$

The constant K_2 for SMCs was obtained from the experiments of Davies and Kerr (1982), where, similar to the experiments for fibroblasts (Brown and Goldstein, 1976), the binding and degradation of LDL by bovine SMCs were measured simultaneously. For the experiments with low LDL concentration in the external medium, the degradation of LDL via the non-receptor mediated pathway is insignificant (Brown and Goldstein, 1976). Therefore, the ratio of the degradation and binding in Davies and Kerr (1982) gives the value of K_2 for SMCs,

$$K_2 = 0.02\ \mu g \text{ cholesterol/ng LDL protein/day}$$

which is one order of magnitude smaller than that for fibroblasts. The reason for this difference is unknown at the present time.

2.3.4 Reesterification of free cholesterol

Equation (19) can not be integrated analytically to determine Q_e; nor can it be solved numerically, because the four constants appearing in (19) are unknown. Fortunately, U_e can be measured

separately from U_H. In Fig.3F of Brown and Goldstein (1976), the incorporation of [^{14}C]oleate into cholesteryl [^{14}C]oleate was measured. Equation (16) can be rewritten as

$$R_H = a_1 \frac{R_H}{U_e} - b_1 \qquad (26)$$

Since all the curves in Fig.3 of Brown and Goldstein (1976) are for the same experimental conditions, at the indicated concentration of LDL in the external medium, U_e and the corresponding $R_H(=K_2B)$ can be determined. Using the method of least squares, a_1 and b_1 were evaluated as:

a_1 = 53.0 μg cholesterol/mg cell protein/day

b_1 = 33.1 μg cholesterol/mg cell protein/day

The result of this curve fitting of the data relating U_e and the LDL concentration in the external medium is shown in Fig.4, where $R_H = K_2B$, and B was obtained from equation (11), rather than the experimental binding data. The experimental data are from Fig.3F of Brown and Goldstein (1976).

It should be mentioned here that the amount of cholesteryl oleate only accounts for 35% of the total cellular content of cholesteryl ester (Goldstein et al., 1975). If the rate of the incorporation of any fatty acid into cholesteryl ester is assumed to be the same, the rate of the total cholesterol reesterification should be equal to that of the incorporation of [^{14}C]oleate into cholesteryl [^{14}C]oleate divided by 0.35. This correction had been made in solving for the constants a_1 and b_1.

The constants a_2 and b_2 can be obtained from another set of experiments in Goldstein et al. (1975). In these experiments, the rate of reesterification of free cholesterol was zero, because the fibroblasts were incubated in LPDS. Therefore, only the nonlysosomal hydrolysis of endogenous cholesteryl [^{14}C]oleate were measured. In this case, equation (19) can be integrated analytically and the solution is

$$t = - \left(Q_e - Q_e^0 + b_2 \ell n \frac{Q_e - Q_{eo}}{Q_e^0 - Q_{eo}} \right) / a_2 \qquad (27)$$

where Q_e^0 is the cellular content of cholesteryl ester at t=0. Let

$$x = t \; / \; \ell n \frac{Q_e - Q_{eo}}{Q_e^0 - Q_{eo}}$$

$$y = (Q_e - Q_e^0) \; / \; \ell n \frac{Q_e - Q_{eo}}{Q_e^0 - Q_{eo}}$$

then

$$y = - a_2 x - b_2 \qquad (28)$$

The experimental data in Table 1 of Daniels et al. (1981) gives Q_{eo}= 1 μg cholesterol/mg cell protein. Using the method of least squares and the experimental data in Fig.9A of Goldstein et al. (1975), a_2 and b_2 were obtained,

a_2 = 13.4 μg cholesterol/mg cell protein/day

b_2 = 1.57 μg cholesterol/mg cell protein

where the cellular content of cholesteryl [^{14}C]oleate was converted to cellular content of total cholesteryl esters by dividing the experimental data by 0.35, which is similar to that in solving for a_1 and b_1. The results of curve fitting equation (27), using the above

values for a_2 and b_2 and the experimental data in Fig.9A of Goldstein et al. (1975) for nonlysosomal hydrolysis of endogenous cholesteryl ester are compared in Fig.5.

2.3.5 Cholesterol synthesis

Equation (20) can be rewritten as

$$\ell n(R_s - K_3Rb_s) = -a_sL_e + \ell n(K_3R) \qquad (29)$$

where K_3Rb_s is the minimum rate of synthesis, and is equal to R_s at large L_e (>50 μg/ml). A least square curve fit of the experimental data in Fig.4 of Brown and Goldstein (1979) provides the following values for the constants a_s,b_s and K_3 in equation (29).

a_s = 0.155 ml/μg LDL protein

b_s = 0.039

$K_3 = 1.13\times10^{-3}$ μg cholesterol/ng LDL protein/day

In the cholesterol synthesis experiments (Brown and Goldstein, 1979), only the rate of incorporation of [^{14}C]acetate into [^{14}C]cholesterol was measured. Since the synthesis of 1 mole cholesterol requires 15 moles of acetate (Stryer, 1988), this factor has been considered in determining the values for a_s, b_s and K_3 above. The results of curve fitting are shown in Fig.6.

2.3.6 Efflux

The constant K_4 in equation (21) can be determined from the experimental data in Table 1 of Daniels et al. (1981). These data are for cells which have been incubated in the LPDS for 2 days and thus have attained steady state; i.e. $\frac{dC}{dt} = 0$ and $\frac{dQ_e}{dt} = 0$. For the case L_e = 0, the cholesterol balance equation (22) reduces to

$$R_{s(max)} = K_4 C_0 \tag{30}$$

where $R_{s(max)}$ and C_0 are the maximum rate of cholesterol synthesis and the steady state concentration of free cholesterol at $L_e = 0$, respectively. Therefore, equations (20), (30) and the experimental data in Table 1 of Daniels et al. (1981) give

$$K_4 = 6.52 \times 10^{-3} \text{ day}^{-1}$$

2.4 Discussion

The primary purpose of this model is to predict the regulatory ability of cells to adapt to a changing environment of extracellular LDL on a time scale of typically half a day or longer. The results of this theoretical model will now be compared with several experiments involving different aspects of the overall cellular LDL metabolism. These comparisons test the validity of the model since all the constants in the model have now been determined.

2.4.1 Regulation of LDL receptor

When we determined the constant K in (9), the experimental results for the down-regulation of the LDL receptor in Fig.2a of Goldstein and Brown (1977) were used. These results provided the experimental data used in curve fitting the data for $L_e = 10$ μg protein/ml in Fig.3. We shall now try to predict additional results for the down-regulation of LDL receptors shown in Fig.2b of Goldstein and Brown (1977) and for the up-regulation of LDL receptors due to the incubation of the cells in LPDS shown in Fig.8 of Brown and Goldstein (1975).

Fig.2b of Goldstein and Brown (1977) also shows results for the time-dependent down-regulation of receptor number when $L_e = 50$ μg

protein/ml. In this experiment R_0 is prescribed and we assume $\dot{R}_0 = 0$, since the cells have been incubated in LPDS for 3 days before the experiments were started. The comparison of the theoretical predictions and the experimental data for the decrease receptor binding is shown by the second curve in Fig.3, labeled by $L_e = 50$ μg protein/ml. The theoretical predictions are obtained by solving equation (9) to obtain R and converting R to the amount of binding using equation (11).

Representative initial conditions for the up-regulation of the LDL receptor can be obtained from Fig.8 of Brown and Goldstein (1975). In this case $\dot{R}_0$ is approximated by numerically differentiating the experimental data at $t = 0$ and $t = 4$ hours. Solving the same equations as for the down-regulation of LDL receptor, i.e. (9) and (11), one obtains the results shown in Fig.7. In this figure three points require further discussion. First, the amount of LDL bound to its receptor was initially determined by measuring the amount of heparin-releasable LDL bound to the cells (Goldstein et al., 1976a). The data obtained from Fig.8 in Brown and Goldstein (1975), however, represents the total amount of ^{125}I- bound to the cells. For the 2-hr binding experiment, this is about 6 times greater than the heparin-releasable radioactivity, which represents the amount of LDL bound to its receptors (Goldstein et al., 1976a). This correction has already been considered in predicting the results in Fig.7. Second, the theoretical results are inaccurate at the beginning of the experiment ($t<10$ hr). This is due to the neglect by the model of those processes which occur on a time scale of less than half a day. Finally, the difference between the theoretical and

experimental results at the steady state for curve 4 is attributable to the simplification of the model in assuming that the amount of mRNA only depends on the concentration of LDL in the medium, instead of the intracellular cholesterol level. In the case of curve 4, the cells were incubated in a medium containing 100 μg/ml LDL before the experiment, so that the initial cholesterol level in the cells was very high. Although the extracellular concentration of LDL was reduced to zero immediately by changing the medium, it could take a significant time to reduce the cellular content of cholesterol, to normal levels for this initial condition. We believe that the number of LDL receptors will eventually approach the same asymptote as the other curves, and thus be determined by the LDL concentration in the external medium.

2.4.2 Regulation of cellular content of sterol

Two other experimental results can be used to confirm the model. One is the change in the cellular content of cholesteryl ester with time at a given concentration of LDL in the medium (Goldstein and Brown, 1977); the second is the increase of the cellular content of the free cholesterol and the cholesteryl ester with the LDL concentration of the medium for cells which have been incubated for 24 hours in LPDS and then exposed to a new medium containing varying amounts of LDL (Brown et al., 1975).

For the first case, equation (19) was solved using a Runge-Kutta method, using the expressions (9) through (12) for R, B and R_H. The initial conditions for the two sets of experiments in Fig.2 of Goldstein and Brown (1977) are that $Q_e = Q_{eo}$ and $R_0 = 184$ ng/mg for $L_e = 10$ μg/ml; and $Q_e = Q_{eo}$ and $R_0 = 208$ ng/mg for $L_e = 50$ μg/ml,

respectively. In addition, we assumed that $\dot{R}_0 = 0$ for both sets of experiments, since the cells had been incubated in the LPDS for 3 days before the start of the experiment. The theoretical results (dashed lines) and the experimental data (symbols) in Goldstein and Brown (1977) are compared in Fig.8. The theoretical prediction for Q_e has the correct shape but falls far below the experimental data. The possible explanation for this large difference is described below.

If one integrates equation (12) for the rate of LDL degradation, from t=0 to t=1 day, using the value $K_2 = 0.2$ μg cholesterol/ng LDL protein/day and the amount of binding obtained from the experimental data in Fig.2 of Goldstein and Brown (1977), one finds that the total amount of lysosomal LDL degradation during the first day is 8.4 and 22.2 μg cholesterol/mg cell protein, for $L_e = 10$ and 50 μg LDL protein/ml, respectively. This is less than one half of the measured increase in cellular content of cholesteryl esters during the first 24 hours. Direct measurement of the total intracellular trichloroacetic acid-soluble content provides the similar results (Brown and Goldstein, 1976), for the cells incubated in growth medium containing the aforementioned concentrations of LDL for the same time period. There are two explanations to this apparent paradox, if we assume that the rate of LDL degradation is proportional to the amount of surface binding. The first possibility is that LDL receptor-mediated pathway may not be the only pathway which contributes to the storage of cholesteryl ester. However, the experimental results for receptor-negative FH homozygote fibroblasts (Brown and Goldstein, 1976) do not support this explanation. The second possibility is that the rate of LDL degradation depends on the confluency of the cell

monolayer. Experiments for endothelial cells (ECs) (Fielding et al., 1979) have shown that the rate of LDL degradation for quiescent confluent ECs is only 0.4 percent of that for sparse ECs which are dividing. The value of K_2 used in our previous calculations is based on the experiments of Brown and Goldstein (1976). In these experiments the cells have been incubated in growth medium containing 10 percent fetal calf serum (FCS) for 6 days, before they are transfered to the LPDS and studied. In this case, the fibroblast monolayer is almost confluent and nearly quiescent when the experiments started. However, the cells in the experiments of Goldstein and Brown (1977) were incubated in the medium containing 10 percent FCS for only one day, before transfered to the LPDS. Thus, the fibroblast monolayer in (Goldstein and Brown, 1977) would have to be far from confluent at the start of the experiment. In order to test this second explanation, we increased the value of K_2 and redid the calculations. Finally, we found that, when K_2= 0.8 μg cholesterol/ng LDL protein/day, the predicted results provided a much better fit of the experimental data as shown in Fig.8 (solid lines). Additional support for our second explanation is provided by the experiments of Daniels et al. (1981) and Rinninger and Pittman (1988). In these experiments the cells were incubated in the LDL-rich medium (L_e> 200 μg LDL protein/ml) and were nearly confluent, when the cellular content of cholesteryl esters was measured. The results in Daniels et al. (1981) and Rinninger and Pittman (1988) show that the cholesteryl ester content for these nearly confluent fibroblasts is approximately 20 μg cholesterol/mg cell protein. It is clear from these results that the value of K_2 is strongly dependent on the

degree of confluency of the monolayer. This effect needs to be studied further.

Dr. Ira Tabas (Columbia College of Physicians and Surgeons, New York) suggested a third possibility to explain the discrepancy between the model and the experimental data for the reesterification of the cellular free cholesterol as shown in Fig.8. He suggested that, for non-confluent cell monolayer, the number of LDL receptors on each cell membrane might be higher than that for confluent cell monolayer. This indicates that the cellular uptake of free cholesterol for non-confluent cell monolayer is higher than that for the confluent cell layer. In addition, the slope of the enzyme ACAT activation as the result of LDL-CE (cholesteryl ester) hydrolysis varies with time (i.e. becomes steeper when the amount of free cholesterol hydrolyzed from LDL is increased). Therefore, the rate of cholesterol reesterification in non-confluent cells is higher than that in confluent cells.

The second experimental test of the model is its ability to predict the cellular content of free cholesterol and cholesteryl ester, when the cells have been incubated for 24 hours in a medium containing varying concentrations of LDL, as shown in Fig.9. The theoretical predictions in Fig.9 were obtained by substituting equations (9) through (12), (20) and (21) into (19) and (22), and solving the latter two equations numerically using a Runge-Kutta method. These results are in reasonably close agreement with the experimental data in Fig.3 of Brown et al. (1975). The initial condition for R in Fig.9 was R_0= 200 ng LDL protein/mg cell protein obtained from Fig.1 of Goldstein and Brown (1974), since the cells in culture in both experiments were prepared by the same procedure. In

order to obtain the initial conditions for C and Q_e in Fig.9, we first calculated dC/dt and dQ_e/dt at the moment of measurement (t=24 hours), using equations (19) and (22) and the experimental data in Fig.3 of Brown et al. (1975) for $L_e = 0$. Since the initial conditions in Fig.3 of Brown et al. (1975) are the same for each LDL concentration, the initial conditions for C and Q_e can be obtained by extropolating C and Q_e to t=0, using the calculated values for dC/dt and dQ_e/dt. The results in Fig.9 directly reflect the changes in the sterol content of the cells in their attempt to adapt to the change of the LDL concentration in the external medium.

There are two limiting cases for the balance of cellular cholesterol content at steady state conditions, (i) $L_e = 0$ and (ii) $L_e > 50$ μg protein/ml. In (i), the rate of receptor-mediated LDL hydrolysis is zero and thus the endogenous synthesis of free cholesterol must just balance the efflux of cholesterol through the cell membrane; In (ii), the number of LDL receptors and the amount of LDL bound to its receptors have both reached saturation values. From equations (10) through (12) and (20), R_s/R_H must in this case equal $K_3 b_s$, which is of the order of 10^{-4} and much smaller than R_x/R_H. Therefore, the rate of LDL hydrolysis and the rate of efflux of cholesterol must just equal one another. For intermediate LDL concentrations in the external medium, the rate of LDL hydrolysis, the endogenous synthesis of free cholesterol and the efflux of cholesterol must balance one another for steady state intracellular equilibrium. In all these predictions we assume that the free

cholesterol from both the cytoplasmic and membrane associated pools enters into the intracellular regulation and thus the results are independent of new membrane synthesis.

2.4.3 Hydrolysis of LDL at steady state

An important application of the model is its ability to predict the rate of hydrolysis of LDL in SMCs and fibroblasts in the quasisteady state as shown in Fig.10. These curves are obtained from equations (10) through (12), and show how the receptor-mediated degradation of LDL changes when the extracellular LDL concentration is slowly increased over a period that is longer than the time needed for the regulation of LDL receptor number, due to diet or other factors. When the extracellular LDL concentration is increased, the rate of LDL degradation by SMCs is increased, but finally becomes saturated. For fibroblasts, however, the increase in extracellular concentration of LDL leads to an increase in the lysosomal degradation of LDL only for very low LDL concentrations in the medium; if the extracellular LDL concentration increases further and exceeds 3 μg/ml, the model predicts that a decrease in the lysosomal degradation of LDL will occur. However, this predicted positive-negative response of fibroblasts to the altering LDL environment is based on the assumption that the synthesis of LDL receptors is controlled by the extracellular concentration of LDL instead of the intracellular level of free cholesterol. In view of limitation, the weak minimum in the curve of fibroblasts at L_e= 14 μg LDL protein/ml will require experimental conformation. Further verification of this characteristic feature of fibroblasts needs to be done in the future studies. In addition, the model predicts that the rate of LDL degradation of fibroblasts is about one order of magnitude greater

than that of SMCs when $L_e < 2$ μg protein/ml, whereas the degradation rates for these cell types. are almost the same if $L_e > 10$ μg protein/ml. The predictions in Fig.10 are important in developing a mathematical model to study the accumulation and degradation of LDL in the arterial wall, which is one of the primary features of atherogenesis.

One of the paradoxes in the study of lipid accumulation and degradation in the intima of the rabbit aorta is described below. The experiments summarized in Steinberg (1983) have shown that approximately 40 percent of the total LDL degradation products in normal rabbit aorta at steady state in vivo were contained in the intima. This thin layer comprises only a small fraction (<5 percent) of the total arterial tissue space. In addition, the amount of LDL degradation per milligram of cell protein in the intima is about 50 times the specific activity of the rest of the aorta (Steinberg, 1983). However, it is well known that there are few SMCs in the normal intima of the rabbit aorta. Furthermore, the rate of LDL degradation by confluent bovine ECs is only 2 percent of that by confluent bovine SMCs (Fielding et al., 1979). Therefore, if the rates of LDL degradation for the same kind of cells in different animal species are roughly comparable, one is hard pressed to explain the high specific activity for LDL degradation in the normal rabbit intima. However, we can make some rough estimations for the distribution of LDL degradation using the results in Fig.10.

The experimental results of Fielding et al. (1979) were for cells in culture, whose lipid environment differs significantly from that in the artery wall. The luminal side of the ECs in the artery wall are exposed to the plasma, in which the average extracellular

concentration of LDL in rabbits was 182 μg cholesterol/ml (Schwenke and Carew, 1988). This value is much higher than the LDL concentration in the cell culture medium. Thus, the LDL degradation by ECs is saturated, and its rate is about 2 percent of the maximum rate of LDL degradation by SMCs (Fielding et al., 1979) using the data for bovine ECs. In contrast, the LDL concentration in the media of artery wall is very low; its average value in normal rabbit is only 0.4 percent of that in the plasma (Schwenke and Carew, 1988). Hence, the rate of LDL degradation by SMCs obtained from Fig.10 is less than 10 percent of the cell culture experiments (Fielding et al., 1979), where the extracellular LDL concentration is 20 μg LDL protein/ml. Based on the above estimations, the rate of LDL degradation by ECs in the artery wall is approximately 20 percent of that by SMCs. Therefore, this prediction still cannot explain the above paradox (Steinberg, 1983), where the rate of LDL degradation by ECs is 50 times that of SMCs and other factors which may affect the LDL concentration and degradation in artery wall must be considered. One possibility is the binding of LDL molecules to the extracellular tissue matrix. This binding will both increase the LDL concentration in the subendothelial space and decrease the degradation of LDL by SMCs, because the matrix bound LDL molecules can not reach the membrane receptors on the SMCs. The quantitative analysis of these competing mechanisms is currently being analyzed in a separate study in which the present model for LDL degradation is being combined with a model for arterial macromolecular transport proposed in Chapter 4 of this thesis and matrix binding.

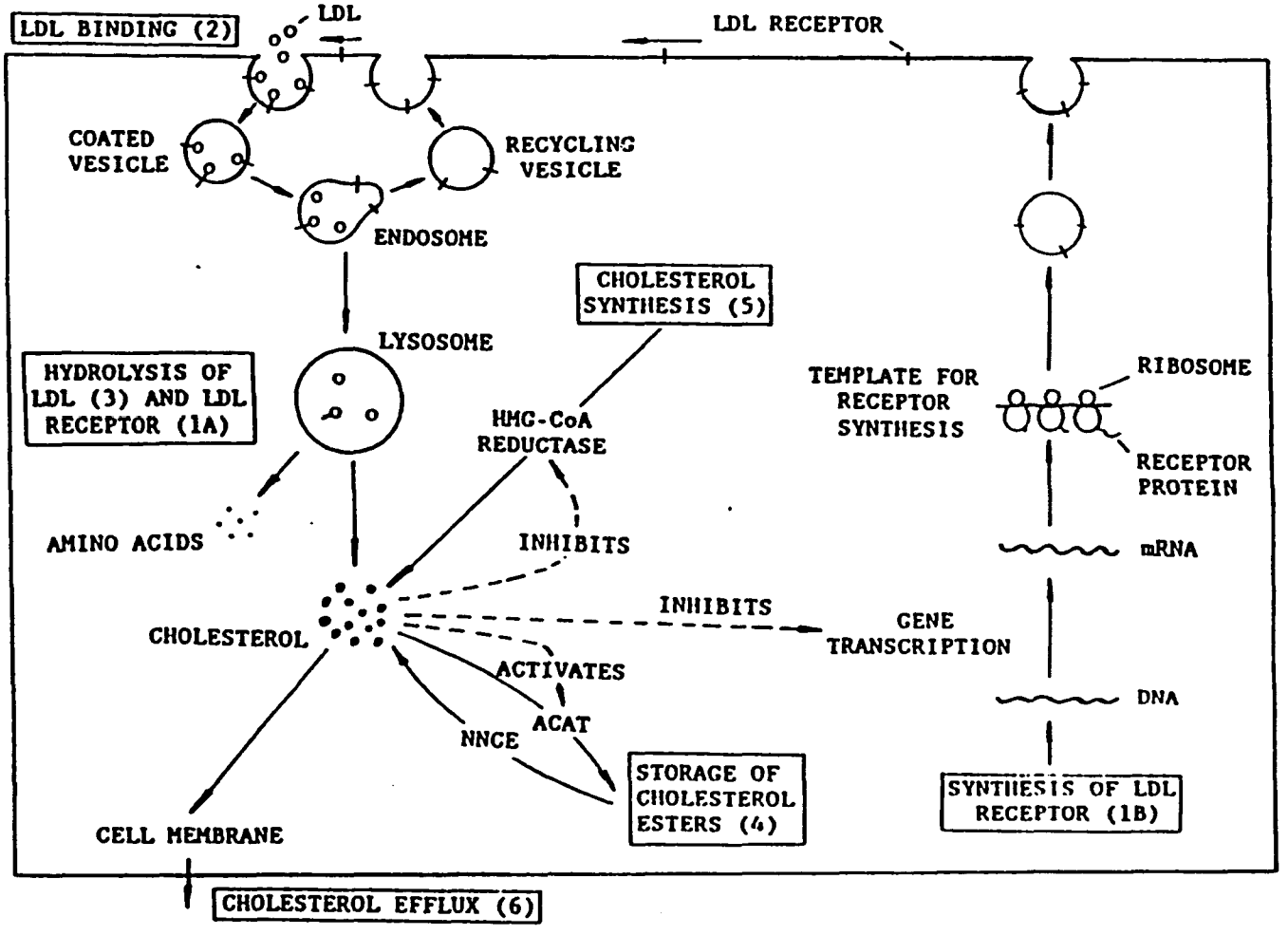
LDL BINDING (2)
LDL
LDL RECEPTOR
COATED VESICLE
RECYCLING VESICLE
ENDOSOME
CHOLESTEROL SYNTHESIS (5)
LYSOSOME
HYDROLYSIS OF LDL (3) AND LDL RECEPTOR (1A)
TEMPLATE FOR RECEPTOR SYNTHESIS
RIBOSOME
RECEPTOR PROTEIN
HMG-CoA REDUCTASE
AMINO ACIDS
INHIBITS
mRNA
INHIBITS
CHOLESTEROL
GENE TRANSCRIPTION
ACTIVATES
ACAT
DNA
NNCE
STORAGE OF CHOLESTEROL ESTERS (4)
SYNTHESIS OF LDL RECEPTOR (1B)
CELL MEMBRANE
CHOLESTEROL EFFLUX (6)

Figure 1

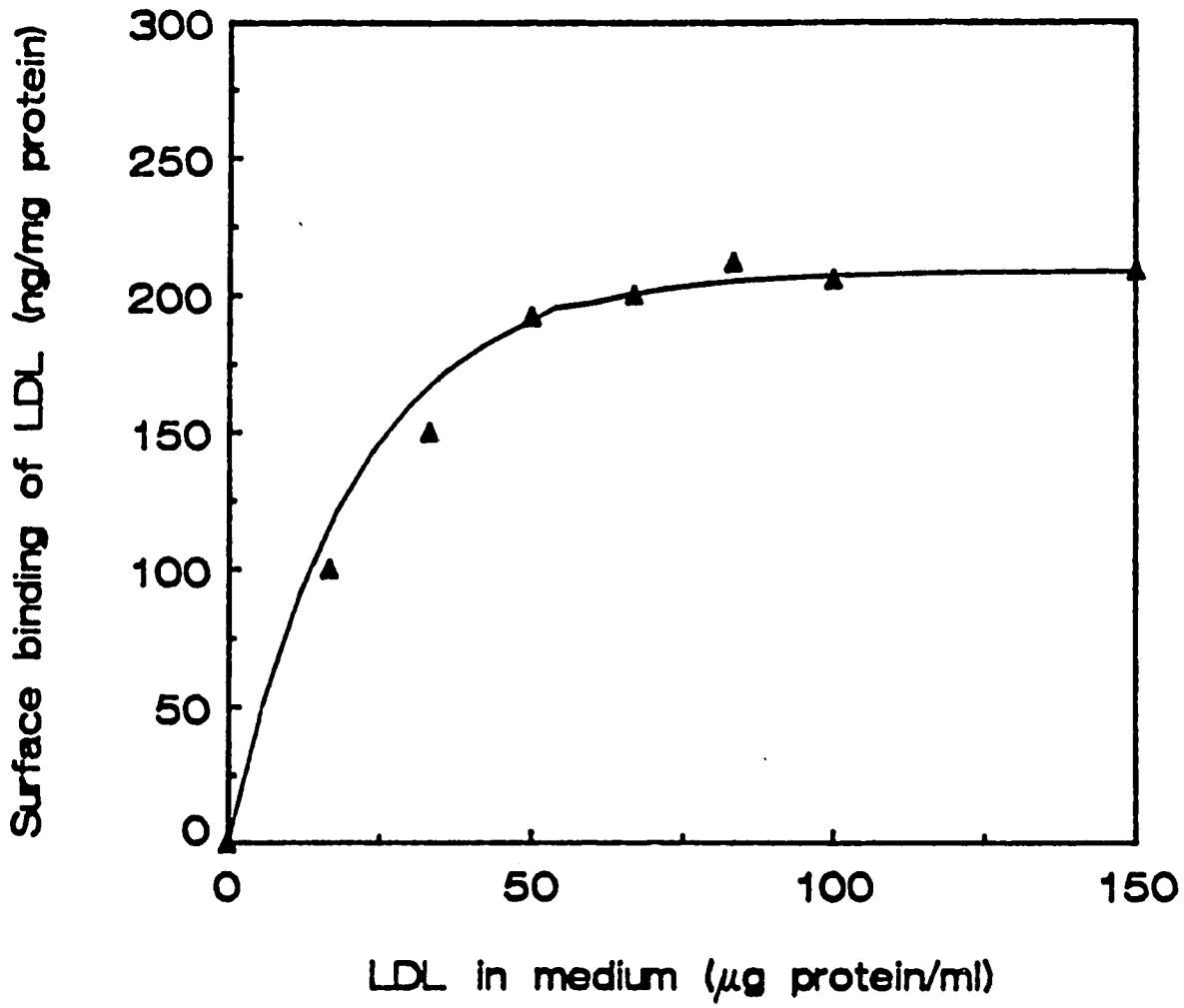
Surface binding of LDL (ng/mg protein)
300
250
200
150
100
50
0
0
50
100
150
LDL in medium (μg protein/ml)

Figure 2

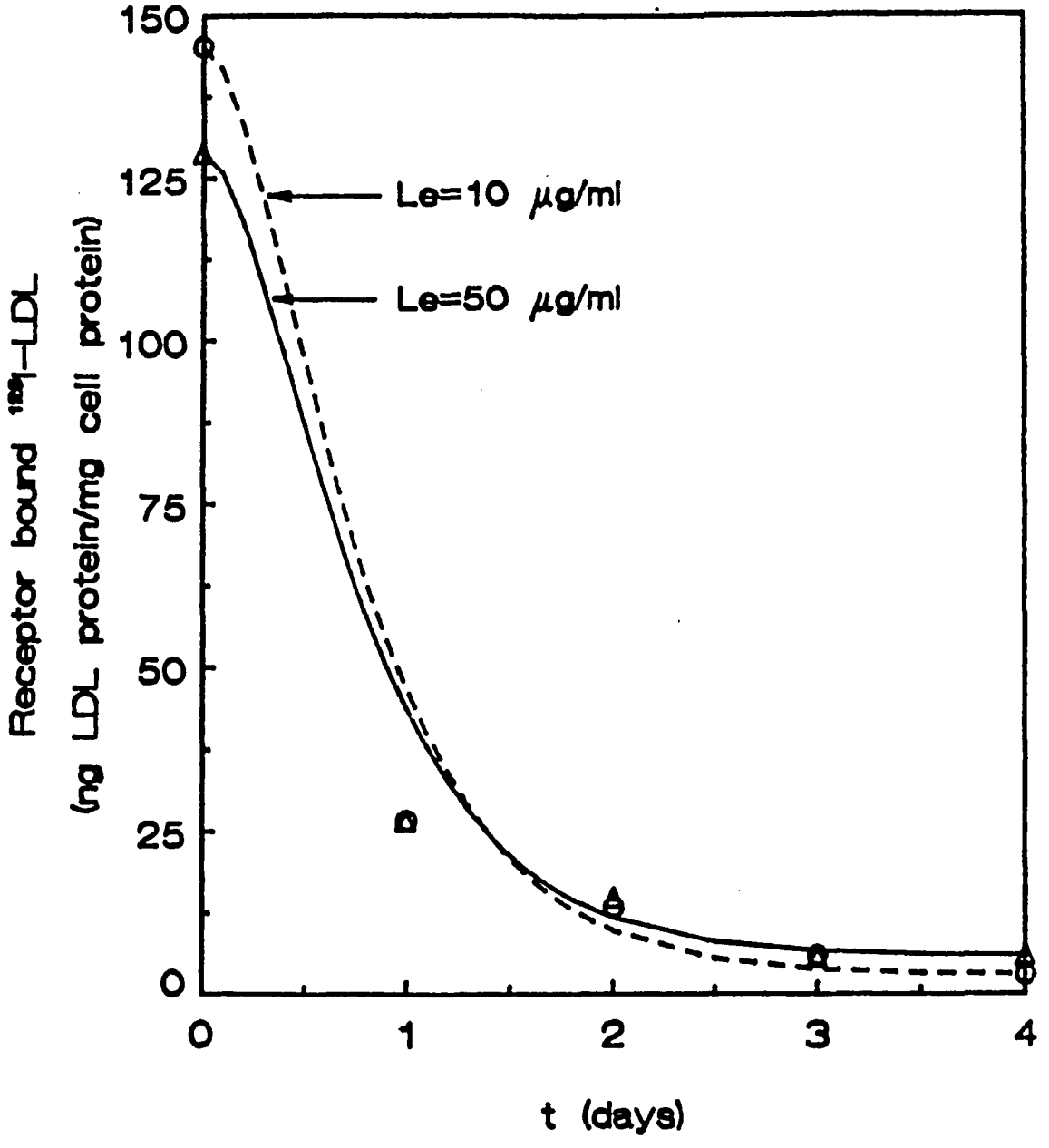
150
125
100
75
50
25
0
0
1
2
3
4
Le=10 μg/ml
Le=50 μg/ml
Receptor bound ¹²⁵I-LDL
(ng LDL protein/mg cell protein)
t (days)

Figure 3

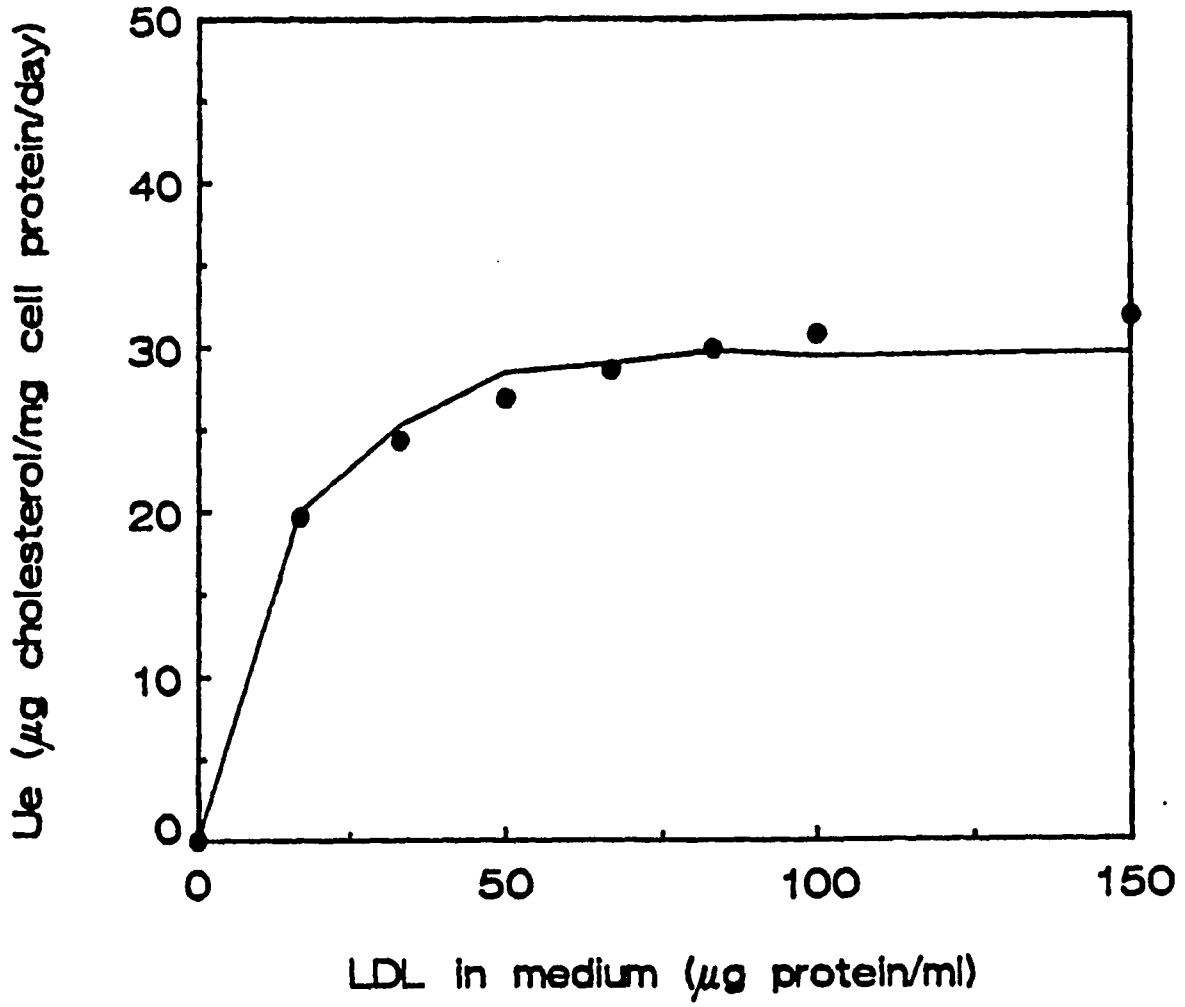
50
40
30
20
10
0
Ue (µg cholesterol/mg cell protein/day)
0
50
100
150
LDL in medium (µg protein/ml)

Figure 4

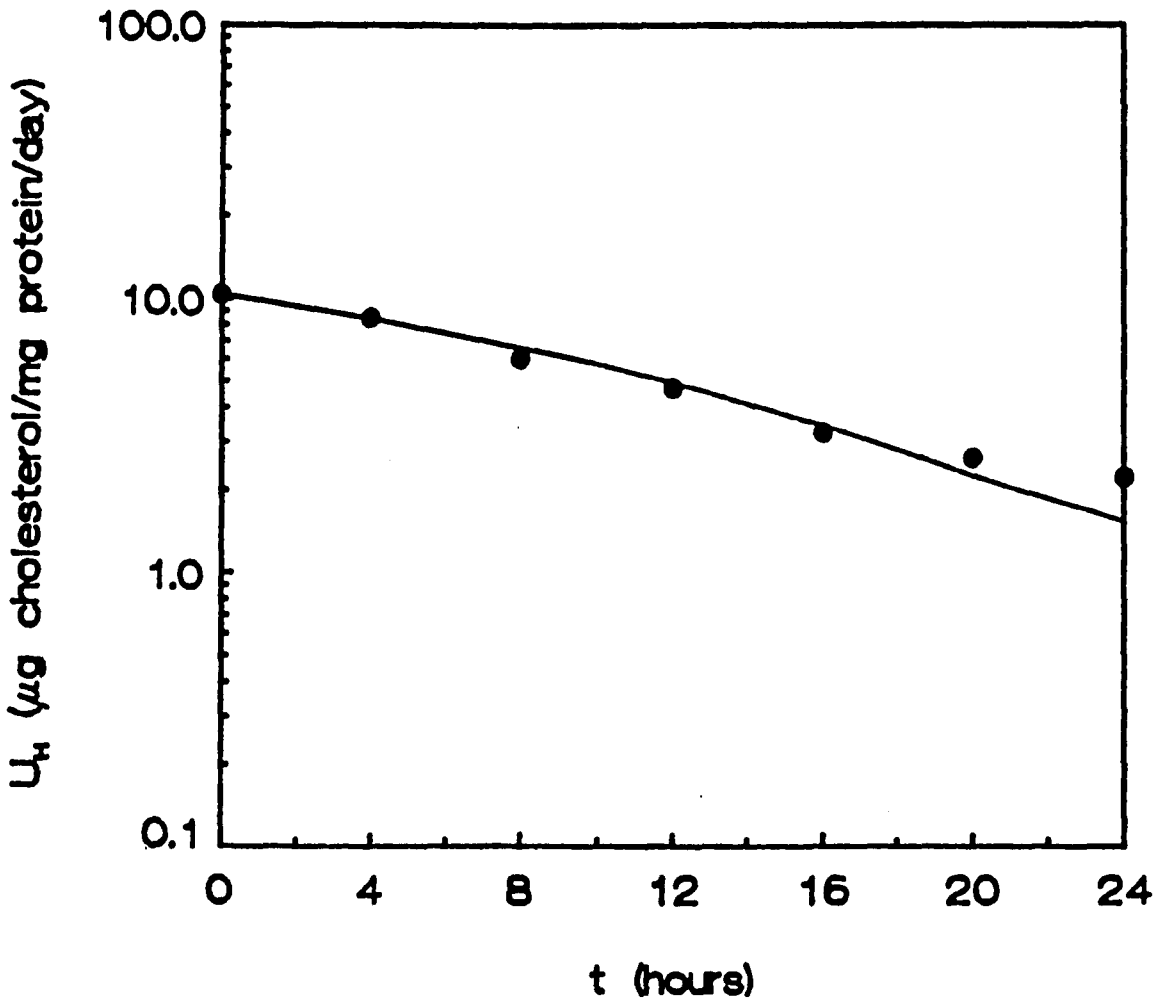
100.0
10.0
1.0
0.1
U_4 (μg cholesterol/mg protein/day)
0
4
8
12
16
20
24
t (hours)

Figure 5

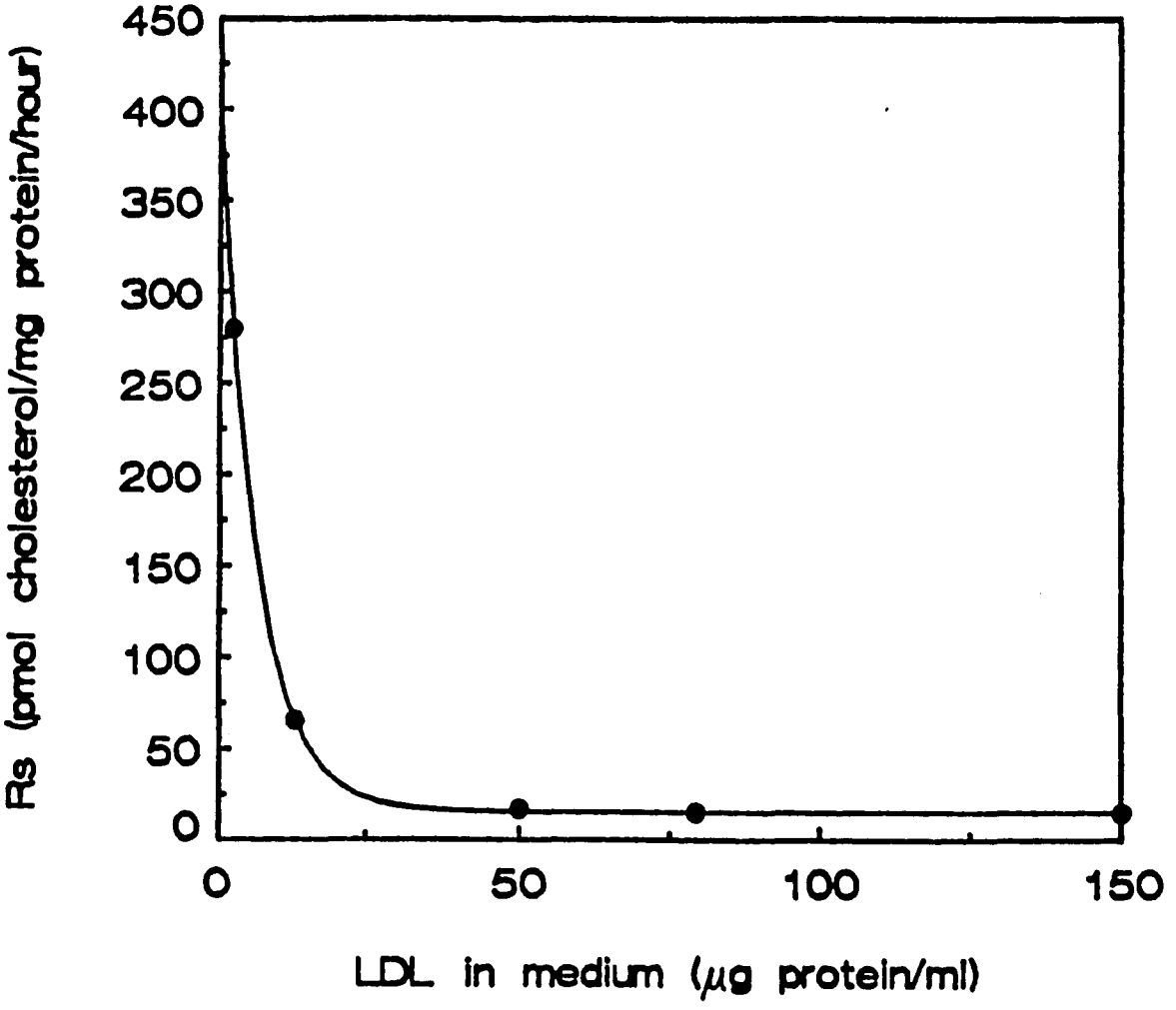
Rs (pmol cholesterol/mg protein/hour)
450
400
350
300
250
200
150
100
50
0
0
50
100
150
LDL in medium (μg protein/ml)

Figure 6

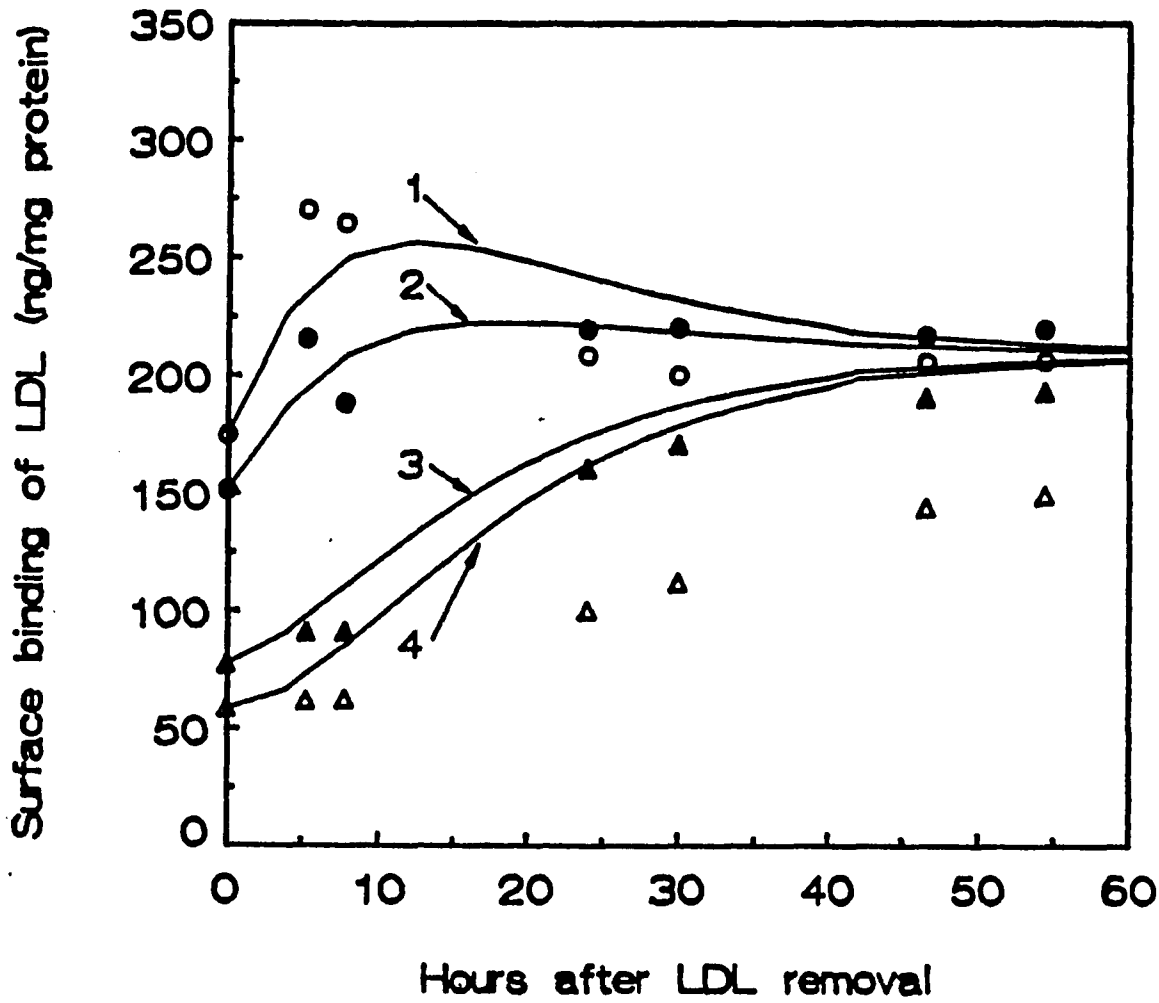
Surface binding of LDL (ng/mg protein)
350
300
250
200
150
100
50
0
0
10
20
30
40
50
60
Hours after LDL removal
1
2
3
4

Figure 7

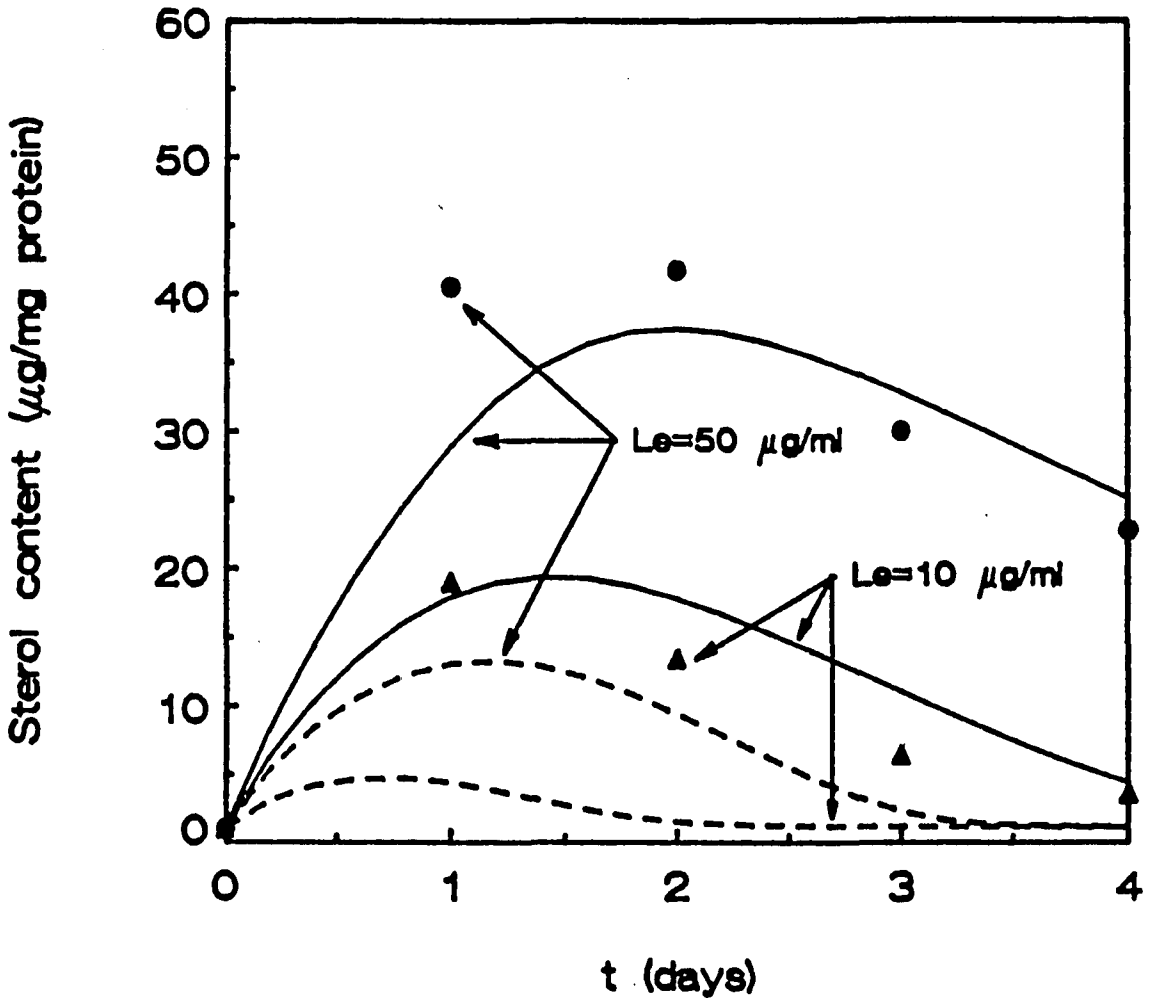
Sterol content (µg/mg protein)
60
50
40
30
20
10
0
0
1
2
3
4
t (days)
Le=50 µg/ml
Le=10 µg/ml

Figure 8

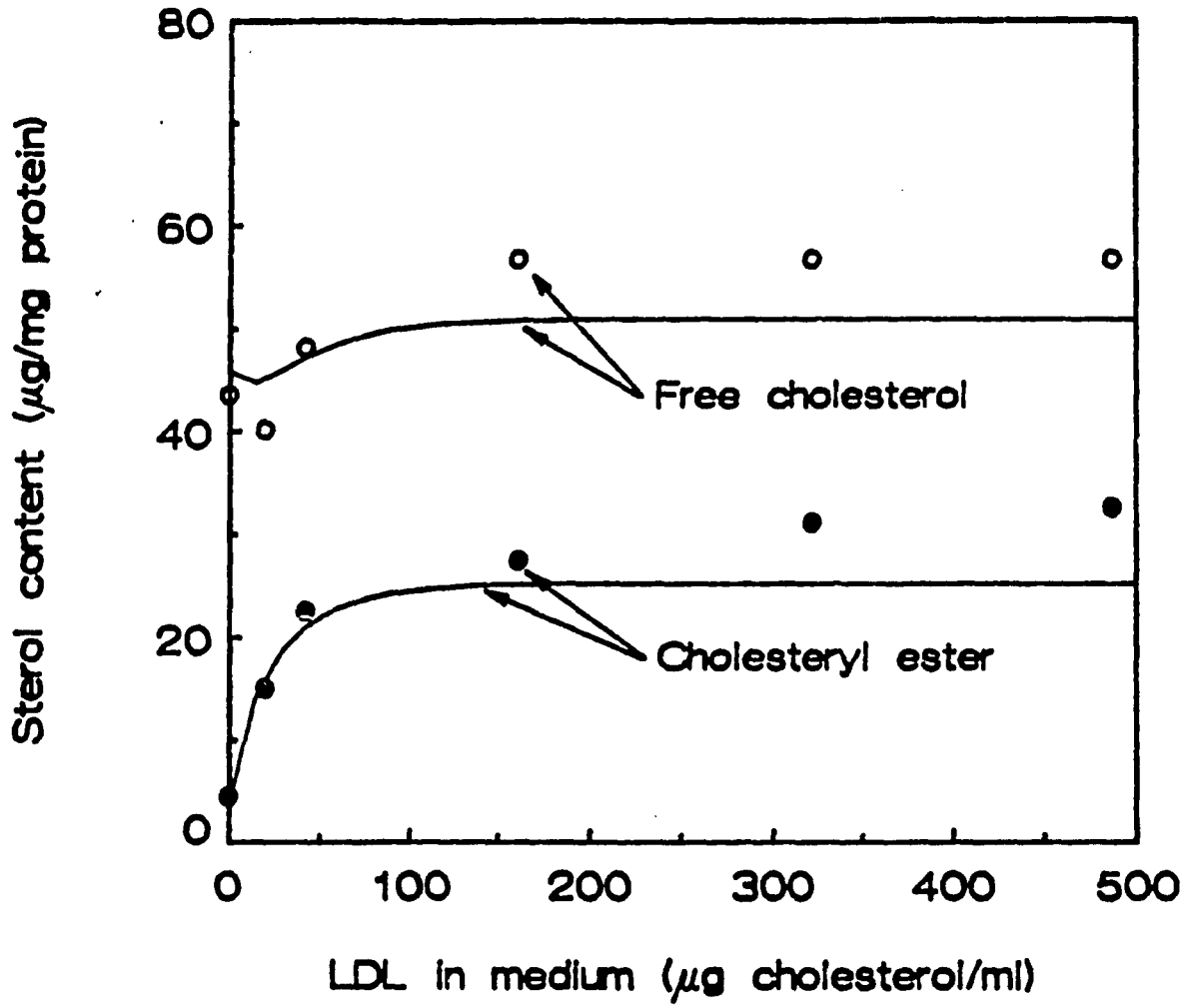
80
60
40
20
0
Sterol content (μg/mg protein)
Free cholesterol
Cholesteryl ester
0
100
200
300
400
500
LDL in medium (μg cholesterol/ml)

Figure 9

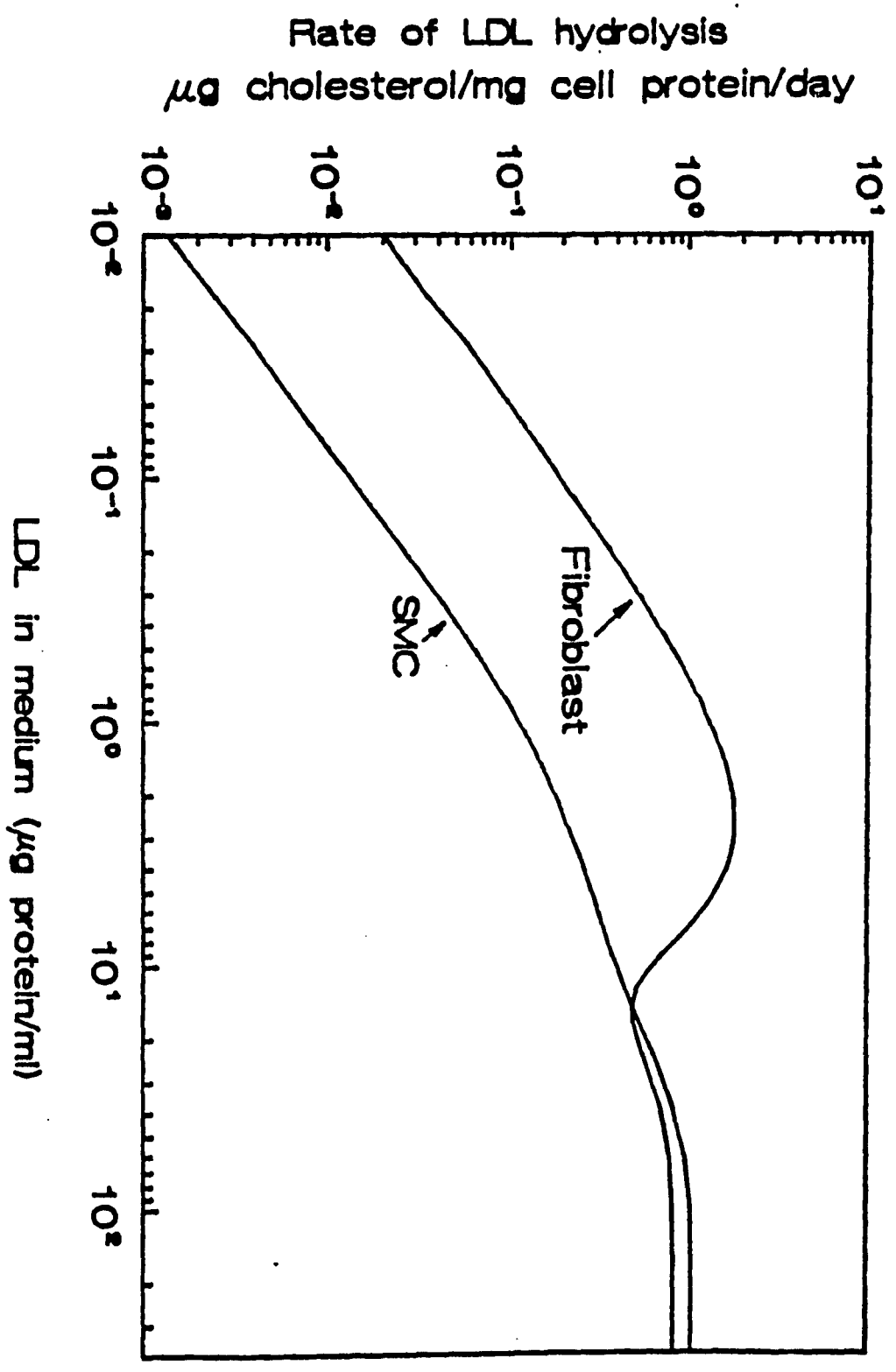
Rate of LDL hydrolysis
μg cholesterol/mg cell protein/day
10⁻⁹
10⁻⁶
10⁻³
10⁰
10³
10⁻⁴
10⁻¹
10²
LDL in medium (μg protein/ml)
Fibroblast
SMC

Figure 10

CHAPTER 3

Effects of Endothelial Filtration, Mitotic Cells and Internal Elastic Lamina on Macromolecular Transport across Artery Wall

3.1 Introduction

Macromolecular transport across the arterial wall is closely linked to a variety of processes in the intima that are believed to play an important role in the subendothelial accumulation of lipid and the formation of the early foam cell lesion (Ross,1986; Weinbaum et al.,1988a). The possible relationship between lipid transport and atherogenesis has been the subject of numerous experimental and theoretical investigations (Bratzler et al., 1977; Fry, 1983, 1985 and 1987; Smith and Staples, 1982; Tzeghai, et al. 1986; Weinbaum et al., 1985 and 1988b; Wen et al., 1988). In this chapter we shall present a two-dimensional, time-dependent model for this transport in which special emphasis will be placed on the coupling between convective-diffusive processes in the interendothelial clefts, the subendothelial intima (SI), i.e. the intimal layer between the endothelium and the internal elastic lamina (IEL), the IEL and the media. Unfortunately, this convective-diffusive model is incorrect, because of the assumption of 1-D convective velocity in the normal direction in the artery wall. We shall show in the next chapter that the major convective transport processes occur parallel rather than normal to the endothelial surface in the vicinity of the leaky cleft exit due to the unique ultrastruture of the intima. The major incorrect results from this model are: (1) the subendothelial concentrations are higher than that in the lumen; and (2) the solute and water fluxes in this model are overestimated by at least one

order of magnitude. However, the results of this model for the pure diffusive transport are still valid. The purpose of including this incorrect model here is to show how the 1-D transport assumption in the artery wall could lead to the physically spurious results.

The leaky junction-cell turnover hypothesis was first proposed by Weinbaum et al.(1985) on the basis of a 2-D purely diffusive model. The theory led to the prediction that the measured local increases (typically 50 to 100 percent) in macromolecular transport in regions with focal intimal staining of Evans blue dye could be quantitatively accounted for by an increase in permeability through leaky junctions involving only a few cells per thousand. It was suggested that, except for a minor contribution due to vesicle transcytosis, the primary transendothelial pathway for molecules the size of albumin or larger would be leaky junctions associated with cells which were either in the mitotic (M) phase or in the process of sloughing due to cell death. The enface area of the leaky junctions surrounding these cells in turnover could be as little as 10^{-6} of the total endothelial surface area. The basic steady state model of Weinbaum et al. (1985) was first extended to include convection by Tzeghai et al. (1986) and time-dependent diffusion and the non-isotropy of the underlying elastic layers by Weinbaum et al. (1988b) and Wen et al. (1988) . These models showed that there were steep lateral concentration gradients in the subendothelial concentration profiles at the leaky cleft exit. These gradients could produce a large local flux in the arterial wall and thus provide a basic mechanism wherein a very small fraction of leaky junctions could account for a significant increase in the average concentration throughout the subendothelial space. The theoretical results in

Weinbaum et al. (1988b) and Wen et al. (1988) also predicted that if the entire cell were removed, the leakage area would increase by $O(10^3)$, but the flux would incre only a factor of roughly two.

The models of Weinbaum et al. (1988b) and Wen et al. (1988) have been used to predict the time window and probe molecule size for which the endothelial leakage sites could be observed in the experiments (Lin et al., 1988 and 1989). Lin et al. (1988) first reported that when the entire aorta of a rat was scanned nearly 99 percent of all cells in M phase had junctions which were leaky to Evans blue-albumin conjugate (EBA). In addition, Lin et al. (1989) observed that 80 percent of all cells in M phase had junctions which were leaky to the much larger molecule Lucifer yellow-low density lipoprotein (LY-LDL). This suggested that the junctions in M phase opened and closed gradually (Chien et al., 1988). While the vast majority of cells in M phase leaked, these cells accounted for roughly 30 percent of the total leakage sites for EBA and 45 percent of the total leakage sites for LY-LDL. Studies just completed using IgG as marker for cell death (Lin, 1989) show that a large fraction of the unidentified leakage sites can be accounted for by cells in the process of dying and/or sloughing. The combined frequency of leakage sites was approximately 5 cells in 10^4. The cell turnover as indicated by ^{3}H-thymidine was roughly twice the background normal level in the regions surrounding branch orifices. These regions have been shown in other animal species to exhibit a typically twofold increase in macromolecular permeability (Bell et al., 1974a & 1974b; Packham et al., 1967; Schwartz et al., 1983). One of the puzzling features of these new results (Chien et al., 1988; Lin, 1989; Lin et al., 1988 and 1989) is that the frequency of the observed leakage

sites (a few cells per ten thousand) is roughly one order of magnitude lower than the predicted frequency of leakage sites using our earlier purely diffusive models (Weinbaum et al., 1985 and 1988b; Wen, 1988) . The new convective-diffusion model developed herein provides a rational explanation for this behavior.

It is well recognized that convective transport of macromolecules is at least as important as diffusive transport in the artery wall in vivo. Significant differences in media concentration profiles due to transmural pressure have been measured by Fry (1983) and Fry et al. (1986) and experimental measurements of transmural albumin transport within the media of rabbit thoracic aorta (Tedgui and Lever, 1985) have shown that the Peclet number in the normal direction in this vessel is between 4 and 5 for an intact endothelium and increases to 6-11 when the endothelium is denuded. In Tzeghai et al. (1986), an initial attempt was made to include convection in the 2-D diffusion models. It is now recognized that this initial 2-D convective-diffusive model did not properly describe the distribution of water fluxes through cleft of the mitotic cell and the clefts of surrounding normal cells which contain junctional discontinuities. In normal junctions, the protein strand arrays are an effective seal for the passage of water and small solutes except for small tortuous discontinuities (Wissig, 1979), which have been shown to occupy less than five percent of the endothelial cell perimeter in mammalian muscle capillary endothelium (Curry, 1986). Freeze cleavage studies of junctions in arterial endothelium suggest a similar result in large vessels (Jan, 1984). As will be shown in the present model, the partitioning of water fluxes through the two parallel pathways (normal junction discontinuities vs leaky junctions) can affect the

subendothelial macromolecular concentration. When there is a large convective flux through the leaky junction, a steep standing gradient can be established within the cleft with the result that macromolecular concentrations at the cleft exit can become significantly greater than that in the lumen. The fractional length ℓ_r of such junction discontinuities (normalized to total cell perimeter) thus plays a critical role in intimal macromolecular transport which will be examined herein for the first time.

A principal motivation for the present study and the formulation of the present model with its four layers (endothelium, SI, IEL and media) with a discrete convective-diffusive barrier at the IEL is the very interesting 1-D model proposed by Fry (1985 and 1987) and its provocative results. Using baseline parameter values given in Table 1 of Fry (1987), this model predicted that the IEL in muscular arteries can act as a molecular sieve and produce a large concentration drop between the SI and media interfaces of the IEL. The results of the model were then used to explain the findings of Smith and Staples (1982) which indicated that the subendothelial LDL concentration in post-mortem human arteries exceeded that in the lumen and the measurements by Fry et al.(1986) on pressurized, deendothelialized minipig aorta which suggested macromolecular sieving in the superficial regions of the intima. The present study was designed to analyze this problem in greater detail with a new 2-D model with the following features. First, the present model takes into account the interactions of fluxes through small pores in an otherwise impermeable diffusion barrier; this includes the fenestrae of the IEL as well as the leaky junctions of the endothelium. Second, the present model deals with the interface matching conditions between

layers, when there is an abrupt change in the area available for diffusion as occurs at the endothelial and IEL interfaces. At these interfaces the concentrations are continuous only at the pore exit, but large discontinuities in the average concentration can exist in the plane of the exit in contrast to the 1-D models when the average concentration is assumed to be continuous. Third, the distinction is made for the water fluxes between normal and leaky junction pathways. Fourth, a separate formula is developed in the present model to describe the resistance of the IEL as a function of the number density and size of the fenestra on the IEL surface, and this resistance is evaluated by using the experimental data of Roach and coworkers (Campbell and Roach, 1981; Song and Roach, 1983) for the IEL structure.

For simplicity, the binding and the degradation of macromolecules in the arterial wall are neglected in the present model. This is a reasonable approximation for albumin transport; however, for LDL a more complicated model which considers binding and degradation is needed, though the qualitative predictions should be similar.

3.2 Mathematical models

3.2.1 Model description:

The arterial wall consists of three layers: the intima, the media and the adventitia (Ferrans, 1980) . The intima is composed of the lining layer of endothelial cells, a thin layer of subendothelial intima (SI), and the IEL. The media is composed of alternating layers of smooth muscle cells (SMCs) and elastic tissue, and is separated from the adventitia by the external elastic lamina. The adventitia

will not be considered in the present model, since it is not considered to be a significant transport barrier.

The macromolecular transport in the arterial wall is non-isotropic, mainly due to the elastic layers in the wall. The transport resistance in the lateral direction is much smaller than that in the normal direction (Weinbaum et al., 1988b), i.e. the diffusion coefficient in the lateral direction (D_r) is much larger than that in the normal direction (D_z). In addition, the ratio D_r/D_z varies significantly across the intima, making it difficult to choose a single appropriate value without treating the IEL as a separate barrier. In this chapter, we shall adopt the four layer structure proposed by Fry (1987) in which separate models are developed for the endothelium, the SI, the IEL and the media. Each layer is described by different governing equations, boundary conditions and baseline parameters.

The diffusion of the macromolecules in the SI is assumed to be isotropic, i.e. D_r/D_z in the SI is equal to unity. Since the distribution of the elastic layers in the media beyond the IEL is quite regular and uniform (Ferrans, 1980) , D_r/D_z is assumed to be greater than unity but constant in this region.

A major difficulty in modeling the IEL is that the size and the distribution of the fenestra in the IEL are randomly related to the leakage sites in the endothelium, hence the exact treatment of the IEL structure is a 3-D convective-diffusion problem. This problem can be simplified, however, due to the similarity in dimensions of the inter-fenestral spacing in the IEL, roughly 10 μm (Song and Roach, 1983), and the effective diameter of an endothelial cell (Tzeghai et

al., 1986). Since the number of the cells with leaky junctions is typically one in a thousand cells or less (Lin et al., 1988), there are at least one thousand fenestrae associated with each mitotic cell. Therefore, in our new model the IEL is approximated by a continuous uniform porous layer across which the local flux is proportional to the local difference in concentration across the IEL.

The distribution of leakage sites in the endothelial layer is random. Based on the discussions in Weinbaum et al. (1988b) and Wen et al. (1988), we have made the same assumption that the cells with transiently leaky junctions can be arranged in a periodic surface array whose number density on a regional basis is the same as the average density in the random array. If the spacing between the cells with leaky junctions is 2ξ in this periodic array, then one can draw a circle of radius ξ centered on each leaky cell and define a periodic unit in the subendothelial space as shown in Fig.1, which is a cylinder enclosed by the circumference of this circle and whose height L_w is the summation of the thicknesses L_j of the endothelial layer, L_i of the SI, L_I of the IEL and L_m of the media. The transport of macromolecules in the SI and the media can thus be treated as an axisymmetric boundary value problem, if the IEL is replaced by an uniform porous layer as described above. The cellular turnover frequency ϕ is defined as R_1^2/ξ^2, where R_1 is the effective radius of the endothelial cell.

3.2.2 Mathematical Formulation:

The four layers of the arterial wall treated in this chapter are each denoted by a subscript. These subscripts are j for the leaky endothelial junctions, i for the SI, I for the IEL, and m for the

media; the subscripts ji and Im are used to denote the exits of the leaky junction into the SI and of the fenestra into the media.

The tilde on top of a parameter indicates that it is dimensional, and the tilde is removed when the parameter is non-dimensionalized. The concentration in a given region x is normalized by using the concentrations in the plasma ($\tilde{C}_p$) and the adventitia ($\tilde{C}_A$):

$$C_x = \frac{\tilde{C}_x - \tilde{C}_A}{\tilde{C}_p - \tilde{C}_A} \tag{1}$$

The dimensionless time is given as

$$t = \frac{D_{zm}\tilde{t}}{L_m^2} \tag{2}$$

where D_{zm} is the diffusion coefficient in the media in the normal direction.

The Peclet number (Pe_x) in any region x is given by

$$Pe_x = \frac{f_x U_x L_x}{\gamma_x D_{zx}} \tag{3}$$

where f_x, U_x, L_x, γ_x and D_{zx} are the solute retardation coefficient (ratio of solute to water velocities), the water velocity in the normal direction, the layer thickness, the tissue-plasma partition coefficient, and the diffusion coefficient in the normal direction, respectively, in region x. These general equations apply to each of the four layers and will not be repeated below.

(A) The transiently leaky junction

Our model for the leaky junction assumes one-dimensional quasi-steady convective-diffusion with a time-varying concentration $C_{ji}(t)$ at its exit into the SI. The quasi-steady behavior in the leaky junction on the much longer time scale for subendothelial spreading has been justified by Weinbaum et al. (1988b). Therefore, the boundary value problem for the concentration in the leaky junction is:

$$\frac{\partial^2 C_j}{\partial z_j^2} - Pe_j \frac{\partial C_j}{\partial z_j} = 0 \qquad (4)$$

$$C_j(0,t) = 1 \ , \quad C_j(1,t) = C_{ji}(t) \qquad (5a,b)$$

where z_j is the centerline coordinate in the leaky junction non-dimensionalized by the depth of the leaky junction L_j. The dimensionless concentration at the cleft exit $C_{ji}(t)$ is required to satisfy the initial condition

$$C_{ji}(0) = 0 \qquad (6)$$

and $C_{ji}(t)$ is to be determined for all times by matching the concentration and the flux at the cleft exit with the values of these unknown variables in the SI.

The dimensionless flux in the leaky junction is

$$q_j(z_j,t) = - \frac{\partial C_j}{\partial z_j} + Pe_j \left(C_j + \frac{\delta}{1 - \delta} \right) \qquad (7)$$

where $\delta = \tilde{C}_A/\tilde{C}_P$.

(B) The SI layer

The boundary value problem for the SI region is approximated by an axisymmetric convective-diffusion process as discussed before, so that the governing equation is

$$D_i^2 \left(\frac{\partial^2 C_i}{\partial r^2} + \frac{1}{r}\frac{\partial C_i}{\partial r} + \frac{\partial^2 C_i}{\partial z_i^2} + \frac{Pe_i}{\eta}\frac{\partial C_i}{\partial z_i} \right) = \frac{\partial C_i}{\partial t} \qquad (8)$$

where r and z_i are the coordinates in the lateral and normal directions, respectively. These coordinates are non-dimensionalized by the media thickness L_m. η is length ratio defined by $\eta = L_i/L_m$, and $D_i^2 = D_{ri}/D_{zm}$ is a dimensionless diffusion coefficient ratio in the SI. The dimensionless flux q_i in the normal direction in the SI is

$$q_i(r,z_i,t) = \frac{\partial C_i}{\partial z_i} + \frac{Pe_i}{\eta}\left(C_i + \frac{\delta}{1-\delta} \right) \qquad (9)$$

The boundary and matching conditions at the endothelial interface with the SI are

$$C_i(r,\eta,t) = C_{ji}(t) \qquad R_1 < r < R_2 \qquad (10)$$

$$q_i(r,\eta,t) = \frac{\gamma_j D_j^2 L_m}{\gamma_i D_i^2 L_j} q_j(1,t) \qquad R_1 < r < R_2 \qquad (11)$$

$$q_i(r,\eta,t) = \sigma[1 - C_i(r,\eta,t)] \qquad \begin{matrix} 0 < r < R_1 \\ R_2 < r < \xi \end{matrix} \qquad (12)$$

Whereas the symmetric condition at the center $r = 0$ and the periodic condition at the border $r = \xi$ are

$$\frac{\partial C_i}{\partial r}(0,z_i,t) = \frac{\partial C_i}{\partial r}(\xi,z_i,t) = 0 \qquad 0 < z_i < \eta \qquad (13a,b)$$

In (11) and (12) $R_2 = R_1 + \Delta R$, ΔR is the width of the leaky junction, $D_j^2 = D_{zj}/D_{zm}$ is the dimensionless diffusion coefficient ratio in the

leaky junction, and σ is the relative resistance of the artery wall without its endothelium with respect to that in the intact endothelium without leaky junctions (Weinbaum et al., 1976). Equation (12) with q_i given by (9) evaluated at z_i=η states that the net flux of molecules across the intact endothelium through tortuous pathways between the junctional strands of the normal interendothelial clefts and by vesicular transport should be balanced by the net flux of molecular diffusion and convection directly beneath the endothelium. The permeability in this region of the endothelium is due to the medium-sized pores discussed in Weinbaum et al. (1988a), so that σ will be equal to zero for macromolecules such as LDL. Equations (10) and (11) represent the continuity conditions on concentration and flux at the exit of the leaky junction.

The boundary condition at the IEL surface is obtained from the assumption that the IEL functions approximately as a uniform porous barrier with a flux that is proportional to the concentration difference across this barrier, i.e. the concentration in the SI layer just above $C_i(r,0,t)$ vs the concentration in the media just below $C_m(r,1,t)$.

$$q_i(r,0,t) = \frac{\sigma_I}{D_i^2\gamma_i}\,[C_i(r,0,t) - C_m(r,1,t)] \qquad 0 < r < \xi \qquad (14)$$

where σ_I is a dimensionless permeability coefficient which is related to the dimensional coefficient $\tilde{\sigma}_I$ for the IEL by $\tilde{\sigma}_I L_m/D_{zm}$. An approximate 2-D theory for estimating σ_I for a convective-diffusive barrier with small circular pores will be developed in the next section. The initial condition for the SI is

$$C_i(r,z_i,0) = 0 \qquad (15)$$

(C) Approximate model for the IEL

We shall assume that the convective-diffusive transport resistance of the IEL is an intrinsic property of this barrier that depends on its geometry and filtration flux and is thus independent of time and the concentration of macromolecules. σ_I can therefore be obtained from an equivalent steady state model which takes into account the interaction between fenestrae in the IEL and the underlying media. We shall also assume that the distribution of the fenestrae is periodic on the surface of the IEL such that their number density on a regional basis is the same as the measured average density in the random array. Based on these assumptions, we can define a periodic unit for the IEL as shown in Fig.2. This is a circular cylinder with a fenestra at the center of the top surface, whose height is L_I+L_m. The diameter of the cylinder is $2\xi_I$ which is equal to the average distance between the fenestrae. This distance is given by $2\epsilon/\sqrt{\phi_I}$, where ϵ and ϕ_I are the radius and the fractional area of the fenestra, respectively.

The separate steady state boundary value problem and its solution to determine σ_I are given in Appendix A. This solution leads to the following expression for σ_I by integrating (A.8) in the lateral direction over the local periodic unit and then substituting the resulting relation into (14).

$$\sigma_I = \frac{\gamma_I L_m D_I^2 \phi_I q_{Is}}{\gamma_m L_I (1-\bar{C}_{ms})} \qquad (16)$$

where $D_I^2=D_{zI}/D_{zm}$ is the dimensionless diffusion coefficient in the fenestra of the IEL, q_{Is} is the dimensionless macromolecular flux through the fenestra, and $\tilde{C}_{ms}$ is the average concentration in the media of the local periodic unit at the IEL-media interface. q_{Is} and $\tilde{C}_{ms}$ are given in Appendix A.

(D) The media

The governing equation for the media is similar to equation (8) for axisymmetric convective-diffusion in the SI except that $D_{rm}\neq D_{zm}$ due to the non-isotropy of the media elastic tissue.

$$D_m^2\left(\frac{\partial^2 C_m}{\partial r^2}+\frac{1}{r}\frac{\partial C_m}{\partial r}\right)+\frac{\partial^2 C_m}{\partial z_m^2}+Pe_m\frac{\partial C_m}{\partial z_m}=\frac{\partial C_m}{\partial t} \qquad (17)$$

where $D_m^2=D_{rm}/D_{zm}$ is a non-isotropic diffusion parameter, r and z_m are the coordinates in the lateral and normal directions, respectively. These coordinates are non-dimensionalized by the media thickness L_m.

The dimensionless flux q_m in the normal direction in the media is

$$q_m(r,z_m,t)=\frac{\partial C_m}{\partial z_m}+Pe_m\left(C_m+\frac{\delta}{1-\delta}\right) \qquad (18)$$

The continuity of flux across the IEL requires that

$$q_m(r,1,t)=\frac{D_i^2\gamma_i}{\gamma_m}q_i(r,0,t) \qquad 0<r<\xi \qquad (19)$$

The symmetry condition at the center $r=0$ and the periodicity condition at the border $r=\xi$ are

$$\frac{\partial C_m}{\partial r}(0,z_m,t)=\frac{\partial C_m}{\partial r}(\xi,z_m,t)=0 \qquad 0<z_m<1 \qquad (20a,b)$$

The boundary condition at the adventitia surface and the initial condition are,

$$C_m(r,0,t) = 0 \qquad 0 < r < \xi \qquad (21)$$

$$C_m(r,z_m,0) = 0 \qquad (22)$$

(E) The water flux relations

The relation between the Peclet numbers at the different layers can be estimated by the conservation of water flux across the arterial wall. This requires that for a steady state water flux

$$U_i A = U_m A = U_j A_j + U_{nj} A_{nj} \qquad (23a,b)$$

where A, A_j and A_{nj} are the cross-sectional areas of the periodic unit and the leaky and normal junctions, respectively; U_{nj} is the water velocity in the normal junctions.

There are two alternative ways to estimate the water velocity-pressure relations in intercellular junctions.

(i) Fiber matrix model

If the wide portion of intercellular junction is assumed to be filled with a glycocalyx of proteoglycans, as proposed in (Curry, 1986), then the velocity-pressure relation obeys Darcy's law and the velocity in both the normal and leaky junctions is proportional to the pressure gradient across the junctions. The theoretical analysis in Tzeghai et al. (1985) has shown that the pressure distributions in the lateral direction in the subendothelial space are almost uniform, if $L_w \geq 0.2$ mm, and the pressure drops across the normal cleft and the leaky cleft will therefore be nearly equal. Thus,

$$U_j = U_{nj} \qquad (24)$$

Substituting (24) into (23), we obtain

$$U_j = U_m \frac{1}{A_j/A + A_{nj}/A} \tag{25}$$

where

$$A = \pi\xi^2, \qquad A_j = 2\pi R_1 \Delta R, \qquad A_{nj} = \pi R_1 \Delta n \ell_{rf}/\phi \tag{26a,b,c}$$

Here Δn is the width of normal junction, and ℓ_{rf} is the fractional length of the normal junction that permits the passage of water in the fiber matrix model. The fiber matrix model of Curry (1986) assumes that the primary resistance of the intercellular water pathway resides in the matrix in the wide part of the cleft as opposed to the constricted regions associated with the junction strands. Thus in the fiber matrix model the effective width of the normal cleft where there are breaks in the junction strand is equal to the actual width of leaky junction ΔR. Note that the perimeter of cells is shared and the effective perimeter of each cell is πR_1 in calculating A_{nj}.

(ii) Junctional strand model

Based on the freeze fracture electron microscopic studies (Firth et al., 1983; Simionescu et al., 1975; Wissig, 1979) and serial section reconstruction techniques (Bundgaard, 1984; Bundgaard and Frokjaer-Jensen, 1982), Tsay et al. (1989) have proposed a new model for capillary filtration. In this model the pores are short discrete holes formed by individual missing proteins in an interlaced arrangement of intramembraneous protein strands in opposing membranes that form the junctional complexes. In this new model the multidimensional hydrodynamic interaction between the fluxes entering and leaving these discrete pores are considered. For large vessels, we believe that the structure of the normal endothelial cleft is

similar to capillary junctions except for the values of parameters in the model, such as the depth of the cleft and the number of missing proteins in the junctional protein strands. The water velocity through the pores formed by these missing junction proteins is given by

$$U_{nj} = \frac{A}{A_{nj}} L_p \Delta P \qquad (27)$$

where ΔP is the pressure drop across the leaky junction, and L_p is the hydraulic conductivity of the endothelial surface per unit area. The expression for L_p includes the resistance of the wide parts of the cleft on each side of the junction strand Rs_1 and Rs_3 and the resistance of the junction strand with its pores Rs_2.

$$L_p = (Rs_1 + Rs_2 + Rs_3)^{-1}$$

The expressions for these resistances are given by Tsay et al. (1989) by

$$Rs_k = \frac{3\mu}{B^3 L_{jt}} [L_k/2 + \frac{1}{d^2} \sum_{n=1}^{\infty} \tanh(\lambda_n L_k) \sin^2(\lambda_n d)/\lambda_n^3] \qquad k=1,3$$

$$\lambda_n = n\pi \ell_{rp}/r_p \qquad n=1,2,3,\ldots$$

$$Rs_2 = \frac{16\mu L_2}{\pi r_p^3 \ell_{rp} L_{jt}}$$

where μ is the viscosity of water, L_1 and L_3 are depths between the protein strand and the lumen and abluminal margins of the cleft, respectively, L_2 and r_p are the depth and radius of the pores in the protein strands, respectively, B is the half width of the wide portion of the cleft, $d = \pi r_p^2/4B$, L_{jt} is the total junctional length per unit endothelial surface area, and ℓ_{rp} is the fractional length

of the pores in the junction strand. ℓ_{rp} defined as the ratio of the diameter of pores to the distance between the pores.

For the leaky junction we assume a uniform open channel; therefore,

$$U_j = \frac{(\Delta R)^2 \Delta P}{12\mu L_j} \tag{28}$$

Substituting (28) into (27) to eliminate ΔP, and then substituting the resulting relation into (23), we have

$$U_j = \frac{1}{A_j/A + 12\mu L_j L_p/(\Delta R)^2} U_m \tag{29}$$

Substituting (23a), (25) and (29) into (3), we can finally estimate the Peclet numbers in the SI and leaky junction, respectively

$$Pe_i = \frac{f_i \gamma_m \eta}{f_m \gamma_i D_i^2} Pe_m \tag{30}$$

$$Pe_j = \frac{f_j L_j \gamma_m}{K_p f_m L_m \gamma_j D_j^2} Pe_m \tag{31}$$

where

$$K_p = \begin{cases} A_j/A + A_{nj}/A & \text{for fiber matrix model} \\ A_j/A + 12\mu L_j L_p/(\Delta R)^2 & \text{for junctional strand model} \end{cases}$$

It is of interest to evaluate the ratio of the transendothelial water fluxes through the leaky junction and normal junction pathways.

For the 1-D fiber matrix model this ratio is

$$[A_j U_j / A_{nj} U_{nj}]_f = 2\phi/\ell_{rf} \tag{32}$$

whereas for the 3-D junction strand model,

$$[A_j U_j / A_{nj} U_{nj}]_p = (\Delta R)^3 \phi/(6\mu R_1 L_j L_p) \tag{33}$$

Here the subscripts f and p denote the fiber matrix and junction strand models, respectively. If we equate the ratio of fluxes in (32)

and (33), then the relationship between ℓ_{rf} and ℓ_{rp} is obtained. This relationship will be discussed later.

3.3 Solutions

The 1-D model equations in the leaky junction can be readily integrated, whereas it is difficult to solve the boundary value problem for the model in the SI and media, because the boundary conditions for the concentration in the SI are coupled with the concentration in the media, as shown in (14) and (19). In this case, although the governing equations and the boundary conditions are linear in the regions considered, the method of separation variables can not be directly used, because the function of time and the function of radius can not be separated at the boundary of the IEL. In order to solve this problem, we first performed a Laplace transform of the model equations in the SI and media, solved the resulting problem by the method of separation variables, and then performed the Laplace transform inversion to obtain the final solutions. This solution procedure is summarized below.

3.3.1 Solution in the leaky junction:

From (4), (5) and (7), one obtains

$$C_j(z_j,t) = \exp(Pe_j z_j) + [C_{ji}(t) - \exp(Pe_j)] \frac{1 - \exp(Pe_j z_j)}{1 - \exp(Pe_j)} \qquad (34)$$

$$q_j(t) = Pe_j [\frac{C_{ji}(t) - \exp(Pe_j)}{1 - \exp(Pe_j)} + \frac{\delta}{1 - \delta}] \qquad (35)$$

where $C_{ji}(t)$ is an unknown function of time, which is coupled with the solutions of the model in the SI.

3.3.2 Solution in the SI and the media:

The first step of the solution procedure in the SI and media is to take the Laplace transform with respect to time t of equations (8)

through (14), and (17) through (21). The solutions for the Laplace transforms of the concentrations $C_i(r,z_i,t)$ and $C_m(r,z_m,t)$, which we denote by $\psi_i(r,z_i,s)$ and $\psi_m(r,z_m,s)$, respectively, can be obtained by the method of separation variables in the transformed space. These solutions, which satisfy the boundary conditions (13) and (20), are

$$\psi_i = \sum_{n=0}^{\infty} \{C_{1n}(s)\exp[\lambda_{1n}(s)z_i] + C_{2n}(s)\exp[\lambda_{2n}(s)z_i]\}J_0(\lambda_n r) \quad (36)$$

$$\psi_m = \sum_{n=0}^{\infty} \{C_{3n}(s)\exp[\lambda_{3n}(s)z_m] + C_{4n}(s)\exp[\lambda_{4n}(s)z_m]\}J_0(\lambda_n r) \quad (37)$$

where $C_{kn}(s)$ (k=1,2,3,4) are unknown functions of the transform variable s, the eigenvalues λ_n are the roots of $J_1(\lambda_n\xi) = 0$, n=0,1,2,...,∞; and

$$\lambda_{1n,2n}(s) = -\left(\frac{Pe_i}{2\eta}\right) \pm \sqrt{\left(\frac{Pe_i}{2\eta}\right)^2 + \lambda_n^2 + s/D_i^2} \quad (38)$$

$$\lambda_{3n,4n}(s) = -\left(\frac{Pe_m}{2}\right) \pm \sqrt{\left(\frac{Pe_m}{2}\right)^2 + \lambda_n^2 D_m^2 + s} \quad (39)$$

By satisfying the boundary conditions, which were obtained from the Laplace transforms of equations (10) through (12),(14),(19) and (21), two sets of four simultaneous linear algebraic equations were obtained as shown in (B.1) and (B.2). This linear matrix of equations can be truncated at any value of n to determine the coefficients C_{k0} and C_{kn} (k=1,2,3,4 and n=1,2,...,∞) in (36) and (37) in terms of the unknown function $\psi_{ji}(s)$, which is defined as the Laplace transform of $C_{ji}(t)$.

An independent expression for $\psi_{ji}(s)$ can be obtained by integrating equation (10) from R_1 to R_2 and performing a Laplace transform. This yields

$$\psi_{ji}(s) = 2[\int_{R_1}^{R_2} r\psi_i(r,\eta,s)\,dr\,]/(R_2^2 - R_1^2) \qquad (40)$$

Substituting (36) into (40) and evaluating the resulting integrals, one obtains

$$\psi_{ji}(s)=C_{10}(s)\exp[\lambda_{10}(s)\eta]+C_{20}(s)\exp[\lambda_{20}(s)\eta]+\frac{2}{R_2^2 - R_1^2}\sum_{n=1}^{\infty}(C_{1n}(s)\cdot$$

$$\exp[\lambda_{1n}(s)\eta] + C_{2n}(s)\exp[\lambda_{2n}(s)\eta])\frac{R_2J_1(\lambda_nR_2)-R_1J_1(\lambda_nR_1)}{\lambda_n} \qquad (41)$$

From (B.1) and (B.2), C_{kn} (k=1,2,3,4 and n=0,1,2,...,∞) are known linear functions of $\psi_{ji}(s)$. Equation (41) thus reduces to a linear equation which can be solved for $\psi_{ji}(s)$. Substituting $\psi_{ji}(s)$ back into the linear equations (B.1) and (B.2) for C_{kn} (k=1,2,3,4 and n=0,1,2,...,∞), one obtains closed form expressions for these coefficients, which depend only on the variable s.

The macromolecular concentrations averaged in the r direction can be obtained by integrating (36) and (37) analytically. These averages are denoted by $\bar{\psi}_i$ and $\bar{\psi}_m$,

$$\bar{\psi}_i(z_i,s)=\frac{2\int_0^{\xi} r\psi_i dr}{R_2^2 - R_1^2}=C_{10}(s)\exp[\lambda_{10}(s)z_i]+C_{20}(s)\exp[\lambda_{20}(s)z_i] \qquad (42)$$

$$\bar{\psi}_m(z_m,s)=\frac{2\int_0^{\xi} r\psi_m dr}{R_2^2 - R_1^2}=C_{30}(s)\exp[\lambda_{30}(s)z_m]+C_{40}(s)\exp[\lambda_{40}(s)z_m] \qquad (43)$$

The last step of the solution procedure is to invert the Laplace transform of the expressions for C_{kn} (k=1,2,3,4 and n=0,1,2,...,∞). Since ψ_i, ψ_m and ψ_{ji} are complicated functions of s, it is very difficult to perform these inversions analytically. In this chapter, these inversions have been performed numerically using the "collocation" inversion method proposed by Schapery and described in Rizzo and Shippy (1970).

3.4 Results

All of the results shown in this section for convective-diffusive transport are incorrect due to the assumption of 1-D continuity relations for water velocity in each layer, whereas the results for pure diffusive transport are still correct. The purpose of putting these physically spurious results into this dissertation is to show why the previous 1-D convective-diffusive model can not be used to study the arterial macromolecular transport.

3.4.1 parameter values:

There are eight important parameters in this model. They are D_j^2, D_i^2, D_m^2, Pe_m, ϕ, σ, σ_I and ℓ_r. The diffusion coefficients in the present model differ from those in Wen et al. (1988), since the diffusion coefficients in Wen et al. (1988) already include the partition coefficients. Thus the present coefficients correspond to the experimentally measured diffusion coefficients. Based on the discussions in the previous model (Wen et al., 1988), reasonable values for D_j^2 in the large arteries are 140, 14 and 1.4 for HRP,

albumin and LDL, respectively; D_m^2 for albumin is of the order of 10. For simplicity we have assumed that $D_{ri}=D_{rm}$; thus, $D_i^2=D_m^2$.

The parameter ϕ represents the frequency of the cells whose junctions are leaky to macromolecules. The experimental studies by Lin et al.(1988) have revealed that about five cells in ten thousand are leaky to albumin in normal rat aortic endothelium. In this case, $\phi = 0.0005$. However, the cells with junctions leaky to macromolecules have a non-uniform distribution over the endothelial surface. The endothelial cell turnover rate at the distal edges of the major branch orifices of the abdominal aorta and the branch orifices of the intercostal arteries are two to three times that at non-branch areas (Lin, 1989). $\phi = 0.001$ is thus representative of the so-called blue areas near branches. In the previous model (Wen et al., 1988), σ was set equal to 0.2 for canine carotid artery and 0.08 for rabbit aorta based on in vitro measurements for albumin uptake in the presence and absence of the arterial endothelium and the assumption that significant amounts of albumin could pass through intact endothelium without leaky junctions. The experimental results (Lin, 1989; Lin et al., 1988 and 1989) indicate that these cells in the endothelial layer are largely impermeable to macromolecules, thus the value of σ, which reflects the macromolecular permeability of the part of the endothelium outside the leaky junction, should be equal to zero. To determine σ_I in our model for the IEL we shall assume that the diffusion coefficient in the fenestra of the IEL is the same as that in the SI, and the thickness of the IEL is taken as 1 μm. The diameter of the fenestrae varies between 0.45 to 1.35 μm, and the fenestrae occupy 0.1 to 4.6% of the surface area for the thoracic

aorta of sheep (Song and Roach, 1983). Based on these values, the dimensionless parameter σ_I was estimated to lie in the range 20 to 45.

Measurements of small ion permeability and hydraulic conductivity in frog and mammalian muscle capillaries summarized by Crone and co-workers (Crone, 1984; Crone and Levitt, 1984) suggest that typically 5 to 10 percent of the normal cleft is open in these mivrovessels using existing 1-D slit models (Crone and Levitt, 1984) for capillary filtration. For rabbit aorta, the hydraulic conductivity of its endothelial layer is of the same order as muscle capillaries (Tzeghai et al., 1985). Therefore, we assume in the present model that ℓ_{rf} lies in the range 0.01 to 0.1 for 1-D slit models. The corresponding range for ℓ_{rp} for junction strand model will be discussed in the next subsection.

Similar to our previous model (Wen et al., 1988), we shall assume that the width of the leaky junction ΔR is 20 nm, the junctional length L_j is 2 μm, the effective endothelial diameter $2R_1$ is 30 μm, the total wall thickness L_w is 0.2 mm for rabbit aorta, the SI thickness L_i is 1 μm, C_A/C_L is zero, the average Peclet number in the media for the intact endothelium is 4.4 (Tedgui and Lever, 1985), and the partition coefficients are unity in the leaky junction (no fiber matrix) and 0.16 in the SI, the fenestra of the IEL and the media (Thurn, 1982), respectively. The radius of the periodic unit ξ is calculated from $R_1/\sqrt{\phi}$. To determine the hydraulic conductivity L_p of the endothelium, we assume that μ is 0.0072 g/cm/sec, r_p is 5.5

nm, L_1=0.4L_j, L_2=2r_p, L_3=L_j-L_1-L_2, B is 8.5 nm, and L_{jt} is 2000 cm/cm^2.

Generally, the solute retardation coefficient f_x in region x could be less than unity in tissues with fiber matrix structure and narrow interstitial spaces. For the arterial wall, the most likely sites of sieving are the leaky junctions of the endothelial layer or the basement membrane. However, Ganatos et al. (1982) have shown that the retardation coefficient is 0.96 for a sphere moving in a channel with a sphere diameter/channel height ratio of 0.33, which is close to the ratio of the equivalent diameter of the albumin to the assumed height of the open cleft. Thus, if there is no extracellular fiber matrix in the leaky junction, f_j in the leaky junction is nearly unity. It is possible that basement membrane components may lie beneath both denuded endothelium and open junctions; this possibility is currently under study. At present, we have assumed, for simplicity, that the interstitial tissues in the SI, IEL and media are continuous and that their structure in these three layers is uniform and does not introduce large sieving effects. The maximum sieving effect for albumin that has been measured by Fry et al. (1986) in the superficial layers of the intima is only approximately 15 percent in denuded minipig aorta. Based on these arguments, we have assumed that the solute retardation coefficients are unity in the other three layers in the present study.

3.4.2 The water flux ratio

The ratios of the water fluxes through the leaky and normal junctions are shown in Fig.3 for different ϕ. The solid lines are obtained from the fiber matrix model (32), and the dashed lines are

from the junction strand model (33). When this water flux ratio is the same in the two models, the hydraulic conductivity L_p of the endothelial layer will be the same. Since the hydraulic resistances of the fiber matrix and junction pore pathways differ, different fractional lengths of junction discontinuity are predicted by the two models for the same value of L_p or water flux ratio. Thus the fractional open junction lengths ℓ_{rf}=0.01 and 0.1 for the fiber matrix model correspond to ℓ_{rp}= 4.63×10^{-4} and 4.45×10^{-3}, respectively, for the junction strand model. This relation is independent of ϕ. The ratio of the number of proteins in a continuous strand of a given length to the number of missing proteins in a protein strand of the same length is defined as $n_p=1/\ell_{rp}$, the number period of missing proteins. Using the values of ℓ_{rp} cited above, n_p will vary from 225 to 2160.

The results shown in Fig.3 are quantitatively incorrect due to the assumption of constant pressure distribution in the SI. In fact, more than 99 percent of the water entering the artery wall through the normal clefts of endothelium (see the results in the next chapter).

3.4.3 The validity of the numerical Laplace transform inversion

In order to check the accuracy of the numerical Laplace transform inversion, we have compared the results of the new solution method with the predictions of previous papers (Tzeghai et al., 1986; Wen et al., 1988), as shown in Fig.4. The latter are the special cases of the present model in which there is no IEL, i.e. ϕ_I= 1 and L_i= 0. The solid lines are the present results and the symbols are

the results presented by Tzeghai et al. (1986) and Wen et al. (1988). One can see that the solutions obtained by the different solution procedures are very close to each other. The only significant difference occurs at the exit of the leaky-junction for curve 3. One cannot determine which solution is more accurate, because the solution procedure in Wen et al. (1988) also involved approximations, and the concentration gradient is very large in the vicinity of the exit of the leaky junction. On the other hand, the width of the leaky junction is very small, so that the error in the concentration in this small region will not have a significant effect on the average concentration.

3.4.4 The axisymmetric concentration distribution

Typical time-dependent concentration distributions in the SI at $z_i=\eta$ in the lateral direction are shown in Fig.5 for rabbit aorta, where L_w=0.2 mm. The ratios of the diffusion coefficients D_j^2, D_i^2, and D_m^2 for albumin are 14, 10 and 10, respectively. The average value for ϕ is 0.001, which is typical of branch areas. The diameter of the fenestra in the IEL and their fractional area are 0.9 μm and 2 percent in that order. The shape of the concentration distributions shown in Fig.5 is similar to the results in the previous model (Wen et al., 1988), which neglected convection, but the level of the concentration in the vicinity of the leaky junction exit is much greater than unity in comparison with the purely diffusive model where this concentration was always less than unity. The large lateral concentration gradient at the exit of the leaky junction is, therefore, independent of the convective transport and the presence of the IEL. These steep lateral gradients indicate that large local

increases in macromolecular permeability of the endothelial surface can be accounted for by a small fraction of cells involved in cell turnover.

It is very important to mention here that the results of the concentrations in the vicinity of the leaky cleft exit that are higher than in the lumen are the artifact due to the assumption of 1-D convective velocity across the artery wall. It will be shown in the next chapter that the subendothelial concentration can not exceed that in the lumen unless a macromolecular sieving structure exists in the intima.

The effects of convection and the number period n_p of missing proteins in the normal junctions on the steady state concentration profile are shown in Figs.6 and 7. When n_p increases from 225 to 2160, the concentration in the subendothelial space will increase markedly, but the pattern of the concentration profile remains almost the same. The large increase in cleft exit concentration when n_p is increased to 2160 (ℓ_{rf}=0.01) is explained by the relative preponderance of water flux through the leaky junctions as a result of the decrease in water flux through the discontinuities in the normal junctions. This leads to a large value of Pe_j and a steep standing gradient at the cleft exit.

At steady state, the concentration distributions in the lateral direction at $z_i = \eta$ and $z_m = 1$ are nearly indistinguishable except in the vicinity of the exit of the leaky junction, as shown in Figs.6 and 7. The concentration profile at $z_i = 0$ is not shown because it is almost identical to that for $z_i = \eta$. These results indicate that the

resistance of the IEL to macromolecular transport at steady state is very small.

3.4.5 The average concentration distribution

The time-dependent average concentration distribution across the wall is shown in Fig.8. As the time increases, the average concentration in planes parallel to the endothelial surface increases and changes from a concave to a convex profile in the media. The concentration profile in the SI is flat. This is not because the concentration gradients in the SI are small compared to the media, but because the SI is much thinner than the media. Thus, the change of the concentration in the SI can not be reflected by the scale of the media in Fig.8. Even for $L_i = 10$ μm, the change in C_i is very small, and the results are almost the same as those shown in Fig.8 for $L_i = 1$ μm.

The discontinuity of the average concentration profile across the IEL is also shown in Fig.8. One can see this discontinuity is very small and decreases with time. The relative concentration difference across the IEL is about three percent at dimensionless time $t=0.01$, which corresponds to 800 seconds, for $D_{zm} = 5\times10^{-9}$ cm^2/sec (Thurn, 1982) and $L_w = 0.2$ mm for albumin.

The effects of the diameter and the fractional area of the fenestra in the IEL on the average concentration profile were also investigated. If the diameter 2ϵ is increased from 0.45 to 1.35 μm and all other parameters in Fig.8 held fixed, with $\phi_I = 2$ percent, the average concentration will increase, but this increase will lessen with time. At $t=0.001$, the maximum increase is about 10 percent in

the SI. If 2ϵ is fixed at 0.90 μm and ϕ_I increased from 0.1 to 5 percent, the average concentration will decrease, and this the relative decrease will again lessen with time. At t=0.001, the maximum decrease in concentration is about 24 percent in the SI, when ϕ_I is increased by a factor of 50. This increase or decrease of the concentration with ϕ_I and/or ϵ brackets the maximum anticipated changes in the resistance of the IEL to macromolecules. In all these cases, the maximum average concentration difference across the IEL is less than 5 percent. These results indicate again that the resistance of the IEL to macromolecular transmural transport is very small and can be neglected, if the interstitial structure in the fenestra is the same as that in the SI and media above and below it.

The effects of the Peclet number on the average concentration profile at steady state are shown in Fig.9. The increase in the average concentration due to the increase in Peclet number from 0 to 4.4 with n_p= 2160 (ℓ_{rf}=0.01) is about 10 times higher than that with n_p=225 (ℓ_{rf}=0.1). If n_p=90, the concentration will even decrease as the Peclet number in the media is increased from 0 to 4.4. The sharp drop in the average wall concentration profile at a given Pe_m as n_p is decreased from 2160 to 225 is due to the decrease in the unstirred layer effect in the leaky junction when the water flux through the normal clefts increases.

The change in the average wall concentration profiles as ϕ increases is shown in Fig.10. An increase in ϕ results in a non-linear increase in concentration in the subendothelial space. Increasing ϕ by a factor of 2 at 0.0005 leads to a 1.84 fold increase in the average SI concentration, whereas increasing ϕ by a

factor of 5 at 0.001 results in only a 2.76 fold increase in the average SI concentration. The reason is that when ϕ is much less than unity, the major resistance of the arterial wall to macromolecular transport comes from the endothelial layer. However, as ϕ is increased, the resistance of the endothelium to macromolecular transport falls sharply to become less than the resistance provided by the rest of the wall (see below) when $\phi > 0.01$. The effect of n_p on the concentration profile for different ϕ is also shown in Fig.10. This effect is the same as described in Fig.9.

The ratio β of the average concentration in the SI to that at the leaky junction exit varies as a function of the time and ϕ as shown in Fig.11 for n_p=2160 (ℓ_{rf}=0.01). The value of β increases with time and ϕ and asymptotically approaches a maximum value at steady state. For the physiological range of ϕ, β is much less than unity, and for ϕ<0.005 the maximum value of β is less than 0.05 for n_p=2160 (ℓ_{rf}=0.01). This indicates that the average concentration in the SI is much less than the concentration in the leaky junction when n_p>2000 and that the average concentration profile across the endothelial-SI interface is sharply discontinuous.

3.4.6 A modified 1-D model

A modified version of Fry's 1-D steady state model (Fry, 1987) has been developed in Appendix C. The primary purpose of this model is to examine the effect of the discontinuity in average concentration β at the endothelial-SI interface that is shown in Fig.11. In Fry's model, the arterial wall is composed of four layers as shown in Fig.1 and β is assumed to be unity. The 1-D model in Appendix C represents a modification from Fry's model (Fry, 1987) in

three respects. First, the average concentration profile across the endothelial-SI interface in the present model is allowed to be discontinuous; it is described by the unknown parameter β which is prescribed. Second, we have assumed, based on the experimental results (Lin et al., 1988 and 1989; Weinbaum et al., 1988b), that only the leaky junctions in the endothelial layer and the fenestrae in the IEL are permeable to macromolecules in these two layers. Thus, in the present model, the permeability of the normal endothelial cells to macromolecules is zero. However, water can pass through both the normal and leaky junctions in the endothelial layer. In the model of Fry (1987), no distinction is made between normal and leaky junctions, and water and macromolecules are allowed to pass through both the interendothelial clefts and the endothelial cell itself. The value of α_m for macromolecular transport is of the order of 10^{-6} in the present model, which is three orders of magnitude less than the minimum non-zero value of α_m in Fig.2 of Fry (1987). Finally, in Fry's model the solute retardation coefficients in the IEL and the media layer are assumed to be less than unity, whereas in the present 1-D model we have assumed that the solute retardation coefficients in the four layers are unity for the reasons discussed in the first part of this section.

The modified 1-D model in Appendix C can be obtained by integrating the present 2-D model in the lateral direction and defining an average concentration as shown in Figs.8,9,10. The principal difference between this averaged 2-D model and the modified 1-D model is that the 1-D theory can not be used to determine the unknown parameter β. This parameter can only be obtained from 2-D

analysis; however, we shall show that there are certain regions where the solution is very insensitive to the value of β in the steady state and the 1-D model with β=1 can be used with surprisingly small error.

The results of the modified 1-D model are shown in Tables 1, 2 and 3 for Pe_m= 0 and 4.4 and n_p=225 (ℓ_{rf}=0.1) and 2160 (ℓ_{rf}=0.01). When there is no convection (Pe_m=0) the solutions become independent of n_p or ℓ_{rf}. Also shown for comparison are the results for the average concentrations obtained from the 2-D model. The parameter values used in obtaining these three tables are the same as those used in Fig.9. β in the 1-D model is treated as a free parameter which is allowed to take values which cover the range from zero to one. The actual value of β is shown with the 2-D model results. One observes that for Pe_m=4.4 (see Tables 1 and 3) the solutions for the average concentration are insensitive to the value of β except inside and close to the exit of the leaky junction. The maximum deviation from 2-D model in the subendothelial average concentration is 20 percent, when n_p=225 and β=0.001. When Pe_m= 4.4 the dominant term for macromolecular transport in all four layers is convection if ϕ<<1. The parameter β which describes the effect of lateral diffusion in the SI is not significant when there is a large convective flux through the leaky cleft. In contrast, as shown in Table 2, the value of β has a significant effect on the average concentration profiles for Pe_m= 0. In this case, diffusion plays an important role in the overall macromolecular transport and the concentration discontinuity across the endothelial-SI interface has to be considered.

3.4.7 Effect of ϕ on average flux of macromolecules

At the steady state, the average flux of macromolecules across each layer is a constant and depends only on the values of the parameters in the model. In Fig.12, the integrated average mass flux Q is scaled relative to Q_d, the mass flux with the endothelium completely denuded. The dependence of Q/Q_d on ϕ is highly non-linear as suggested by the results in Fig.12. When the Peclet number in the media is increased from zero to 4.4, the entire flux curve is shifted to the left. Unfortunately, these results are incorrect due to the assumption of 1-D continuity relations for water velocity in each layer (see discussions in the next chapter). The solute flux Q in Fig.12 of this chapter is overestimated by at least one order of magnitude.

When ϕ=1, the total macromolecular flux through the arterial wall is very close to the flux through a wall whose endothelium is denuded. When ϕ=1 the fractional area of the leaky junctions are still only of $O(10^{-3})$, since the endothelial cells are present and only their junctions are open. This result is similar to that shown in Fig.3(c) of Wen et al. (1988) when Pe_m= 0. This value of ϕ corresponds to α_m= 0.001 in Fry's model (Fry, 1987).

3.5 Discussion

The transport of LDL in the arterial wall involves the binding of the LDL to the cell membrane or the extracellular matrix of the arterial wall and the degradation of LDL by the endothelial cells or smooth muscle cells (Steinberg, 1983). The present model, which has neglected these two processes, is thus only a rough approximation for

the LDL transport in the arterial wall. However, some of the key insights obtained in this chapter relating to the resistance of the IEL, the importance of convection in the different layers, the role of n_p (ℓ_{rf}) in establishing an unstirred layer in the leaky cleft and the discontinuity of the concentration profile across the endothelial-SI interface for the 1-D model are also applicable to the problem of LDL transport. These considerations govern the LDL delivery into the arterial wall for binding and degradation.

3.5.1 Permeability of endothelial layer and IEL to macromolecules

The experimental results (Lin et al., 1988 and 1989; Weinbaum et al., 1988b) have shown that the normal endothelial cells, the junctions between them and the elastic tissues of the IEL are impermeable to macromolecules the size of albumin or larger. Therefore, the primary large pore for macromolecular transport across the endothelial layer is the leaky junction associated with cells in turnover (Weinbaum et al., 1988a). Similarly, the macromolecular transport across the IEL is largely through the fenestra.

The fractional area of the leaky junctions is the first of two key parameters in estimating the macromolecular flux across the endothelial layer. The experiments (Lin et al., 1988 and 1989) indicate that this fractional area is of the order of 10^{-6}. The 2-D mathematical model for convective-diffusion in this chapter has shown that such a tiny area of leaky junctions due to an increase in cell turnover involving only a few cells in ten thousand can account for a twofold increase in macromolecular permeability through the endothelial layer. The total junctional area for filtration, which includes both normal and leaky junctions, is the second key parameter. The total fractional junctional area for filtration,

assuming n_p lies in the range 225 to 2160 (ℓ_{rf}=0.01 to 0.1), varies from 10^{-5} to 10^{-4}. This is one to two orders of magnitude larger than the fractional area of the leaky junctions. Thus, more than eighty percent of the water molecules cross the endothelial layer through normal junctions, as shown in Fig.3 for $\ell_{rp}>0.000463$ ($\ell_{rf}>0.01$) and $\phi<0.001$ (note: these results are incorrect, see the discussions in the next chapter). For the same water flux distribution, $\ell_{rp}<<\ell_{rf}$. This difference in open junction length for water flow arises because the fiber matrix model is 1-D and does not account for the extensive lateral spreading of the water on each side of the junction strand. Thus, for the same hydraulic conductivity, a much larger portion of the endothelial cleft must be open in the fiber matrix model than the junction strand model.

In Fry's 1-D model (Fry, 1987), the macromolecules are assumed to cross the endothelial layer through two phases, i.e. the endothelial cells and the junctions between them, and a single fractional area α_m is used to estimate both the macromolecular and water fluxes. The non-zero value of the fractional area α_m used to calculate the results in Fry (1987) is at least one order of magnitude larger than the total fractional junctional area for filtration cited above and three orders of magnitude larger than the fractional area of the leaky junctions observed by Lin et al. (1988) and (1989). This description of the endothelial layer leads to concentration profiles in Fig.2 of Fry (1987) which differ markedly from those in the present study. The numerical testing of the 1-D

model in Fry (1987) revealed that the concentrations in the SI will be less than that in the lumen, if $\alpha_m < 0.001$ or f_I is close to unity.

3.5.2 The boundary conditions for 1-D model

Generally, the concentration profile of macromolecules in the arterial wall is measured by taking sections as a function of time and distance from the lumen to adventitia surface. Therefore, the experimental data correspond directly to the results of a 1-D model. This 1-D model is obtained by integrating the 2-D model in the lateral direction. The equivalent 1-D average results are shown in Figs. 8-10.

The difficulty in formulating a 1-D model is the treatment of the interface matching conditions when there is a discontinuity in area for macromolecular transport between layers. One must first solve a 2-D convective diffusion problem to treat the interaction between pores and determine the discontinuity in the average concentration at the interface. Alternatively, one can solve the 2-D problem and determine an effective permeability coefficient which considers this pore interaction as we have described in our model for the IEL where the effect of the pore interaction is included in the expression for σ_I. The local variations in concentration between the fenestra, however, are small and one can construct an equivalent porous layer wherein one does not need to treat the individual pores. The treatment of the endothelium is more critical since there are large local differences in SI concentration. In the intact region the macromolecular concentration can be close to zero whereas at the cleft exit the concentration can exceed that in the lumen if there is an unstirred layer in the leaky junction. The discontinuity in the concentration profile does not cause difficulty in the 2-D model,

because the local boundary conditions on the flux and concentration are satisfied exactly. If we integrate the boundary conditions in the lateral direction, the mass flux is still continuous across the endothelial-SI interface, but the average concentration is discontinuous and described by the parameter β in Fig.11. Certain simplifications are suggested by Tables 1 to 3. One observes that the continuous concentration profile, i.e. β=1, can be used as the interfacial matching condition without causing much error in the 1-D model, if the Peclet number in the media is greater than unity. However, the results in Table 2 indicate that a proper boundary condition at the endothelial-SI interface is required in a 1-D model for macromolecular transport when the Peclet number in the media is smaller than unity.

3.5.3 Comparison of convective diffusion and pure diffusion

Pure diffusive transport is a special case of convective diffusion, obtained by setting the Peclet number equal to zero. The fundamental difference between these two transports is the level of the subendothelial concentration. Generally, the average macromolecular concentration in the subendothelial space in pure diffusive transport is less than in convective-diffusion. A critical parameter in determining the SI concentration when there is a transmural filtration pressure is the value of n_p or ℓ_{rf}. For a given Pe_m, $n_p(\ell_{rf})$ and ϕ determine the relative water flux through the normal and leaky junctions.

The effect of $n_p(\ell_{rf})$ on macromolecular flux in Fig.12 suggests a novel method for estimating the value of n_p or ℓ_{rf}. As just discussed, experiments suggest that the macromolecular flux is

sensitive to the change of ϕ when ϕ>0.0005 (Lin et al., 1988), whereas the results with n_p=225 (ℓ_{rf}=0.1) in Fig.12 indicate a significant change in permeability only for ϕ>0.001. The latter behavior is inconsistant with the experimental results in Lin et al. (1988). The predictions of the present model suggest that n_p is greater than 225 (ℓ_{rf}=0.1) and close to 2160 (ℓ_{rf}=0.01).

3.5.4 The resistance of the arterial wall to macromolecular transport

The excessive accumulation of the lipid in the subendothelial space is one of the primary features of the atherogenesis (Weinbaum et al., 1988a). Based on the results of the present model, the major resistance to macromolecular transport resides in the endothelial layer. Because the SI and the IEL are very thin compared to the media layer, and the size of the fenestra in the IEL are very large compared with the size of macromolecules, the resistances of the SI layer and the IEL to macromolecules are very small, as shown in Fig.8.

APPENDIX A

This appendix contains the approximate model for the IEL, as shown in Fig.2, and its solution. The value of σ_I is estimated from this model.

Because the macromolecular concentration at the top of the fenestra of the IEL is $\tilde{C}_i$ instead of $\tilde{C}_p$, it is convenient in this model to non-dimensionalize the concentration in a given region x by $(\tilde{C}_i - \tilde{C}_A)$:

$$C_{xs} = \frac{\tilde{C}_{xs} - \tilde{C}_A}{\tilde{C}_i - \tilde{C}_A} \tag{A.1}$$

where the subscript s is used to denote the steady state.

The governing equation and the boundary conditions for steady state convective diffusion in the fenestra of the IEL are

$$\frac{\partial^2 C_{Is}}{\partial z_I^2} - Pe_I \frac{\partial C_{Is}}{\partial z_I} = 0 \tag{A.2}$$

$$C_{Is}(0) = 1, \quad C_{Is}(1) = C_{Im} \tag{A.3a,b}$$

where z_I is the centerline coordinate in the fenestra, and non-dimensionalized by the depth of the fenestra of the IEL.

The dimensionless mass flux in the fenestra is

$$q_{Is} = - \frac{\partial C_{Is}}{\partial z_I} + Pe_I \left(C_{Is} + \frac{\delta_I}{1 - \delta_I}\right) \tag{A.4}$$

where $\delta_I = \tilde{C}_A / \tilde{C}_i$,

Since the distance between the fenestrae is small compared to the media thickness, the 2-D spreading and interaction between the exit jets in the media must be considered. Thus, the governing

equation for the steady state convective diffusion in the media of the artery is

$$D_m^2 \left(\frac{\partial^2 C_{ms}}{\partial r^2} + \frac{1}{r}\frac{\partial C_{ms}}{\partial r}\right) + \frac{\partial^2 C_{ms}}{\partial z_m^2} + Pe_m \frac{\partial C_{ms}}{\partial z_m} = 0 \qquad (A.5)$$

here r and z_m are the coordinates in the lateral and normal directions, respectively, they are non-dimensionalized by the media thickness L_m. The dimensionless flux q_{ms} in normal direction in the media is

$$q_{ms}(r,z_m,t) = \frac{\partial C_{ms}}{\partial z_m} + Pe_m\left(C_{ms} + \frac{\delta_I}{1 - \delta_I} \right) \qquad (A.6)$$

The boundary conditions in the media are

$$\frac{\partial C_{ms}}{\partial r}(0,z_m) = \frac{\partial C_{ms}}{\partial r}(\xi_I,z_m) = 0 \qquad 0 < z_m < 1 \qquad (A.7a,b)$$

$$q_{ms} = \begin{cases} 0 & \epsilon < r < \xi_I \\ \dfrac{\gamma_I D_{zI} L_m}{\gamma_m D_{zm} L_I} q_{Is} & 0 < r < \epsilon \end{cases} \qquad \text{at } z_m = 1 \text{ and } z_I = 1 \qquad (A.8)$$

$$C_{ms}(r,1) = C_{Im} \qquad 0 < r < \epsilon \qquad (A.9)$$

$$C_{ms}(r,0) = 0 \qquad 0 < r < \xi_I \qquad (A.10)$$

where ϵ and ξ_I are the dimensionless radii of the fenestra and the local periodic unit, respectively, and they are non-dimensionalized by L_m.

From continuity of water flow, the Peclet number in the fenestra Pe_I is related to the Peclet number in the media Pe_m by

$$Pe_I = \frac{\gamma_m f_I L_I}{\phi_I \gamma_I f_m L_m D_I^2} Pe_m \qquad (A.11)$$

where $D_I^2 = D_{zI}/D_{zm}$ and ϕ_I is the fractional area of the fenestra on the IEL surface.

Equation (A.2) was solved analytically, and (A.5) was solved by using the separation variable method. Substituting the solutions of (A.2) and (A.5) into the boundary conditions (A.3) and (A.7) through (A.10), one obtains

$$C_{Is} = \frac{2h_2}{\epsilon^2 - 2h_1}, \qquad q_{Is} = h_3 C_{Is} + h_4$$

$$\bar{C}_{ms} = D_I^2 (L_m/L_I) q_{Is} \phi_I [1-\exp(-Pe_m)]/Pe_m$$

where $\bar{C}_{ms}$ is the average concentration in the media of the local periodic unit at the IEL-media interface, and

$$h_1 = \sum_{n=0}^{\infty} \mu_{n1}\mu_{n3}, \qquad h_2 = \sum_{n=0}^{\infty} \mu_{n2}\mu_{n3}$$

$$h_3 = Pe_I/[1-\exp(Pe_I)], \quad h_4 = -\exp(Pe_I)h_3$$

Where ϵ is the dimensionless radius of the fenestra. The coefficients μ_{n1}, μ_{n2} and μ_{n3} $(n=0,1,2,\ldots,\infty)$ are determined by

$$\mu_{10} = \frac{D_I^2 (L_m/L_I)\phi_I}{g_0} h_3, \qquad \mu_{1n} = \frac{2D_I^2 (L_m/L_I) h_3 \epsilon J_1(\lambda_n \epsilon)}{\lambda_n g_n [\xi_I J_0(\lambda_n \xi_I)]^2}, \qquad n\geq 1$$

$$g_n = (\lambda_{1n} + Pe_m)\exp(\lambda_{1n}) - (\lambda_{2n} + Pe_m)\exp(\lambda_{2n}), \quad \mu_{2n} = \frac{\mu_{1n}}{h_3} h_4, \qquad n\geq 0$$

$$\mu_{30} = \epsilon^2 [1-\exp(-Pe_m)]/2, \quad \mu_{3n} = \frac{\epsilon J_1(\lambda_n \epsilon)}{\lambda_n} [\exp(\lambda_{1n}) - \exp(\lambda_{2n})], \qquad n\geq 1$$

where

$$\lambda_{1n,2n} = [-Pe_m \pm \sqrt{Pe_m^2 + 4D_m^2 \lambda_n^2}]/2, \qquad n\geq 0$$

and $J_0(\ )$ and $J_1(\ )$ are the zeroth and the first order Bessel functions and λ_n are eigenvalues satisfying the equation $J_1(\lambda_n \xi_I)=0$, $(n=0,1,2,\ldots,\infty)$.

Appendix B

This appendix contains the linear algebraic equations for C_{kn} $(k=1,2,3,4$ and $n=0,1,2,\ldots,\infty)$.

By satisfying the boundary conditions, which were obtained from the Laplace transform of the equations (10) through (14), and (19) through (21), the following two sets of four simultaneous linear algebraic equations were obtained.

For n = 0

$$(\lambda_{10}+ a_3)\exp(\lambda_{10}\eta)\, C_{10} + (\lambda_{20}+ a_3)\exp(\lambda_{20}\eta)\, C_{20} = [(a_4\psi_{ji}+ a_7/s)\frac{R_2^2- R_1^2}{\xi^2} + (\sigma + a_2)/s \qquad (B.1a)$$

$$(\lambda_{10}+ a_1)\, C_{10} + (\lambda_{20}+ a_1)\, C_{20}+ b_1\exp(\lambda_{30})\, C_{30}+ b_1 \exp(\lambda_{40})\, C_{40}- a_2/s \qquad (B.1b)$$

$$a_6C_{10}+ a_6C_{20}+ (\lambda_{30}+ b_2)\exp(\lambda_{30})\, C_{30}+ (\lambda_{40}+ b_2)\exp(\lambda_{40})\, C_{40}- b_3/s \qquad (B.1c)$$

$$C_{30}+C_{40}= 0 \qquad (B.1d)$$

and for n ≥ 1

$$(\lambda_{1n}+ a_3)\exp(\lambda_{1n}\eta)\, C_{1n} + (\lambda_{2n}+ a_3)\exp(\lambda_{2n}\eta)\, C_{2n} = (a_4\psi_{ji}+ a_7/s)\frac{2[R_2J_1(\lambda_nR_2) - R_1J_1(\lambda_nR_1)]}{\lambda_n\xi^2J_0^2(\lambda_n\xi)} \qquad (B.2a)$$

$$(\lambda_{1n}+ a_1)\, C_{1n} + (\lambda_{2n}+ a_1)\, C_{2n}+ b_1\exp(\lambda_{3n})\, C_{3n}+ b_1 \exp(\lambda_{4n})\, C_{4n}= 0 \qquad (B.2b)$$

$$a_6C_{1n}+ a_6C_{2n}+ (\lambda_{3n}+ b_2)\exp(\lambda_{3n})\, C_{3n}+ (\lambda_{4n}+ b_2)\exp(\lambda_{4n})\, C_{4n}= 0 \qquad (B.2c)$$

$$C_{3n}+C_{4n}= 0 \qquad (B.2d)$$

The expressions for the constants a_k (k=1,2,...,7) and b_k (k=1,2,3) are

$$d_1 = Pe_j/[1-\exp(Pe_j)]$$

$$d_2 = -\exp(Pe_j)d_1 + \delta Pe_j/(1-\delta)$$

$$a_1 = Pe_i/\eta - \sigma_I/(D_i^2\gamma_i)$$

$$a_2 = -Pe_i\delta/[\eta(1-\delta)]$$

$$a_3 = Pe_i/\eta + \sigma$$

$$a_4 = \gamma_j D_j^2 L_m d_1/(\gamma_i D_i^2 L_j) + \sigma$$

$$a_5 = a_2 + (a_4 - \sigma)d_2/d_1$$

$$a_6 = -\sigma_I/\gamma_m$$

$$a_7 = a_5 - \sigma - a_2$$

$$b_1 = \sigma_I/(D_i^2\gamma_i)$$

$$b_2 = Pe_m - a_6$$

$$b_3 = -Pe_m\delta/(1-\delta)$$

APPENDIX C

This appendix contains a modified 1-D steady state model similar to that in Fry (1987). The purpose of this model is to investigate how the discontinuity in average macromolecular concentration profile across the endothelial-SI interface affects the solution predictions of the 1-D model.

This is a four-layers model. These layers are the endothelium, the SI, the IEL and the media. Here, in order to distinguish the results of 1-D and 2-D models, the additional subscripts o is used to denote the quantities in the 1-D model. The subscript iI is used to

denote the entrance of the SI into the fenestra of the IEL. The coordinates z_x represents the dimensionless distances from the lumen to adventitia sides in the region x. It is non-dimensionalized by the thickness L_x of this region.

The governing equations and the boundary conditions of this model are

$$- \frac{\partial^2 C_{jo}}{\partial z_j^2} + Pe_j \frac{\partial C_{jo}}{\partial z_j} = 0 \qquad (C.1)$$

$$C_{jo} = C_{ji}/\beta \quad \text{at } z_j = 1; \quad \text{and } C_{jo} = 1 \quad \text{at } z_j = 0 \qquad (C.2)$$

$$q_{jo} = - \frac{\partial C_{jo}}{\partial z_j} + Pe_j C_{jo} \qquad (C.3)$$

$$- \frac{\partial^2 C_{io}}{\partial z_i^2} + Pe_i \frac{\partial C_{io}}{\partial z_i} = 0 \qquad (C.4)$$

$$C_{io} = C_{ji} \quad \text{at } z_i = 0; \quad \text{and } C_{io} = C_{iI} \quad \text{at } z_i = 1 \qquad (C.5)$$

$$q_{io} = - \frac{\partial C_{io}}{\partial z_i} + Pe_i C_{io}, \qquad (C.6)$$

$$q_{io} = \frac{\gamma_j D_{zj} L_i A_j}{\gamma_i D_{ri} L_j A} q_{jo} \quad \text{at } z_j = 1 \text{ and } z_i = 0 \qquad (C.7)$$

$$- \frac{\partial^2 C_{Io}}{\partial z_I^2} + Pe_I \frac{\partial C_{Io}}{\partial z_I} = 0 \qquad (C.8)$$

$$C_{Io} = C_{iI} \quad \text{at } z_I = 0; \quad \text{and } C_{Io} = C_{Im} \quad \text{at } z_I = 1 \qquad (C.9)$$

$$q_{Io} = - \frac{\partial C_{Io}}{\partial z_I} + Pe_I C_{Io}, \qquad (C.10)$$

$$q_{io} = \frac{\gamma_I D_{zI} L_i \phi_I}{\gamma_i D_{ri} L_I} q_{Io} \quad \text{at } z_I = 0 \text{ and } z_i = 1 \qquad (C.11)$$

$$- \frac{\partial^2 C_{mo}}{\partial z_m^2} + Pe_m \frac{\partial C_{mo}}{\partial z_m} = 0 \qquad (C.12)$$

$$C_{mo} = C_{Im} \quad \text{at } z_m = 0; \quad \text{and } C_{mo} = 0 \quad \text{at } z_m = 1 \qquad (C.13)$$

$$q_{mo} = - \frac{\partial C_{mo}}{\partial z_m} + Pe_m C_{mo}, \qquad (C.14)$$

$$q_{mo} = \frac{\gamma_I D_{zI} L_m \phi_I}{\gamma_m D_{zm} L_I} q_{Io} \qquad \text{at } z_m = 0 \text{ and } z_I = 1 \tag{C.15}$$

where

$$C_{xo} = \frac{\tilde{C}_{xo} - \tilde{C}_A}{\tilde{C}_P - \tilde{C}_A}$$

$\tilde{C}_{xo}$ and Pe_x are the concentration and the Peclet number in the region x, respectively, β is the ratio of the concentrations between the leaky junction and the SI at the endothelial-SI interface, and C_{ji}, C_{iI}, and C_{Im} are the concentrations at the endothelial-SI, SI-IEL, and IEL-media interfaces, respectively. In addition, we have already assumed that the velocity ratio between the water and solute is unity in each layer.

The estimations of the Peclet numbers in each layer are the same as those in the 2-D model.

The solution of the boundary value problem (C.1) through (C.15) is

$$C_{jo} = \frac{(1-C_{ji}/\beta)\exp(Pe_j z_j) + C_{ji}/\beta - \exp(Pe_j)}{1 - \exp(Pe_j)} \tag{C.16}$$

$$C_{io} = \frac{(C_{ji}-C_{iI})\exp(Pe_i z_i) + C_{iI} - C_{ji}\exp(Pe_i)}{1 - \exp(Pe_i)} \tag{C.17}$$

$$C_{Io} = \frac{(C_{iI}-C_{Im})\exp(Pe_I z_I) + C_{Im} - C_{iI}\exp(Pe_I)}{1 - \exp(Pe_I)} \tag{C.18}$$

$$C_{mo} = \frac{C_{Im}[\exp(Pe_m z_m) - \exp(Pe_m)]}{1 - \exp(Pe_m)} \tag{C.19}$$

where C_{ji}, C_{iI} and C_{Im} are determined by the following linear algebraic equation set which is derived from boundary conditions

(C.7), (C.11) and (C.15) requiring that the mass flux be continuous across the each interface.

$$\begin{cases} C_{ji}[y_i + x_1 y_j \exp(-Pe_j)/\beta] - C_{iI} y_i \exp(-Pe_i) = x_1 y_j & (C.23) \\ -C_{ji} y_i + C_{iI}[y_i \exp(-Pe_i) + x_2 y_I] - C_{Im} x_2 y_I \exp(-Pe_I) = 0 & (C.24) \\ C_{iI} x_3 y_I - C_{Im}[y_m + x_3 y_I \exp(-Pe_I)] = 0 & (C.25) \end{cases}$$

Here

$$x_1 = \frac{\gamma_j D_j^2 L_i A_j}{\gamma_i D_i^2 L_j A}, \qquad x_2 = \frac{\gamma_I D_I^2 L_i \phi_I}{\gamma_i D_i^2 L_I}, \qquad x_3 = \frac{\gamma_I D_I^2 L_m \phi_I}{\gamma_m L_I}$$

$y_x = Pe_x/[\exp(-Pe_x) - 1]$ in region x

TABLE 1. The effect of β on the concentration distribution with $Pe_m = 4.4$ and $n_p = 2160$ ($\ell_{rf} = 0.01$)

	In leaky junction			In SI		In IEL		In media		
β \ z	0	0.9	1	0	1	0	1	0	0.5	1
0.001	1.0	5.22	200	0.201	0.201	0.201	0.201	0.201	0.181	0
0.01	1.0	1.40	20.1	0.201	0.201	0.201	0.201	0.201	0.181	0
0.1	1.0	1.02	2.01	0.201	0.201	0.201	0.201	0.201	0.181	0
1.0	1.0	0.98	0.20	0.201	0.201	0.201	0.201	0.201	0.181	0
2-D *	1.0	1.36	18.2	0.204	0.204	0.204	0.204	0.204	0.175	0

TABLE 2. The effect of β on the concentration distribution with $Pe_m = 0$

(concentration × 100)

	In leaky junction			In SI		In IEL		In media		
β \ z	0	0.9	1	0	1	0	1	0	0.5	1
0.001	100	96.4	96.0	0.10	0.10	0.10	0.09	0.09	0.05	0
0.01	100	73.3	70.4	0.70	0.70	0.70	0.69	0.69	0.34	0
0.1	100	27.3	19.2	1.92	1.92	1.92	1.87	1.87	0.94	0
1.0	100	12.1	2.32	2.32	2.32	2.32	2.26	2.26	1.13	0
2-D *	100	42.0	35.6	1.47	1.47	1.47	1.48	1.48	0.72	0

TABLE 3. The effect of β on the concentration distribution with Pe_m= 4.4 and n_p=225 (ℓ_{rf}=0.1)

	In leaky junction			In SI		In IEL		In media		
β \ z	0	0.9	1	0	1	0	1	0	0.5	1
0.001	1.0	13.0	20.3	0.020	0.020	0.020	0.020	0.020	0.018	0
0.01	1.0	1.88	2.43	0.024	0.024	0.024	0.024	0.024	0.022	0
0.1	1.0	0.53	0.25	0.025	0.025	0.025	0.025	0.025	0.022	0
1.0	1.0	0.40	0.025	0.025	0.025	0.025	0.025	0.025	0.022	0
2-D *	1.0	1.75	2.21	0.025	0.025	0.025	0.025	0.025	0.021	0

* The results of the 2-D model are obtained from Fig.9

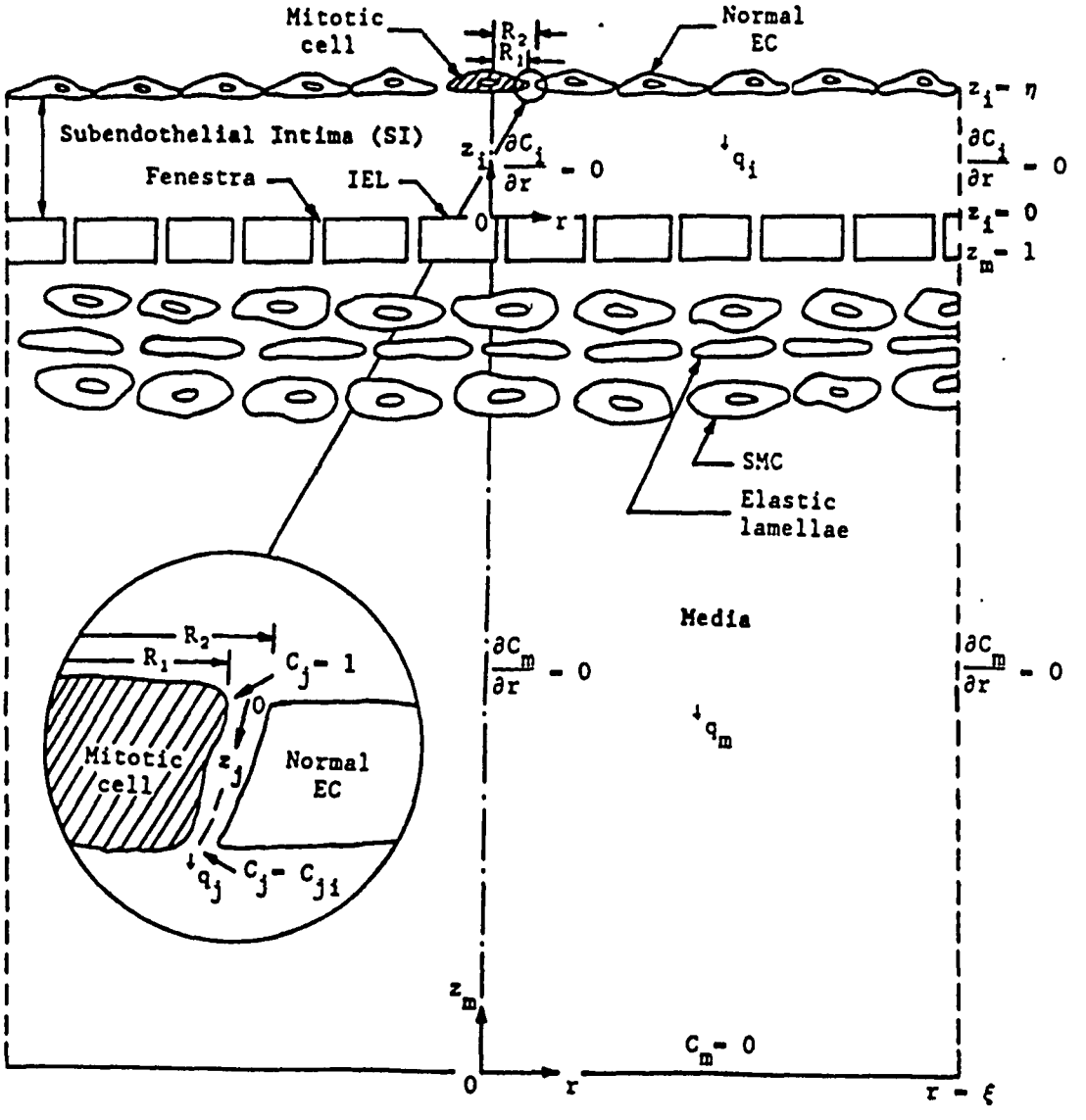
Mitotic cell
R_2
R_1
Normal EC
$z_i = \eta$
Subendothelial Intima (SI)
z_i $\frac{\partial C_i}{\partial r} = 0$
q_i
$\frac{\partial C_i}{\partial r} = 0$
Fenestra
IEL
0
r
$z_i = 0$
$z_m = 1$
SMC
Elastic lamellae
Media
$\frac{\partial C_m}{\partial r} = 0$
$\frac{\partial C_m}{\partial r} = 0$
q_m
R_2
R_1
$C_j = 1$
0
Mitotic cell
z_j
Normal EC
q_j
$C_j = C_{ji}$
z_m
$C_m = 0$
0
r
$r = \xi$

Figure 1

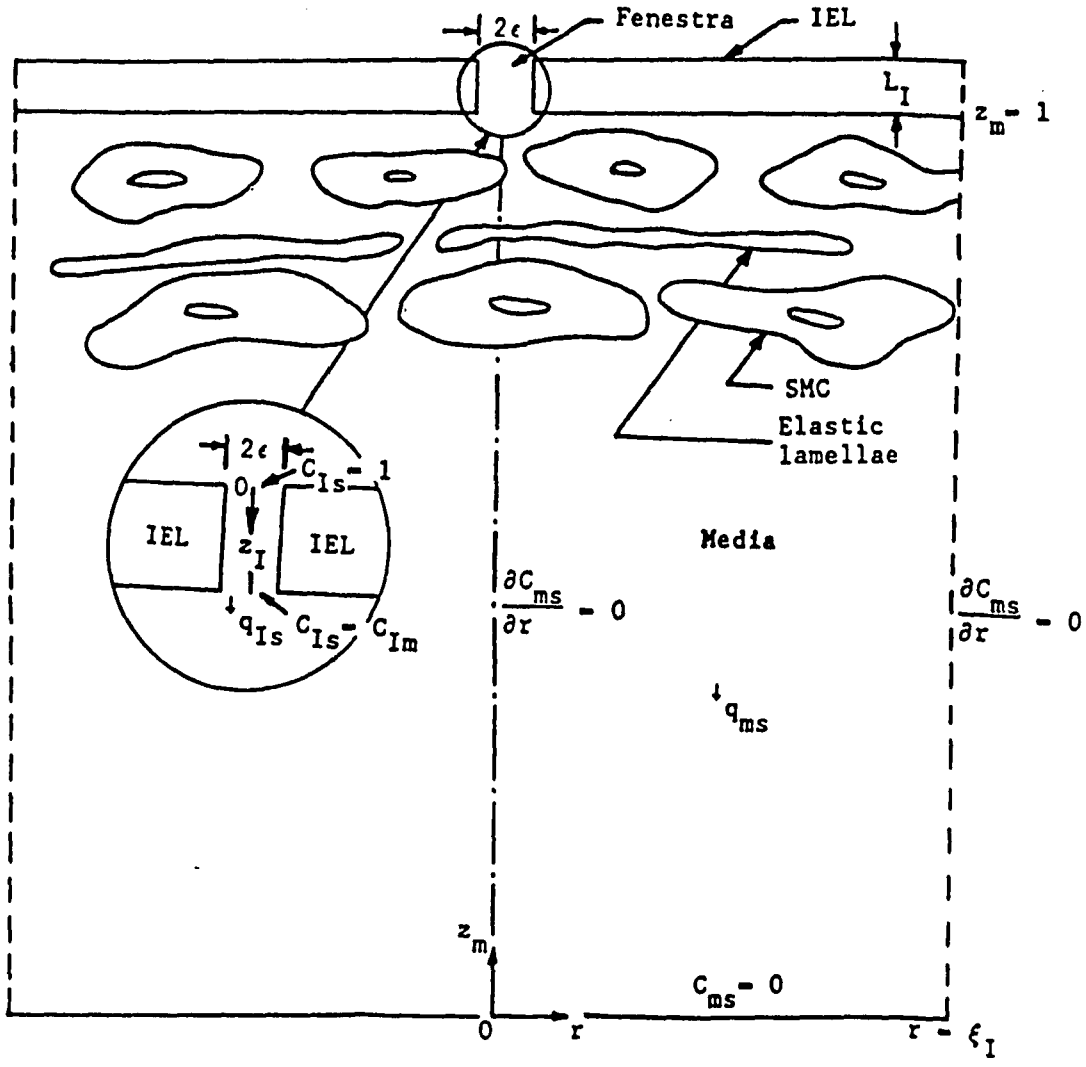
2ε
Fenestra
IEL
L_I
$z_m = 1$
SMC
Elastic lamellae
2ε
$C_{Is} = 1$
0
IEL
z_I
IEL
q_{Is} $C_{Is} = C_{Im}$
Media
$\frac{\partial C_{ms}}{\partial r} = 0$
$\frac{\partial C_{ms}}{\partial r} = 0$
q_{ms}
z_m
$C_{ms} = 0$
0
r
$r = \xi_I$

Figure 2

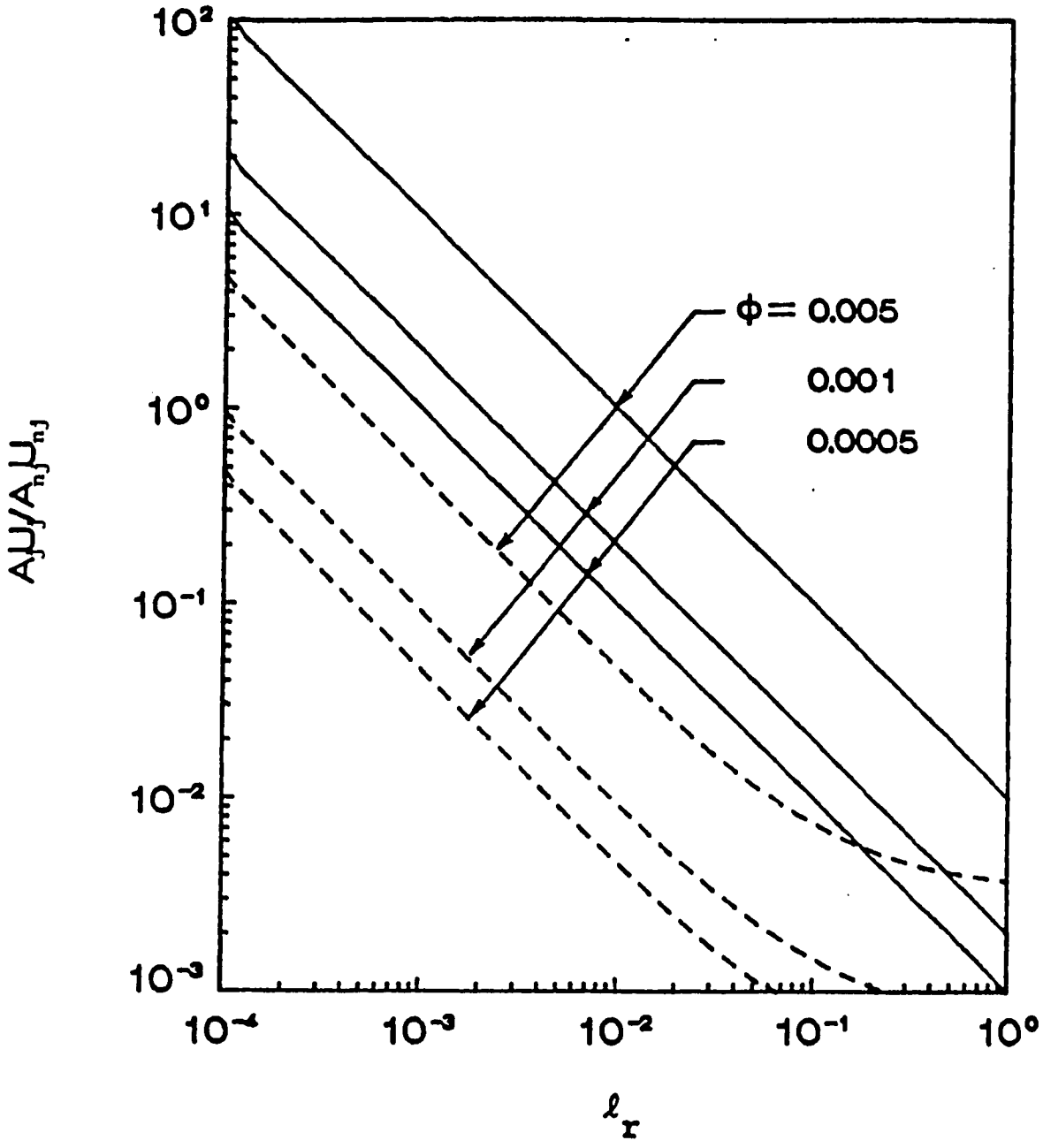
10^2
10^1
10^0
10^{-1}
10^{-2}
10^{-3}
$A_j U_j / A_{nj} U_{nj}$
$\phi = 0.005$
0.001
0.0005
10^{-4}
10^{-3}
10^{-2}
10^{-1}
10^0
ℓ_r

Figure 3

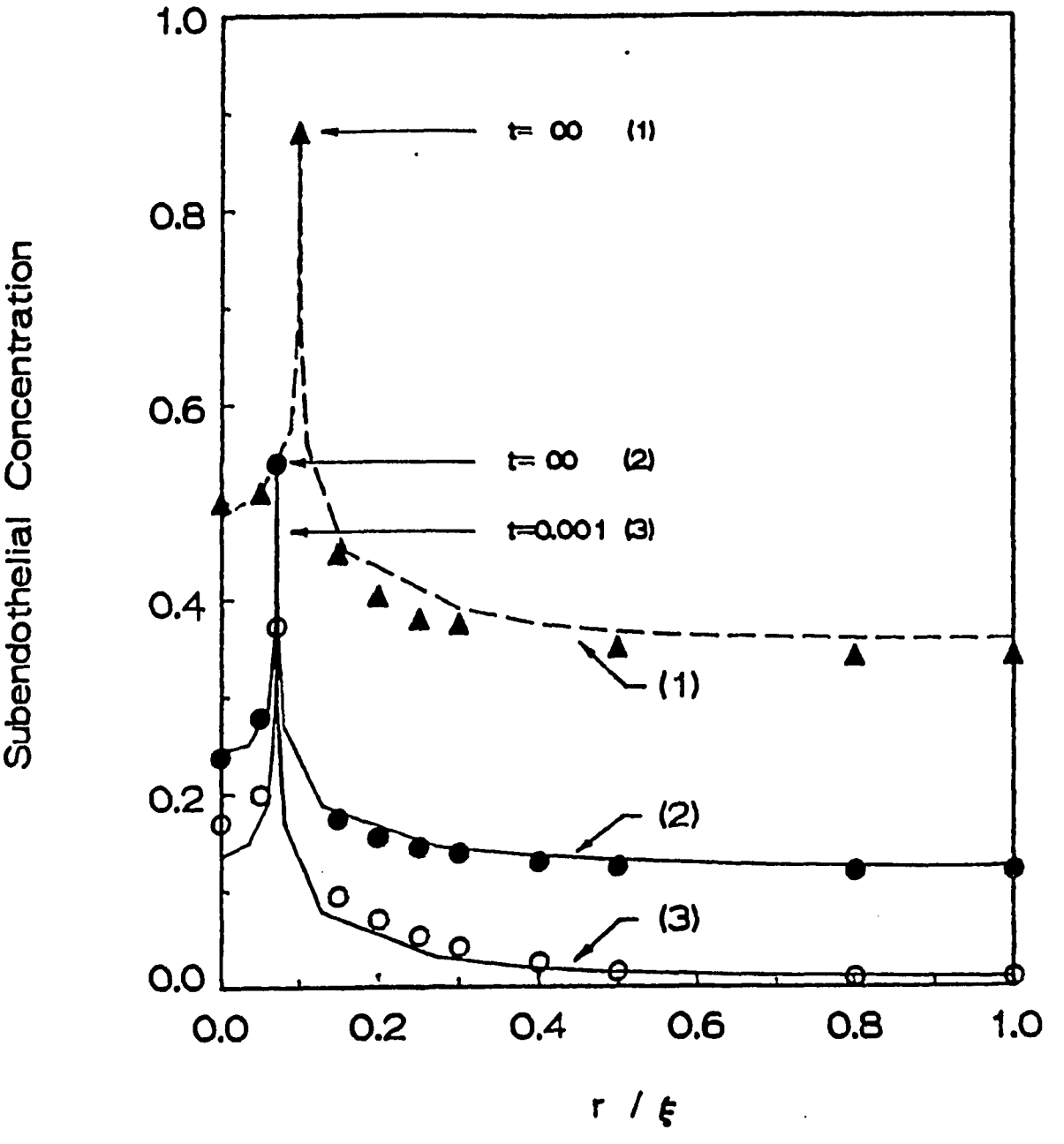
Subendothelial Concentration
1.0
0.8
0.6
0.4
0.2
0.0
0.0
0.2
0.4
0.6
0.8
1.0
r / ξ
t= ∞ (1)
t= ∞ (2)
t=0.001 (3)
(1)
(2)
(3)

Figure 4

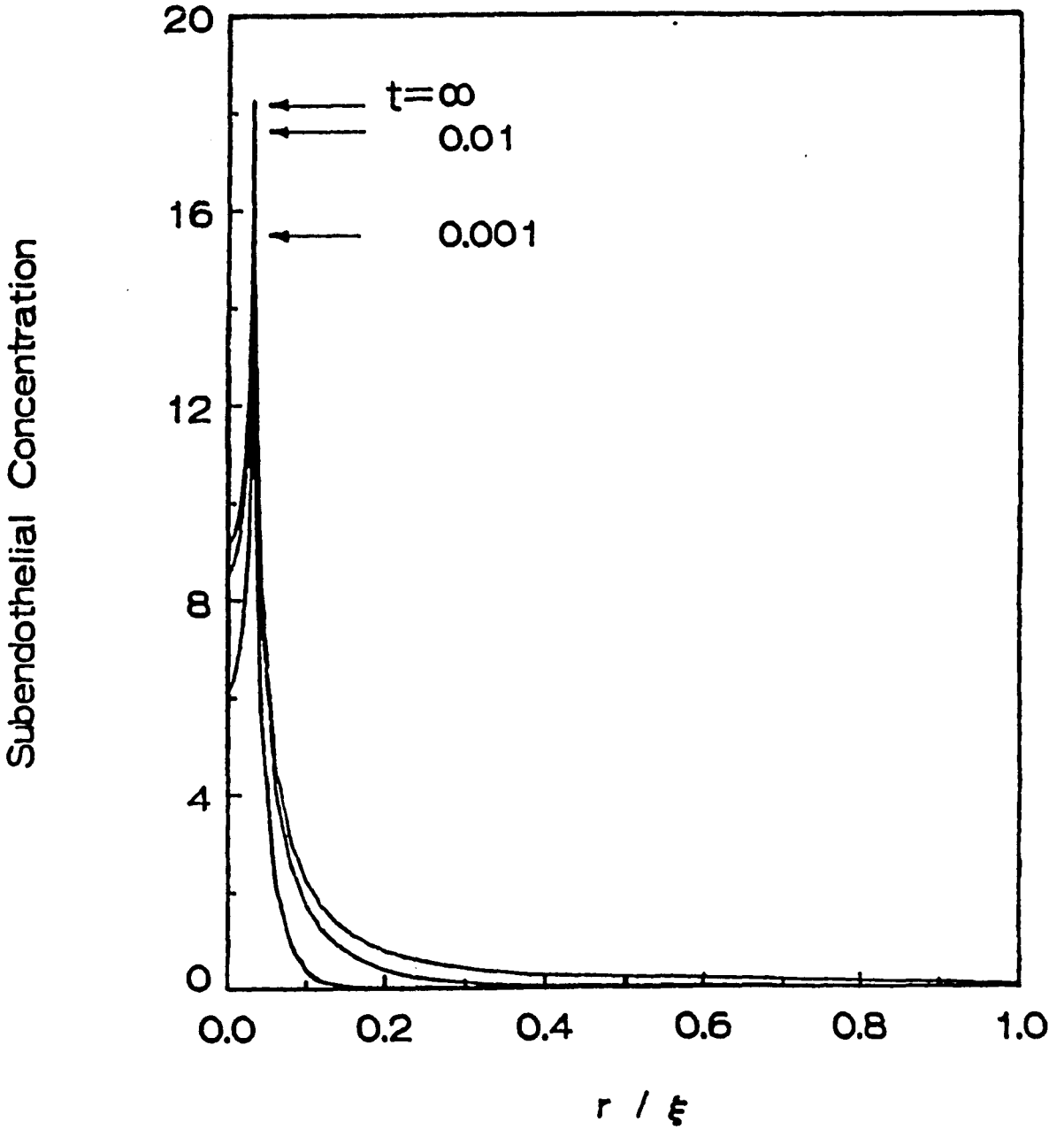
Subendothelial Concentration
20
16
12
8
4
0
t=∞
0.01
0.001
0.0
0.2
0.4
0.6
0.8
1.0
r / ξ

Figure 5

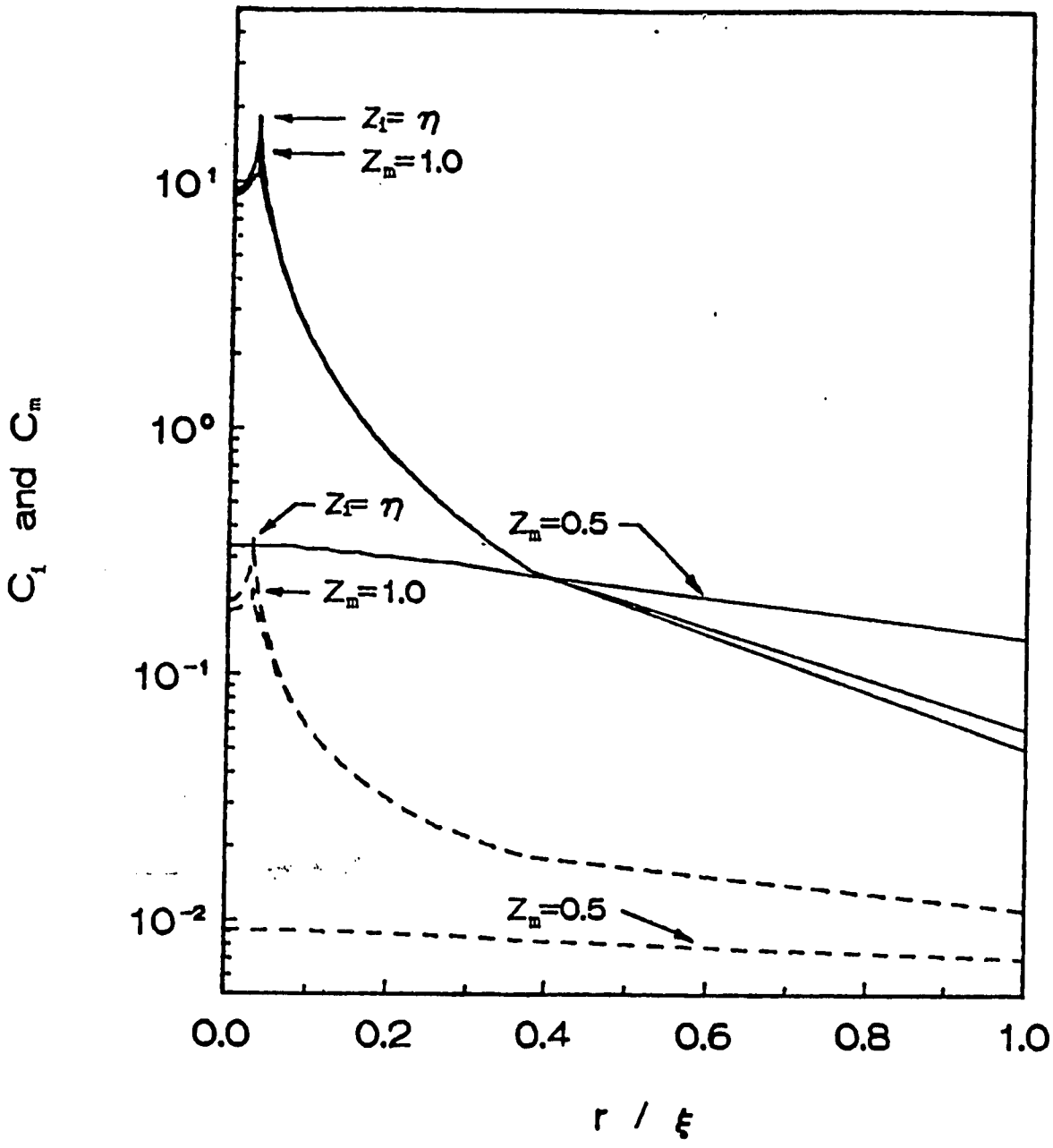
$Z_i = \eta$
$Z_m = 1.0$
10^1
10^0
$Z_i = \eta$
$Z_m = 0.5$
$Z_m = 1.0$
10^{-1}
10^{-2}
$Z_m = 0.5$
C_i and C_m
0.0
0.2
0.4
0.6
0.8
1.0
r / ξ

Figure 6

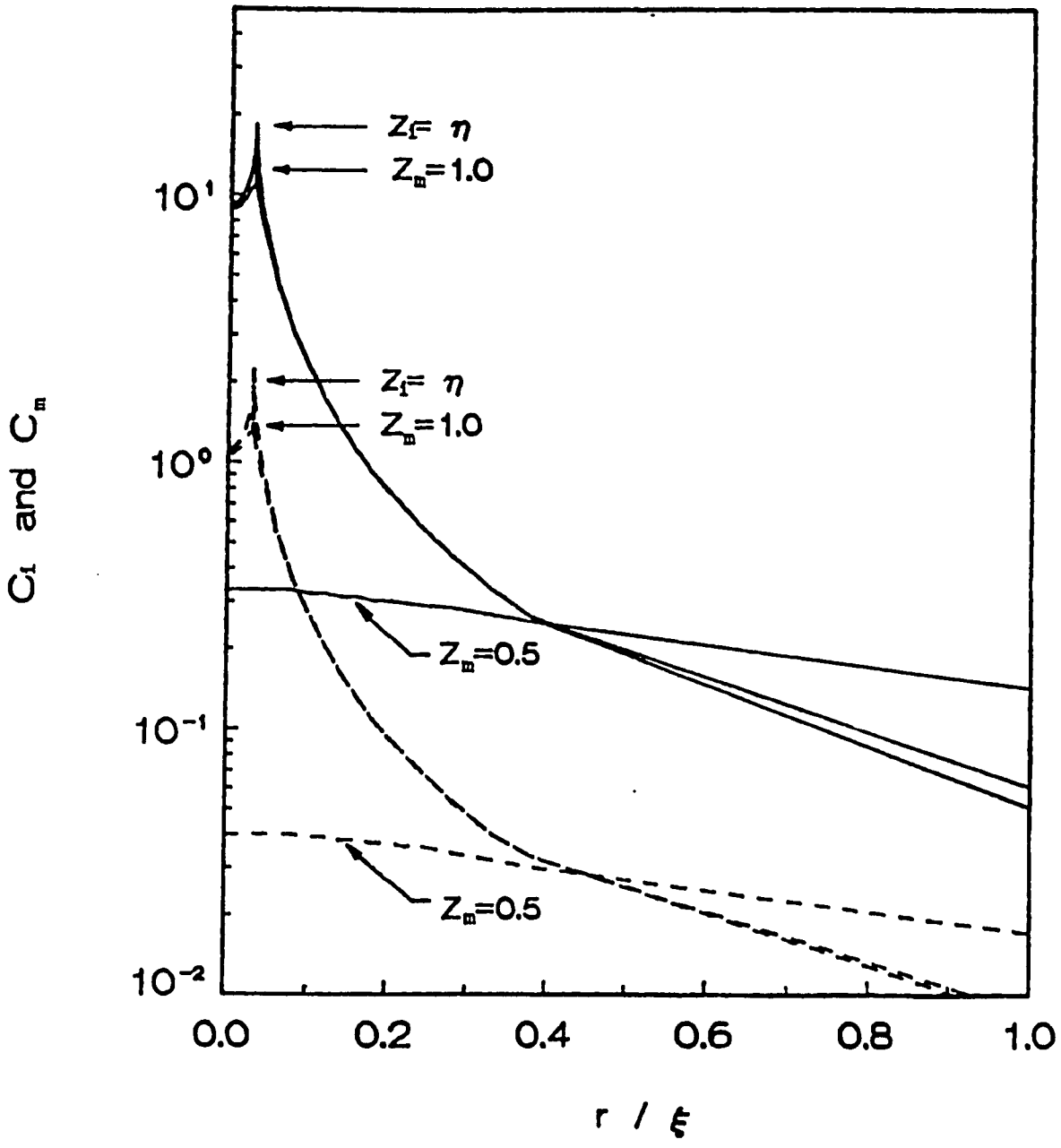
$Z_f = \eta$
$Z_m = 1.0$
$Z_f = \eta$
$Z_m = 1.0$
$Z_m = 0.5$
$Z_m = 0.5$
10^1
10^0
10^{-1}
10^{-2}
C_f and C_m
0.0
0.2
0.4
0.6
0.8
1.0
r / ξ

Figure 7

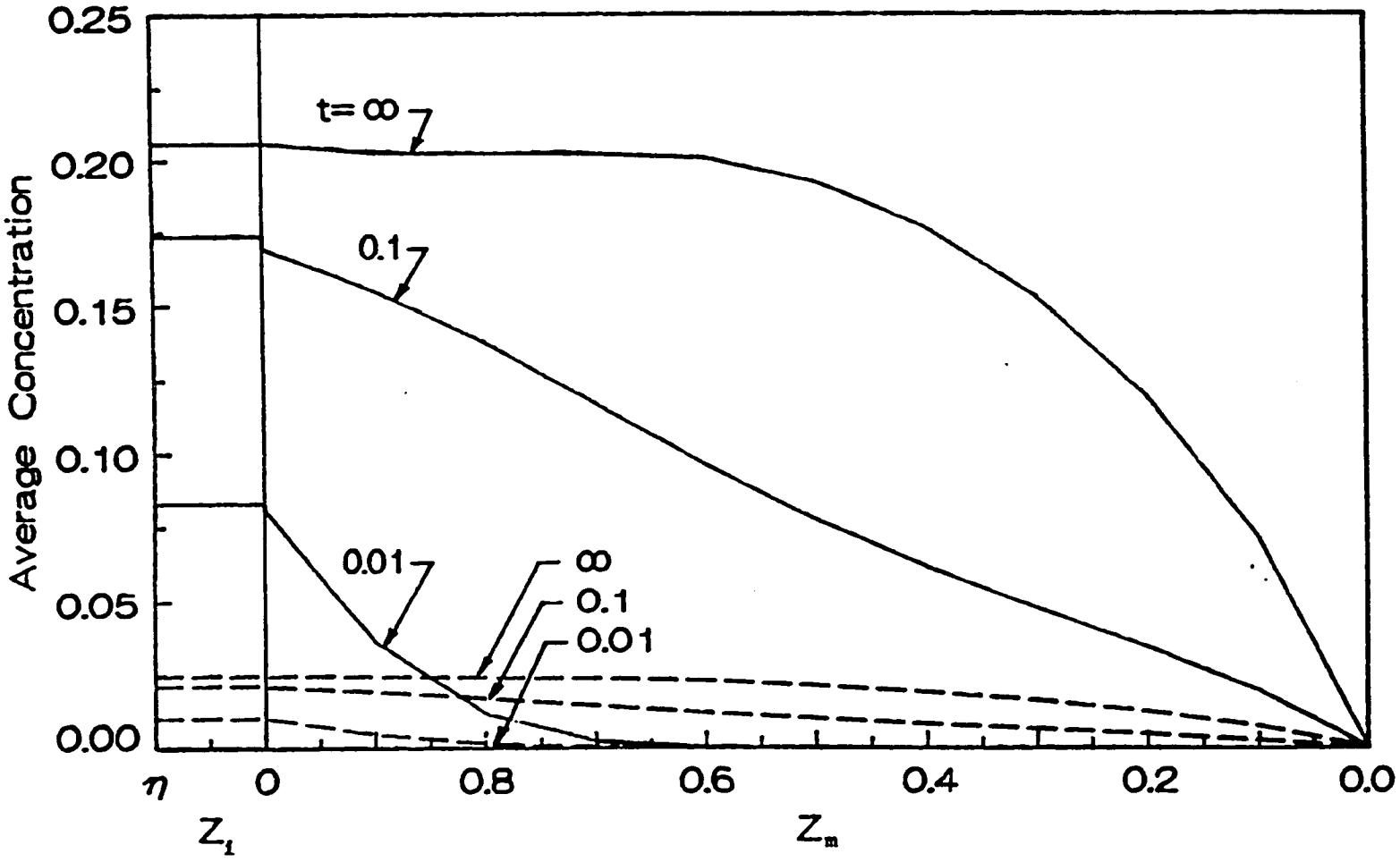
0.25
0.20
0.15
0.10
0.05
0.00
Average Concentration
t=∞
0.1
0.01
∞
0.1
0.01
η
0
0.8
0.6
0.4
0.2
0.0
Z1
Zm

Figure 8

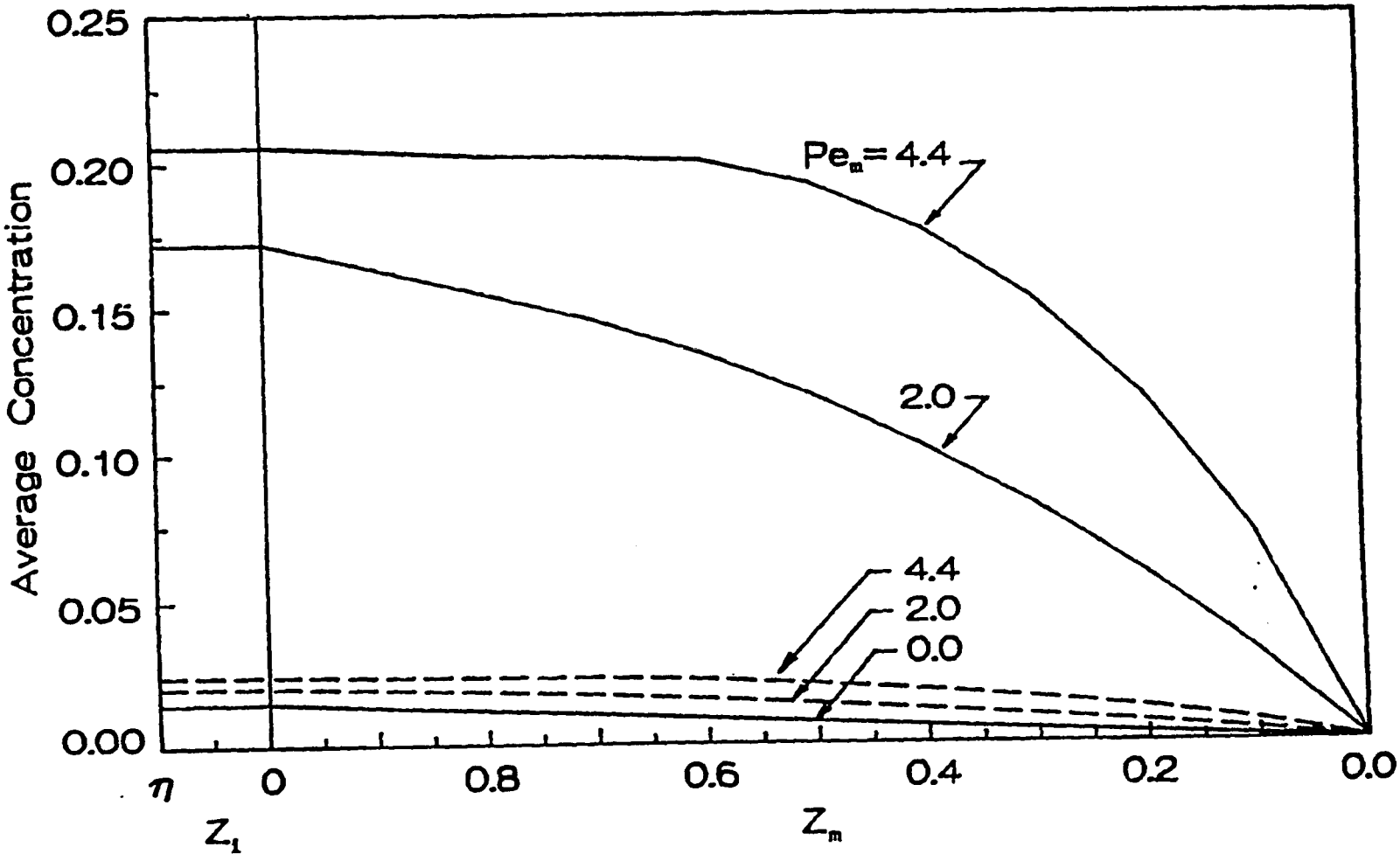
0.25
0.20
0.15
0.10
0.05
0.00
Average Concentration
Pe_m = 4.4
2.0
4.4
2.0
0.0
η
0
0.8
0.6
0.4
0.2
0.0
Z_1
Z_m

Figure 9

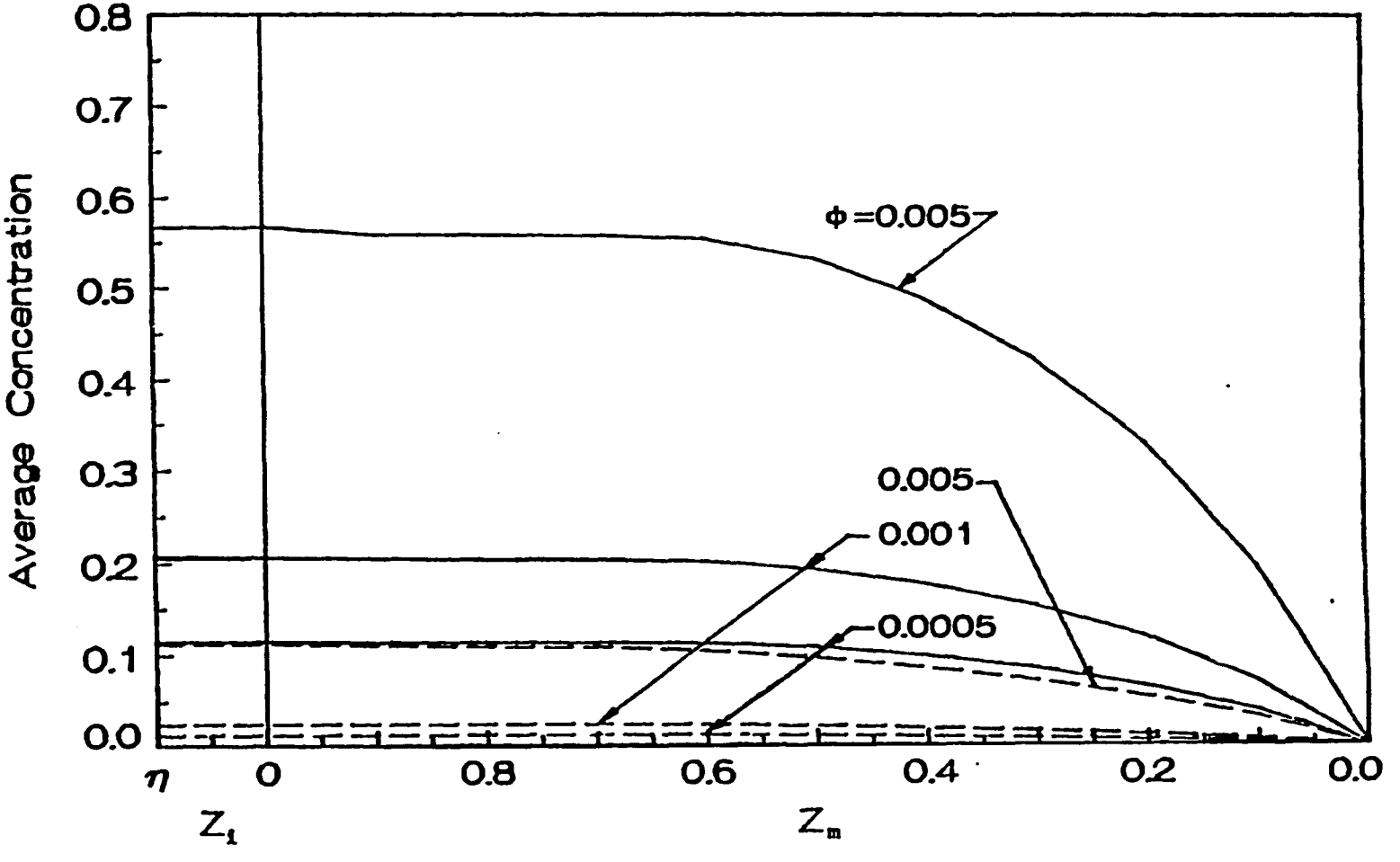
Average Concentration
0.8
0.7
0.6
0.5
0.4
0.3
0.2
0.1
0.0
ϕ=0.005
0.005
0.001
0.0005
η
0
0.8
0.6
0.4
0.2
0.0
Z_1
Z_m

Figure 10

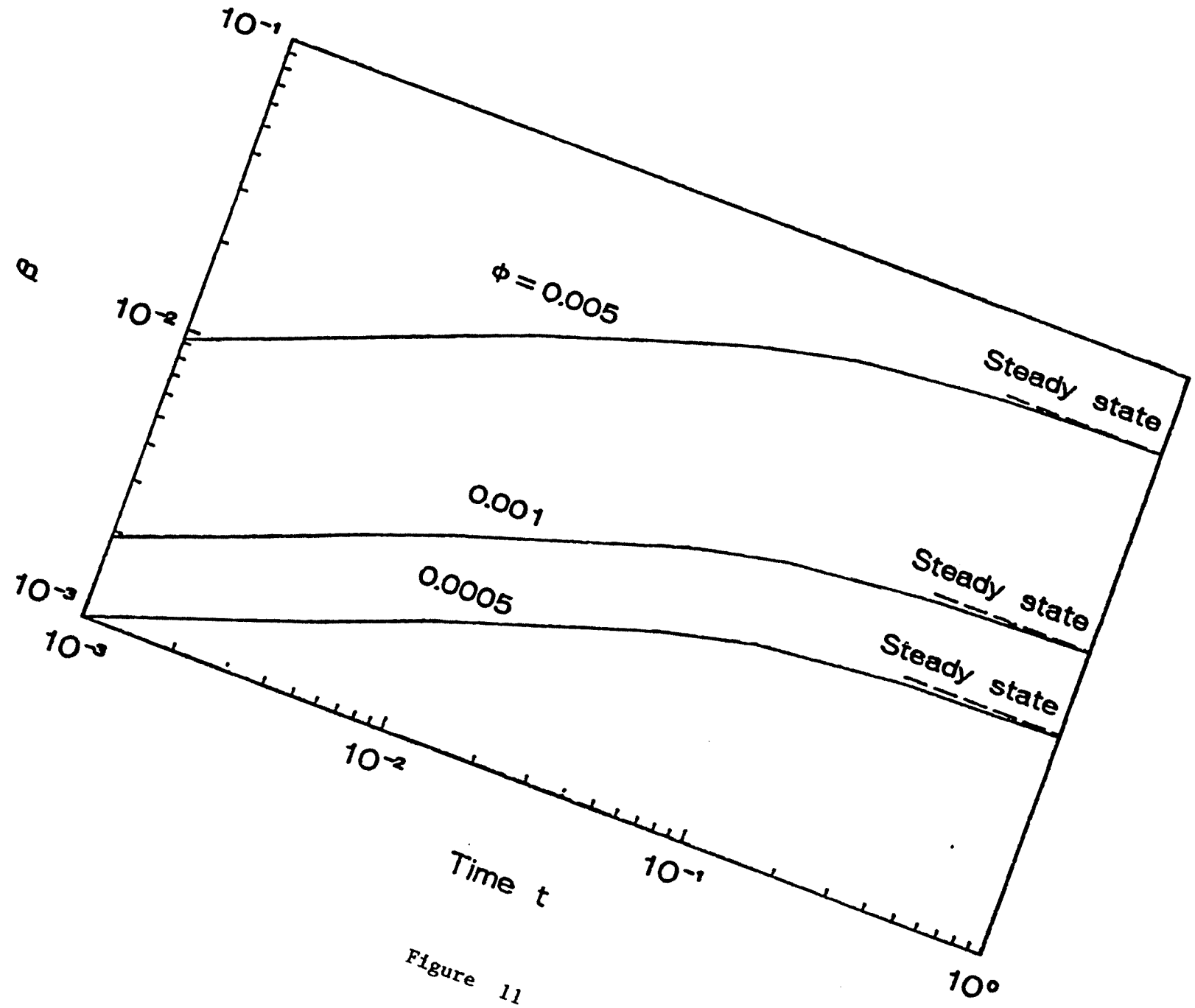
10⁻¹
Q
10⁻²
φ = 0.005
Steady state
0.001
Steady state
10⁻³
0.0005
Steady state
10⁻³
10⁻²
Time t
10⁻¹
10⁰

Figure 11

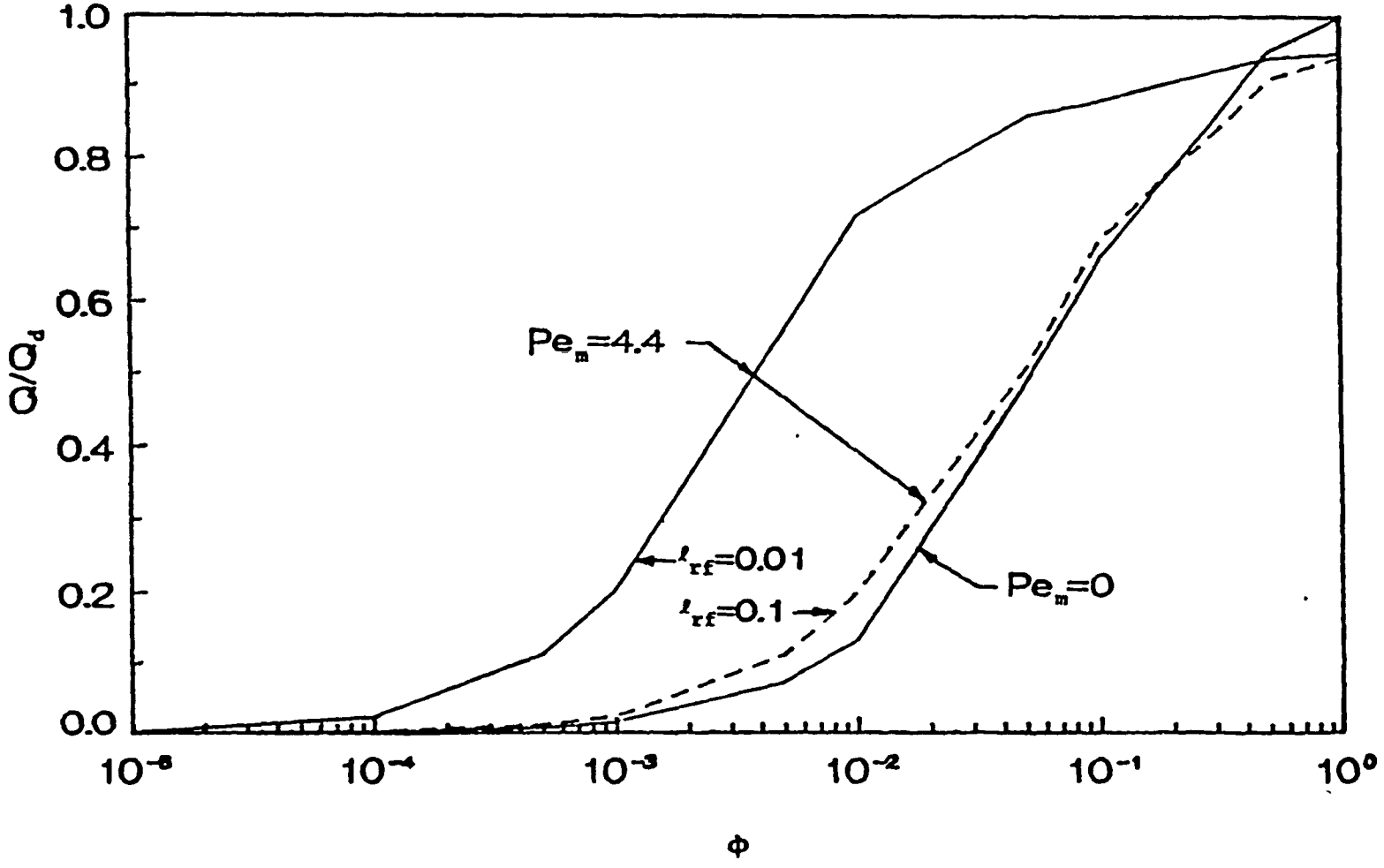
1.0
0.8
0.6
0.4
0.2
0.0
Q/Q_d
Pe_m=4.4
l_rf=0.01
l_rf=0.1
Pe_m=0
10^-5
10^-4
10^-3
10^-2
10^-1
10^0
Φ

Figure 12

CHAPTER 4

A New View of Convective-Diffusive Processes in the Arterial Intima

4.1 Introduction

Macromolecular transport across the arterial wall is closely linked to a variety of processes in the intima that are believed to play an important role in the subendothelial accumulation of lipid and the formation of the early foam cell lesion (Ross, 1986; Weinbaum et al., 1988a; Nerem and Levesque, 1983). The possible relationship between lipid transport and atherogenesis has been the subject of numerous experimental and theoretical investigations (Bratzler et al., 1977; Fry, 1983,1985 and 1987; Smith and Staples, 1982; Tzeghai et al., 1986; Weinbaum et al., 1985 and 1988b; Wen et al., 1988). In this chapter we shall present new models for filtration and for the convective-diffusive transport of macromolecules in the subendothelial intima (SI), which we believe shed a new light on the role that the internal elastic lamina (IEL) plays in modulating both the subendothelial water and macromolecular fluxes in the artery wall. We shall show that one-dimensional (1-D) convective-diffusive models for transport across the wall are inappropriate in the SI and can lead to physically spurious results, because the major transport processes occur parallel rather than normal to the endothelial surface in the vicinity of the leaky cleft exit due to the unique ultrastructure of the intima. It will be shown that the convective transport through the leaky clefts surrounding the small population of endothelial cells in turnover and the subsequent interaction with

the IEL are the dominant processes that determine the distribution of macromolecules in the SI in vivo.

4.1.1 The pore for macromolecules

Weinbaum et al. (1985) have proposed a new hypothesis for the transendothelial pathway via which molecules the size of albumin (effective diameter 7 nm) or larger enter the arterial wall. According to this hypothesis the large pore for macromolecular entry in arteries is not vesicular transport, but a pore created by the temporary disruption of the junction strands of a very small population of cells that are involved in cell turnover (cells either in mitosis (M phase) or in the process of sloughing due to cell death). The ferry boat transendothelial transport mechanism for plasmalemma vesicles proposed in Palade (1960) had been questioned after double labeling methods (Chien et al., 1982) and ultrathin serial section electron microscopic techniques (Bundgaard et al., 1983) both failed to reveal significant numbers of truly free cytoplasmic vesicles that were not attached to the plasma membranes of the cell in other planes of section via invaginating membrane structures. In Weinbaum et al. (1985) a relatively simple periodic axisymmetric two-dimensional (2-D) purely diffusive model of the arterial wall was constructed to test the quantitative feasibility of the leaky junction-cell turnover hypothesis. It was demonstrated in Weinbaum et al. (1985) that the typically two fold regional variations in steady state macromolecular permeability that had been measured in various animal species could be achieved by purely diffusive mechanisms if the number of cells with leaky junctions was increased from a few cells in a thousand to roughly twice this proportion. It was also shown that this behavior could not be

predicted by previous 1-D models since the diffusive flux entering the SI bore little relation to the open pore area. The numerical solutions showed that if the entire leaky cell had been removed, the pore area would increase by a factor of 400 but the flux would increase by only a factor of two. Thus, the fractional pore area required to account for the measured macromolecular permeability using the axisymmetric 2-D theory was of $O(10^{-5})$, whereas 1-D models, assuming that the entire damaged cell was leaky, would require that this fractional pore area be more than two orders of magnitude larger to predict the same diffusive flux.

The initial model in Weinbaum et al. (1985) neglected the varying resistance of the leaky cleft to macromolecules of increasing size and the non-isotropic structure of the underlying tissue due to the IEL and the elastic lamellae in the media. Both these complications, however, need to be considered if one is to design experiments in which the macromolecular leakage sites can be identified at the cellular level. Two models were developed. One was a short time model (Weinbaum et al., 1988b) which predicted the time dependent diffusion in the vicinity of the cleft exit (see inset of Fig.1). The second was a longer time model (Wen et al., 1988) which predicted the labeling of a larger region surrounding the leaky cell and the approach to steady state transport, see Fig.1. Both models included a diffusion coefficient D_{zj} for the leaky cleft which was dependent on the the size of the tracer molecule. Furthermore, the large non-isotropy of diffusion in directions normal and parallel to the endothelial surface caused by the IEL and elastic lamellae in the media was taken into account by introducing separate diffusion

coefficients for each direction. However, the IEL was not treated as a separate discrete barrier as in the present investigation.

4.1.2 Experimental verification of the leaky junction-cell turnover hypothesis

Direct experimental confirmation at the cellular level of the leaky junction-cell turnover hypothesis was first reported in Lin et al. (1988). The entire thoracic aortas of 12 rats were microscopically scanned using hemotoxylin to identify the nuclei of cells in M phase and Evans blue albumin (EBA) to detect the fluorescent leakage sites. This study showed that fluorescent sites for EBA permeability were extremely rare, approximately 5 cells in 10^4 (roughly one cell/mm^2), but that, after five minutes of labeling, 99 percent of all cells in M phase exhibited fluorescent EBA leakage sites that were somewhat larger than a single cell with a maximum fluorescent intensity centered on the cell in question. A second short time study using lucifer-yellow-labelled low density lipoprotein (LY-LDL) (Lin et al., 1989) revealed that the fluorescent regions could be confined to the cleft exit region of the leaky cell for this larger, more slowly diffusing molecules, and that approximately 80 percent of the cells in M phase exhibited leakage. The smaller percentages of M phase leakage sites for LY-LDL suggested that the junctions of cells opened and closed gradually during M phase (Chien et al., 1988). While most cells in M phase had leaky junctions, these cells only accounted for roughly 30 percent of the total leakage sites for EBA and 45 percent of the total leakage sites for LY-LDL. Further studies in (Lin, 1989) using IgG as a marker for cell death showed that a large fraction of the unidentified leakage sites could be accounted for by cells in the process of dying and/or

sloughing. More recent related studies (Chuang et al., 1990; Wu et al., 1990) have shown that the frequency of leakage site surrounding the intercostal branches of the aorta is approximately twice that of nonbranch areas and that in spontaneously hypertensive rats the overall frequency of leakage sites in the entire aorta is approximately 3 times that of normal rats.

At present there is a lack of accurate data to determine whether all or nearly all of the entry of LDL and albumin is through these widely scattered cellular leakage sites. However, there is increasing evidence which suggests that this is the case. Stemerman et al. (1986) first reported localized HRP reaction foci in the descending rabbit thoracic aorta that were roughly 100 cells in area after one minute of labeling and observed that the permeability of radioactive LDL in these areas was 47 times larger than control values. Shorter time studies reported in (Chuang et al., 1990), in which these reaction foci are more localized, indicate that virtually all cells in M phase are leaky to HRP and that the HRP reaction foci first observed in (Wu et al., 1990) represent enlargement due to lateral spread from leakage around a single cell. The localization of EBA leakage has been observed in (Chuang et al., 1990) after labeling periods of up to two hours in vivo. During this period the number of leakage sites approximately tripled, but, for reasons which we shall attempt to explain with the present model, fluoresence remained confined to a region which was roughly only 3 cell diameters from the leaky cell at the origin. These results suggest that even after long times there is very little permeability to EBA outside of these localized cellular leakage sites. A different behavior was observed for HRP which is believed to be just small enough to pass through

normal clefts. In this case a diffuse labeling of the entire wall was observed en face after four minutes of HRP injection, although the initial leakage after 30 seconds was confined to the isolated leakage sites noted above.

4.1.3 Convective transport

The 2-D models described in (Weinbaum et al., 1985 and 1988b; Wen et al., 1988) are limited to diffusion. However, it is well recognized that convective transport of macromolecules is at least as important as diffusive transport in the arterial wall in vivo. Significant differences in media concentration profiles due to transmural pressure have been measured by Fry (1983) and Fry et al. (1986), and experimental measurements of transmural albumin transport within the media of rabbit thoracic aorta (Tedgui and Lever, 1985) have shown that the Peclet number in the normal direction in this vessel is between 4 and 5 for an intact endothelium and increases to 6-11 when the endothelium is denuded. With the exception of the study by Tzeghai et al.(1986), previous models for convective-diffusive transport in the arterial wall have been based on 1-D theories in which there are continuities of water and solute fluxes and of macromolecular concentrations at interfaces between different layers, but discontinuities in water velocity and concentration gradient at interfaces of barriers (endothelium and IEL) where the cross-sectional area for transport changes abruptly (Fry, 1985 and 1987). The model by Fry (1985 and 1987), which has strongly influenced the present study, treats the IEL as a discrete barrier and divides the artery wall into four layers as shown in Fig.1: the endothelium, the SI, the IEL and the media. Using baseline parameter values given in Table 1 of Fry (1987), Fry's model predicted that the

IEL can act as a molecular sieve when convection is present and lead to a higher macromolecular concentration in the SI than in the lumen. These results were used to explain the findings by Smith and Staples (1982) on post-mortem human arteries that the SI concentration of LDL exceeded that in the lumen and Fry's in vitro observations on pressurized, deendothelialized minipig aorta which indicated some macromolecular sieving in the superficial layers of the intima (Fry et al., 1986).

In an earlier investigation (Tzeghai et al., 1986), the authors attempted to incorporate convection into the 2-D diffusion model in Weinbaum et al. (1985). This earlier study introduced two flawed simplifying assumptions, whose consequences were not fully appreciated until the present model was developed. First, it was reasoned that since the normal clefts were much more numerous than the leaky cleft, and therefore provided the major contribution to the total water flux, one would not need to treat the small contribution to the total water flux that passes through the leaky junction separately. Second, the authors assumed a simple 1-D continuity equation for the water flux in each layer that was the same as for the 1-D models in (Fry, 1985 and 1987). The difficulty with the first assumption is that the macromolecular flux that enters the artery wall is strongly dependent on the water flux that enters through the leaky cleft which provides a much lower resistance. Thus, a quantitative model is required to first determine how the total water flux is apportioned between leaky and normal clefts. The leaky cleft can have a much larger Peclet number than a normal cleft since the present theory shows that the hydraulic resistance of a leaky cleft is two orders of magnitude smaller than a normal cleft with an intact

junctional protein strand. The convective flux of macromolecules through the leaky cleft will, therefore, be much larger than that predicted by the model in Tzeghai et al. (1986).

The second assumption in the last paragraph lies at the heart of the new model for the SI developed in the present study. If one uses a 1-D model for filtration there will be a large discontinuity in the water velocity at the leaky cleft exit because of the abrupt change in transport area as the water enters the SI. It will be shown later that this simplifying assumption leads to spurious behavior, which is suggestive of macromolecular sieving in the intima.

A third fundamental difficulty with existing 1-D convective-diffusive models is that the IEL presents a second transport barrier once the solute has entered the SI through the leaky cleft. Ultrastructural studies of the IEL (Campbell and Roach, 1981; and Song and Roach, 1983) in the major arteries have revealed that the fenestra in this layer are typically 1 μm diameter widely dispersed holes which comprise only between 0.5 and 2.0 percent of the surface area of large arteries. The solute is thus trapped in a narrow space which is bordered from below by impervious elastic tissue with widely separated holes and from above by an endothelium with two types of discrete pores: normal clefts through which only water can enter and leaky clefts through which both water and macromolecules can enter, see Fig.1. The convective spreading of the solute in the SI in the vicinity of the leaky cleft exit is thus primarily parallel rather than normal to the endothelial surface. A new model for the SI is, therefore, proposed in this investigation which describes the lateral (horizontal) (see Fig.1) transport in this critical subendothelial layer. An important feature of this model is that it must correctly

describe the lateral variation of the pressure field in the SI since this pressure field controls the distribution of the water flux through the leaky and normal clefts and thus the convective flux of macromolecules through the leaky cleft.

Valuable insight into the proper formulation of the new model for the intima was obtained from a recent model described in Chapter 3 of this dissertation. This model, like the present model, divides the artery wall thickness into the four distinct layers as shown in Fig.1. The key difference between the present model and the model in last Chapter is that the convective transport in the model in last chapter was assumed to be 1-D, i.e. a uniform normal velocity was assumed in each layer and convective transport in the lateral direction was neglected. This assumption leads to a sharp discontinuity of the normal velocity component at the exit of leaky cleft, since the normal velocity in the leaky cleft is much greater than in the SI due to the abrupt change in area discussed earlier. The model in last chapter predicted that the concentration at the exit of the leaky cleft could be as much as 18 times larger than that in the lumen. This increase in concentration was required to conserve solute and thus compensate for the abrupt decrease in the convective flux at the cleft exit. We shall show in the Discussion of this chapter that if a more rigorous model is used for the velocity field in which the discontinuity in the water velocity is not present, subendothelial concentrations greater than that in the lumen can not occur unless a sieving structure is present in the intima.

4.2 Mathematical Models

4.2.1 Model description

In the proposed new model, the arterial wall is divided into four discrete layers as shown in Fig.1. The loose connective tissue of the adventitia layer will not be considered since it is not a significant transport barrier.

The distribution of leakage sites in the endothelial layer is random. Adopting the approach in (Tzeghai et al., 1986; Weinbaum et al., 1985 and 1988b; Wen et al., 1988), we assume that the cells with transiently leaky junctions can be arranged in a periodic surface array whose number density on a regional basis is the same as the average density in the random array. If the spacing between the cells with leaky junctions is 2ξ in this periodic array, then one can draw a circle of radius ξ centered on each leaky cell and define a periodic unit in the subendothelial space as shown in Fig.1. This periodic unit is a cylinder whose height L_w is the sum of the thickness L_j of the endothelial layer, L_i of the SI, L_I of the IEL and L_m of the media. The cell turnover parameter ϕ describing the frequency of leaky cells is defined as R_1^2/ξ^2, where R_1 is the effective radius of endothelial cell (EC). In addition, the leaky cleft is approximated by a ring-source in both the filtration and macromolecular transport models for the SI, with the ring width much narrower than the radius of the EC.

Because the thickness of the SI is two orders of magnitude smaller than that of the media in lesion-free areas, one can integrate all physical variables across the SI in the normal

direction. The resulting equations for filtration and convective-diffusion in the SI are 1-D and depend only on the lateral coordinate r. In these equations the water and solute fluxes in the normal direction at the upper and lower boundaries of the SI can be treated as the source terms.

A major difficulty in modeling the IEL is that the distribution of the fenestra in the IEL are randomly related to the leakage sites in the endothelium, hence the exact treatment of the IEL structure is a 3-D convective-diffusion problem. This problem can be simplified, however, because the typical inter-fenestral spacing in the IEL, roughly 10 μm (Song and Roach, 1983), is comparable to the radius of an endothelial cell (Weinbaum et al., 1985). Since the number of the cells with leaky junctions is typically one in a thousand cells or less (Lin et al., 1988), there are at least one thousand fenestrae in each periodic unit. Therefore, the fenestral pores in the IEL do not have be considered separately and the IEL can be approximated by a continuous uniform porous layer. The transport of macromolecules in the SI and the media in each periodic wall unit can thus be treated as an axisymmetric boundary value problem. The macromolecular diffusion in the media is non-isotropic, mainly due to the elastic lamellae in the media.

4.2.2 Mathematical formulation

The four layers of the arterial wall treated in this chapter are each denoted by a subscript. These subscripts are j for the leaky endothelial junction, i for the SI, I for the IEL, and m for the media; the subscript nj is used for the normal junction and the subscripts ji and Im are used to denote the exits of the leaky junction into the SI and of the fenestra into the media,

respectively. U and W represent the velocities in lateral and normal directions, respectively.

The tilde on top of a parameter indicates that it is dimensional, and the tilde is removed when the parameter is non-dimensionalized. The water velocity $\tilde{U}_x$ (or $\tilde{W}_x$), the pressure $\tilde{p}_x$, the hydraulic conductivity $(\tilde{L}_p)_x$ and the macromolecular concentration $\tilde{C}_x$ in a given region x are non-dimensionalized by using the hydraulic conductivity in the media $(\tilde{L}_p)_m$, the pressure $\tilde{p}_L$ and concentration $\tilde{C}_L$ in the lumen,

$$U_x = \frac{\tilde{U}_x}{(\tilde{L}_p)_m \tilde{p}_L}, \qquad W_x = \frac{\tilde{W}_x}{(\tilde{L}_p)_m \tilde{p}_L} \tag{1}$$

$$p_x = \frac{\tilde{p}_x}{\tilde{p}_L}, \qquad C_x = \frac{\tilde{C}_x}{\tilde{C}_L}, \qquad (L_p)_x = \frac{(\tilde{L}_p)_x}{(\tilde{L}_p)_m} \tag{2}$$

The dimensionless coordinates and time are given as

$$t = \frac{D_{zm}\tilde{t}}{L_m^2}, \quad r = \frac{\tilde{r}}{L_m}, \quad z_j = \frac{\tilde{z}_j}{L_j}, \quad z_I = \frac{\tilde{z}_I}{L_I}, \quad z_m = \frac{\tilde{z}_m}{L_m} \tag{3}$$

where D_{zm} is the diffusion coefficient in the media in the normal direction. These general equations apply to each of the four layers and will not be repeated below.

(1) Model for Filtration

One of the most important features of the filtration in the arterial wall is that the water enters the SI through both the normal and leaky junctions in contrast to macromolecules which enter only through leaky junctions. The pressure drop across the leaky junction will be much smaller than that across the normal endothelium, because

the hydraulic conductivity of the normal endothelial clefts, the present theory indicates, is several orders of magnitude smaller than that of the leaky cleft. Whereas the pressure in the lumen is uniform over a periodic wall unit, large lateral pressure gradients will exist in the SI from the exit of the leaky junction towards the center and edge of the periodic unit, respectively, due to the large differences in hydraulic conductivity for the normal and leaky clefts and the filtration barrier created at the bottom boundary of the SI by the IEL. Therefore, after crossing the leaky cleft, the water flux will be shunted laterally in the SI, and then slowly seep through the fenestral openings in the IEL. The apportionment of the water flux through leaky and normal clefts is very important in determining the macromolecular flux into the artery wall and the lateral spread of the macromolecules in the SI from a leakage site.

The treatment of the filtration boundary value problem just described is subtle since the lateral pressure distribution just above and below the IEL are both unknown. To simplify this problem, we shall treat the endothelial layer, except for the leaky cleft, as an uniform porous barrier across which the local flux is proportional to the local transendothelial pressure drop. The proportionality constant, the hydraulic conductivity of the normal endothelium $(L_p)_e$, is obtained from a newly developed model for filtration flow in an intercellular cleft with both junction strand pores and cross-bridging proteoglycan fibers (Tsay et al., 1989).

(A) Boundary value problem for SI

The boundary value problem for filtration in the SI can be obtained from Fig.1 by replacing the concentration (C) and the solute flux (q) in this figure by the pressure (p) and water velocity (U or

W). Because the leaky cleft is treated as a ring-source, the lateral velocity U_i is discontinuous across $r=R_1$, the exit of the leaky cleft. Therefore, different continuity equations are required for the region $0\le r<R_1$ (denoted by k=1) and the region $R_1<r\le\xi$ (denoted by k=2).

$$\frac{dU_{ik}}{dr} + \frac{1}{r} U_{ik} - \frac{1}{\eta} [W_{njk}(r) - W_{Ik}(r)] \qquad k=1,2 \qquad (4)$$

where $\eta = L_i/L_m$, and U_{ik} (k=1,2) is the lateral velocity component in each region. The water velocities across the leaky cleft, W_j, the normal intact endothelial layer, W_{nj}, and the IEL, W_I, are related to the local pressure drop across the corresponding layer,

$$W_j = (L_p)_j[1 - p_{i1}(R_1)] \qquad (5)$$

$$W_{njk}(r) = (L_p)_e[1 - p_{ik}(r)] \qquad k=1,2 \qquad (6)$$

$$W_{Ik}(r) = (L_p)_I[p_{ik}(r) - p_{Im}(r)] \qquad k=1,2 \qquad (7)$$

Here p_{ik}(k=1,2), the pressure in the SI, and p_{Im}, the pressure at the IEL-media interface , are unknown functions of r. The leaky cleft is treated as an uniform open channel in which the resistance of cross bridging fibers is neglected. Accurate solutions for a periodic cross-bridging fiber array in a channel in Tsay and Weinbaum (1990) show that this resistance is very small for fiber spacings that would permit the passage of LDL (22 nm), as will be discussed later. The dimensionless hydraulic conductivity of the leaky cleft is given by

$$(L_p)_j = \frac{\Delta R^2}{12\mu L_j^2}/(\tilde{L}_p)_m \qquad (8)$$

where μ is the viscosity of water, and ΔR is the width of leaky cleft.

The hydraulic conductivity of the normal endothelium is estimated by a new model proposed in Tsay et al. (1989) and shown in Fig.2. This figure shows the idealized geometry and pertinent dimensions of the mathematical model for the normal cleft with its junction strand and cross-bridging fibers. In this model the pores in the normal junction are circular discrete holes formed by individual missing proteins in an interlaced arrangement of intramembraneous protein strands in opposing membranes that form the junctional complexes. The expression for $(L_p)_e$ includes the resistance of the wide parts of the cleft on each side of the junction strand Rs_1 and Rs_3, which can have cross-bridging fibers as proposed in fiber matrix model of Curry and Michel (1980), and the resistance of the junction strand with its pores Rs_2,

$$(L_p)_e = [(Rs_1 + Rs_2 + Rs_3)(\bar{L}_p)_m]^{-1} \qquad (9)$$

The expression for these resistances are given in Tsay et al. (1989) by

$$Rs_y = \frac{3\mu_{eff}}{B^3 L_{jt}}[L_y/2 + \frac{1}{d^2}\sum_{n=1}^{\infty}\tanh(\lambda_n L_y)\sin^2(\lambda_n d)/\lambda_n^3] \quad y=1,3 \qquad (9a)$$

$$\lambda_n = n\pi/(r_p n_p) \qquad n=1,2,3,\ldots$$

$$Rs_2 = \frac{16\mu n_p L_2}{\pi r_p^3 L_{jt}} \qquad (9b)$$

where L_1 and L_3 are depths between the protein strand and the lumen and abluminal margins of the cleft, respectively; L_2 and r_p are the depth and radius of the pores in the protein strands, respectively, B is the half width of the wide portion of the cleft; $d=\pi r_p^2/4B$; L_{jt} is

the total junctional length per unit endothelial surface area, and n_p is the number period of missing proteins, which is defined as the ratio of the distance between the pores to the diameter of the pores. μ_{eff} in eqn. (9a) is the effective viscosity of the wide part of the cleft which includes the additional hydraulic resistance of possible cross-bridging fiber matrix components as proposed in the fiber matrix theory of Curry and Michel (1980). Rigorous analytic expressions for μ_{eff} for the doubly periodic fiber geometry shown in Fig.2 have been derived in Tsay and Weinbaum (1990). These expressions, which show how μ_{eff} varies with the channel height 2B, the fiber radius a and spacing 2W, are too lengthy to include herein and the reader is referred to the original reference (Tsay and Weinbaum, 1990). The results of this new theory have important implications for the possible structure of the interendothelial cleft of arterial endothelium that will be elaborated upon later in this chapter.

In order to estimate the hydraulic conductivity $(L_p)_I$ of the IEL, a local 2-D model was developed using the simplified periodic unit for the fenestral pore interaction shown in Fig.3. This model is described in Appendix A. $(L_p)_I$ depends on both the geometrical structure of the IEL and the interaction of the water jets through the fenestral pores in the underlying media. In this model we have assumed that the intrinsic hydraulic conductivity of the tissue matrix in the fenestral pores is the same as that in the media. This assumes that the interstitial space across the IEL is continuous in structure.

From Appendix A,

$$(L_p)_I = \frac{W_f \phi_I}{1 - W_f \phi_I} \tag{10}$$

where ϕ_I is the fractional area of the fenestra in the IEL and W_f is the water velocity in the fenestra; the latter depends on the radius ϵ of fenestra, the distance $2\xi_I$ between the fenestrae, L_I and L_m. If the fractional area of the fenestra is small enough such that $\phi_I W_f << 1$, then it can be shown that $(L_p)_I$ is proportional to ϕ_I. In this limit, the interactions between the fenestrae can be neglected.

The relationship between the water velocity and the pressure in the SI is assumed to obey Darcy's law, and the intrinsic hydraulic conductivity in the SI is assumed to be the same as that in the media. Therefore,

$$U_{ik} = - \frac{dp_{ik}}{dr} \qquad (k=1,2) \tag{11}$$

Conservation of water flux and continuity of pressure in the SI at $r=R_1$ require that

$$\eta \, [U_{i2}(R_1) - U_{i1}(R_1)] = \Delta R W_j \tag{12}$$

and

$$p_{i2}(R_1) = p_{i1}(R_1). \tag{13}$$

The axisymmetric condition at r=0 and the periodic condition at $r=\xi$ require

$$U_{i1}(0) = 0 \qquad \text{and} \qquad U_{i2}(\xi) = 0. \tag{14}$$

(B) <u>Boundary value problem for the media</u>

The filtration in the media is assumed to be isotropic and obeys Darcy's law. Thus

$$U_m = - \frac{\partial p_m}{\partial r} \tag{15}$$

and

$$W_m = \frac{\partial p_m}{\partial z_m}, \tag{16}$$

where W_m is in the opposite direction to the z_m axis, as shown in Fig.1.

The continuity equation is

$$\frac{\partial U_m}{\partial r} + \frac{U_m}{r} - \frac{\partial W_m}{\partial z_m} = 0 \tag{17}$$

The axisymmetric condition at r=0 and the periodic condition at $r=\xi$ require that

$$U_m = 0 \qquad \text{at } r=0 \text{ and } r=\xi. \tag{18}$$

The pressure at the adventitia layer was taken as the reference, thus

$$p_m = 0 \qquad \text{at } z_m = 0. \tag{19}$$

The matching condition at $z_m=1$ for the water velocity is

$$W_m = W_I \qquad \text{at } z_m = 1, \tag{20}$$

where W_I is related to the unknown pressure drop across the IEL by eqn.(7).

(2) Model for Macromolecular Transport

The leaky cleft in this model is assumed to be a circular ring-source. Similar to the previous model (Wen et al., 1988), the initial filling of macromolecules in the leaky cleft is assumed to be instantaneous. The time-dependent dimensionless macromolecular flux $q_j(t)$ through the leaky cleft can be related to the unknown time-dependent concentration $C_{ji}(t)$ at the exit of the leaky cleft by

using a 1-D quasi-steady convective-diffusion equation as described in Tzeghai et al. (1986). The solution to this equation is

$$q_j = d_1 - d_2 C_{ji}(t) \tag{21}$$

where

$$d_1 = \frac{Pe_j}{1-\exp(-Pe_j)}, \quad d_2 = d_1 \exp(-Pe_j), \quad Pe_j = \frac{f_j L_j \tilde{W}_j}{D_{zj}\gamma_j} \tag{22}$$

and Pe_j is the Peclet number in the leaky junction. f_j, D_{zj} and γ_j in (22) are the retardation coefficient (defined as the ratio of the solute velocity to water velocity), the diffusion coefficient and the plasma-tissue partition coefficient in the leaky junction, respectively.

(A) Boundary value problem for the SI

Similar to the filtration problem, separate solute conservation equations must be applied in the SI for the regions $0 \le r < R_1$ (k=1) and $R_1 < r \le \xi$ (k=2):

$$\frac{\partial C_{ik}}{\partial t} = -\left(\frac{\partial q_{ik}}{\partial r} + \frac{1}{r} q_{ik} \right) - \frac{D_I^2 \gamma_I L_m}{\eta \gamma_i L_i} q_I \qquad k=1,2 \tag{23}$$

Here $D_I^2 = D_{zI}/D_{zm}$; D_{zI} and γ_I are the diffusion and plasma-tissue partition coefficients in the fenestra, respectively, and γ_i is the plasma-tissue partition coefficient in the SI. The dimensionless flux in the SI in the lateral direction q_i is defined by

$$q_{ik} = - D_i^2 \frac{\partial C_{ik}}{\partial r} + Pe_{ik} C_{ik} \qquad k=1,2 \tag{24}$$

where

$$Pe_{ik} = \frac{f_i L_m \tilde{U}_{ik}}{D_{zm}\gamma_i}, \qquad D_i^2 = \frac{D_{ri}}{D_{zm}} \tag{25}$$

Pe_{ik} (k=1,2) and f_i are the Peclet number and the retardation coefficient in the SI, respectively. In contrast to the filtration problem described in Appendix A, it is difficult to formulate and solve a periodic 2-D convective-diffusive model for the permeability of the IEL which considers the interaction between the fenestra openings in this layer. This is due to the coupling of diffusion and convection. However, if the fractional area of the fenestra ϕ_I in the IEL is very small, we can assume that the local average solute flux q_I across the IEL is proportional to ϕ_I and given by

$$q_I = \phi_I q_f \tag{26}$$

where q_f is the solute flux in the fenestra, which can be estimated by the same quasi-steady 1-D model used to describe the solute transport in the leaky cleft. Thus, from (21)

$$q_f = d_3 C_{ik} - d_4 C_{Im} \tag{27}$$

where

$$d_3 = \frac{Pe_I}{1-\exp(-Pe_I)}, \qquad d_4 = d_3 \exp(-Pe_I), \qquad Pe_I = \frac{f_I L_I \tilde{W}_I}{\gamma_I D_{zI} \phi_I} \tag{28}$$

and Pe_I and f_I are the Peclet number and retardation coefficients in the fenestra, respectively.

The axisymmetric condition at r=0 and the periodic condition at $r=\xi$ are given by

$$\frac{\partial C_{i1}}{\partial r} = 0 \qquad \text{at } r=0 \quad \text{and} \tag{29}$$

$$\frac{\partial C_{i2}}{\partial r} = 0 \qquad \text{at } r=\xi. \tag{30}$$

The matching conditions for the solute flux and concentration require that

$$\eta(q_{i2} - q_{i1}) = \Delta R D_j^2 \frac{\gamma_j L_m}{\gamma_i L_j} q_j \qquad \text{at } r=R_1 \quad \text{and} \qquad (31)$$

$$C_{i1} = C_{i2} = C_{ji}(t) \qquad \text{at } r=R_1, \qquad (32)$$

where $D_j^2 = D_{zj}/D_{zm}$.

The initial conditions are

$$C_{ik} = 0 \qquad k=1,2 \qquad \text{at } t=0 \qquad (33)$$

$$C_{ji}(0) = 0 \qquad (34)$$

(B) Boundary value problem for the media

The solute mass balance equation for convective-diffusive transport in the media is given by

$$\frac{\partial C_m}{\partial t} = -\left(\frac{\partial q_{rm}}{\partial r} + \frac{1}{r} q_{rm}\right) + \frac{\partial q_{zm}}{\partial z_m} \qquad (35)$$

where the dimensionless fluxes q_{rm} and q_{zm} in the r and z directions are defined as

$$q_{rm} = -D_m^2 \frac{\partial C_m}{\partial r} + Pe_{rm} C_m \qquad (36)$$

$$q_{zm} = \frac{\partial C_m}{\partial z_m} + Pe_{zm} C_m \qquad (37)$$

and

$$Pe_{rm} = \frac{f_m L_m \bar{U}_m}{\gamma_m D_{zm}}, \qquad Pe_{zm} = \frac{f_m L_m \bar{W}_m}{\gamma_m D_{zm}}, \qquad D_m^2 = \frac{D_{rm}}{D_{zm}}. \qquad (38)$$

Here Pe_{rm} and Pe_{zm} are the Peclet numbers in the r and z directions in the media, D_{rm} is the diffusion coefficient in the media in the lateral direction, and f_m and γ_m are retardation and plasma-tissue partition coefficients in the media, respectively.

The axisymmetric condition at r=0, the periodic condition at r=ξ and the initial condition in the media are the same as (29), (30) and (33). The concentration in the adventitia layer is assumed to be zero; thus

$$C_m = 0 \qquad \text{at } z_m = 0. \tag{39}$$

The matching condition at the IEL-media interface is given by

$$q_{zm} = D_I^2 \frac{\gamma_I L_m}{\gamma_m L_I} q_I \qquad \text{at } z_m = 1, \tag{40}$$

where q_I is obtained from (26).

4.3 Solutions for filtration and transport models

4.3.1 Filtration model

The coupled boundary value problem for filtration in our periodic wall unit defined by equations (4) through (7) and (11) through (20) can be solved analytically since the governing equations and boundary conditions are linear and the solutions are simply separable functions. The solution procedure is non-trivial since the matching conditions (5) through (7) on the velocity across the endothelium and IEL all involve unknown functions of the pressure distribution in the SI and at the IEL-media interface. However, the boundary value problem for the velocity field can be converted into a boundary value problem for these unknown pressure distributions and the latter solved by tedious but straight forward methods. Closed form solutions for the velocity components and pressure distribution in the SI and media are given below.

$$U_{i1}(r) = a_1 I_1(\lambda_1 r) + \sum_{n=2}^{\infty} B_n J_1(\mu_n r) \qquad 0 \le r < R_1 \tag{41}$$

$$U_{i2}(r) = a_2 K_1(\lambda_1 r) + \sum_{n=2}^{\infty} B_n J_1(\mu_n r) \qquad R_1 < r \le \xi \tag{42}$$

$$U_m(r,z_m) = \sum_{n=2}^{\infty} A_n \mu_n J_1(\mu_n r) \frac{\sinh(\mu_n z_m)}{\sinh(\mu_n)} \tag{43}$$

$$W_m(r,z_m) = A_1 + \sum_{n=2}^{\infty} A_n \mu_n J_0(\mu_n r) \frac{\cosh(\mu_n z_m)}{\sinh(\mu_n)} \tag{44}$$

$$p_{i1}(r) = -\frac{1}{\lambda_1} a_1 I_0(\lambda_1 r) + \sum_{n=2}^{\infty} \frac{B_n}{\mu_n} J_0(\mu_n r) + a_3 \qquad 0 \le r < R_1 \tag{45}$$

$$p_{i2}(r) = \frac{1}{\lambda_1} a_2 K_0(\lambda_1 r) + \sum_{n=2}^{\infty} \frac{B_n}{\mu_n} J_0(\mu_n r) + a_3 \qquad R_1 < r \le \xi \tag{46}$$

$$p_m(r,z_m) = A_1 z_m + \sum_{n=2}^{\infty} A_n J_0(\mu_n r) \frac{\sinh(\mu_n z_m)}{\sinh(\mu_n)} \tag{47}$$

where

$$\lambda_1^2 = \frac{(L_p)_I + (L_p)_e}{\eta}, \qquad \lambda_2 = \frac{(L_p)_I}{\eta}, \qquad B_n = \frac{\lambda_2 \mu_n A_n}{\mu_n^2 + \lambda_1^2}, \tag{48}$$

and J_n, I_n and K_n (n=0,1) are the n^{th} order regular and modified Bessel functions of the first and second kind, respectively. The μ_n are the roots of the eigenvalue equation $J_1(\mu_n \xi)=0$, $(n=1,2,\ldots,\infty)$. Terms involving $K_1(\lambda_1 \xi)/I_1(\lambda_1 \xi)$ have been neglected in (42) and (46) because, based on the physiological values of λ_1 and ξ, these terms are of the order of 10^{-80}. The expressions for the coefficients a_1, a_2, a_3 and $A_n (n=1,2,\ldots,\infty)$ are given in Appendix B.

These solutions allow us to write closed form expressions for the convective transport terms for the solute flux in equations (23) and (35) for the SI and media, respectively.

4.3.2 Macromolecular transport model

The solutions for the velocity field in the SI and media

described by equations (41) through (47) are now substituted into the macromolecular transport equations (23) and (35). It is very difficult to obtain analytical solutions for these transport equations due to the complexity of the velocity field. We have therefore resorted to a finite difference method, called the Hopscotch Method, to solve the boundary value problem for solute transport. This method, which is described in Gourlay (1970), can be shown to be unconditionally stable. The basic idea and computational procedure for this numerical solution scheme are summarized in Appendix C.

4.4 Results

4.4.1 Parameter values:

There are eight important parameters in this model. They are D_j^2, D_i^2, D_m^2, D_I^2, ϕ, ϕ_I, the average pressure in the SI and the average Peclet number in the media. The diffusion coefficients in the present model differ from those in Wen et al. (1988), since the diffusion coefficients in Wen et al. (1988) already include the partition coefficients. Thus the present coefficients correspond to the experimentally measured diffusion coefficients. Based on the discussions in the previous model (Wen et al. 1988), reasonable values for D_j^2 in the large arteries are 140, 14 and 1.4 for HRP, albumin and LDL, respectively; D_m^2 for albumin is of the order of 10. For simplicity we have assumed that $D_{ri}=D_{zI}=D_{rm}$; thus, $D_i^2=D_I^2=D_m^2$.

The parameter ϕ represents the frequency of the cells whose junctions are leaky to macromolecules. The experimental studies by Lin et al. (1988) have revealed that about five cells in ten thousand

are leaky to albumin in normal rat aortic endothelium. In this case, ϕ = 0.0005. However, the cells with junctions leaky to macromolecules have a non-uniform distribution over the endothelial surface. The endothelial cell turnover rate at the distal edges of the major branch orifices of the abdominal aorta and the branch orifices of the intercostal arteries are two to three times that at non-branch areas (Lin, 1989; Chuang et al., 1990). ϕ = 0.001 is thus representative of the so-called blue areas near branches.

Roach and co-workers (Campbell and Roach, 1981; Song and Roach, 1983) have studied the size and frequency of the fenestra in the IEL of cerebral arteries and the thoracic aorta of sheep. In the aorta, the fenestrae occupy 0.2 to 2 % of the IEL surface area. In this chapter, two values for the fractional area of fenestra ϕ_I were used, ϕ_I= 0.005 and 0.02.

Vargas et al. (1979) have shown that, for a 200 μm thick rabbit aorta, the water flux across the artery wall will be doubled at the same transmural pressure gradient, if the endothelium is gently removed. This experiment indicates that the pressure drop across the endothelium is approximately one half of the total pressure drop across the artery wall for a vessel of 200 μm wall thickness. The hydraulic conductivity of the media $(\tilde{L}_p)_m$, based on these measurements of the water flux and corresponding pressure gradient, is 7.73×10^{-8} cm/sec-cmH_2O. The average water velocity in the media, $\tilde{W}_m$, corresponding to this value of $(\tilde{L}_p)_m$, is 3.68×10^{-6} cm/sec. Similar values for $(\tilde{L}_p)_m$ and $\tilde{W}_m$ were first reported in the experiments by Tedgui and Lever (1984). However, it was subsequently

realized in Tedgui and Lever (1985) that these values for $(\tilde{L}_p)_m$ and $\tilde{W}_m$ were an order of magnitude too large, due to the hydration of the interstitial space when the endothelium was removed. A new experiment was designed in Tedgui and Lever (1985) with the albumin introduced from the adventitial side, and the concentration profiles for albumin were curve fitted by a 1-D convective-diffusive equation. These experiments indicated a value for Pe_{zm} of 4.4 for the intact rabbit aorta and roughly twice this value for a denuded vessel. Using these results for the rabbit aorta, we have required that the average value of Pe_{zm} and the average pressure in the SI be 4.4 and one half of the lumen pressure, respectively. These requirements are satisfied in the model by varying the hydraulic conductivity of the media and the number period of missing proteins n_p in the normal endothelial junction strand. For $\phi_I = 0.005$, one finds that to obtain these values of p_i and Pe_{zm}, $(\tilde{L}_p)_m$ and n_p are 9.8×10^{-9} cm/sec-cm H_2O and 1700, respectively. The latter value for n_p is an upper limit that neglects the hydraulic resistance of cross-bridging fibers in the wide part of the normal cleft. If $\phi_I = 0.02$ and the same matching conditions are required, one obtains $(\tilde{L}_p)_m = 5.88\times10^{-9}$ cm/sec-cm H_2O and $n_p = 1750$ when no cross-bridging fibers are present. The influence of cross-bridging fibers and their role in normal arterial cleft structure will be discussed later in connection with Figs.2 and 10.

The remaining input data is the same as our previous model (Wen et al., 1988). We take the width of the leaky junction ΔR to be 20

nm, the junctional length L_j to be 2 μm, the effective endothelial diameter $2R_1$ to be 30 μm, the IEL thickness L_I to be 1 μm, the SI thickness L_i to be 1 μm, the media thickness L_m to be 0.2 mm (rabbit aorta), and the partition coefficients to be unity in the leaky junction (no fiber matrix) and 0.16 in the SI, the fenestra of the IEL and the media (Thurn, 1982). The radius of the periodic unit ξ is calculated from $R_1/\sqrt{\phi}$. The diffusion coefficient in the media in the normal direction D_{zm} was assumed to be 5.05×10^{-9} cm^2/sec for albumin (Thurn, 1982), and the pressure in the lumen $\tilde{p}_L$ was chosen to be 0, 70, 100, or 200 mmHg. To determine the hydraulic conductivities of the endothelium $(L_p)_e$, and the IEL, $(L_p)_I$, we assumed that μ is 0.0072 g/cm/sec, r_p is 5.5 nm, $L_1=0.4L_j$, $L_2=2r_p$, $L_3=L_j-L_1-L_2$, B is 10 nm, L_{jt} is 2000 cm/cm^2, and the distance between the fenestrae $2\xi_I$ is 10 μm. The radius of the fenestra ϵ is determined by $\xi_I\sqrt{\phi_I}$.

Generally, the solute retardation coefficient f_x in region x can be less than unity in tissues with fiber matrix structure and narrow interstitial spaces. However, Ganatos et al. (1982) have shown that the retardation coefficient is 0.96 for a sphere moving in a channel with a sphere diameter/channel height ratio of 0.3, which is close to the ratio of the equivalent diameter of the albumin to the assumed height of the open cleft. It seems reasonable to assume if there is extracellular fiber matrix in the leaky junction, it must be very loose since LDL (22 nm dia.) can also pass through this structure. Thus we assumed $f_j=1$ for albumin in the leaky junction. The possible

effect of $f_j < 1$ for larger macromolecules will be analyzed in the next section. The maximum sieving effect for albumin that has been measured by Fry et al. (1986) in the superficial layers of the intima of denuded minipig aorta is approximately 15 %. This small sieving effect has been neglected in the present study and we have assumed that the solute retardation coefficients are unity in the SI, the fenestra of the IEL and the media. We have also assumed, for simplicity, that the interstitial space of these three layers is uniform and continuous across the fenestra of the IEL.

4.4.2 Water velocity and pressure distribution

The lateral velocity distributions in the SI are shown in Fig.4 for ϕ_I= 0.005 and 0.02. Three important features of the heterogeneous filtration of the SI are revealed by this figure. First, the lateral velocity U_i in the SI is much greater than the normal velocity W_I across the IEL shown in Fig.5 in a region that extends several cell diameters from the leaky cleft exit. This suggests that the lateral convective transport of macromolecules in the SI after they cross the leaky cleft might be the dominant transport mechanism in this region. Second, U_i decreases sharply with r, and after 3 cell diameters decreases to less than 10 % of the maximum value of U_i. This behavior, we shall show shortly, explains why the lateral spreading of macromolecules, after they enter the SI, was observed in Chuang et al. (1990) to be confined to a few cell diameters of the initial leakage site after two hours of labeling. Third, the lateral velocity in the media is much smaller than in the SI, because the lateral pressure distribution in the media is much more uniform (Fig.5). This result indicates that the IEL functions as a pressure equalizer for

the media, allowing for a nearly uniform filtration therein. This behavior is important, if water and small solutes are needed to uniformly perfuse the smooth muscle cells in the artery wall.

The water flux per unit surface area W_{nj} across the normal endothelial cells is shown in Fig.5. One can show by integration of this profile that more than 99.5 % of the total wall flux across the endothelium occurs via normal clefts. Although a small fraction (less than 0.5 %) of the total water flux enters through the leaky cleft, almost all of the macromolecular flux entering the artery wall are through the leaky cleft.

The pressure distribution in the SI shown in Fig.5 is non-uniform. The pressure drop across the leaky cleft is only 5 % of that across the normal endothelial clefts. However, in previous 1-D models (Fry, 1987; Tzeghai et al., 1986; and the model in last chapter) the pressure in the SI is assumed to be uniform. Therefore, the water velocity in the leaky cleft of 1-D models is overestimated by a factor of twenty. One also observes in Figs.4 and 5 that the decrease in the hydraulic resistance of the IEL due to the increase in ϕ_I, will decrease the pressure drop across the IEL and the lateral spread of the water in the SI.

4.4.3 Macromolecular concentration distribution

The time-dependent concentration distributions in the SI are shown in Fig.6 for the same values of ϕ_I used in Figs.4 and 5. An important feature of these SI profiles is that the concentration distribution in the SI varies very slowly with time. At t=0.8, the results are not markedly different from the results at t=1 (22 hr.), indicating that steady state has been achieved. These steady-state

results are meaningful only in a statistical average sense since leakage sites open and close long before t = 1 (measured duration of leakage is tyically 1 to 2 hours.), but their number density ϕ, which determines steady state permeability, does not change. If the SI location, where the concentration of fluorescent-labeled macromolecules falls to 10 % of its value at the center of the leaky cell, is defined as the margin of a leaky spot for this molecule, then the radius of the leaky spot is roughly $3.3R_1$ at 10 minutes, and would increase to only $3.9R_1$ if the leakage site did not close and steady state could be achieved. These results are qualitatively consistent with the new experimental observation in Chuang et al. (1990) for the long time growth of the leakage site. The physical explanation of this phenomenon is as follows. Because the filling of the macromolecules into the leaky cleft is assumed to be instantaneous, the concentration in the SI is overestimated at very short times (of the order of seconds). As the macromolecules continue to enter the SI, they either spread laterally or leak into the media through the fenestrae in the IEL. The convective flux through the leaky cleft rapidly fills the SI region around the leaky cell. The SI concentration profiles do not change substantially after this rapid filling since diffusion in the vicinity of the leaky cleft is relatively unimportant. In contrast, diffusion in the media in lateral direction and in the SI far from the leakage site is important. Thus, the average concentration in the SI which will be shown later increases continuously on a longer time scale.

The effect of convection on the concentration profiles in the SI if steady state could be achieved is shown in Fig.7. As the pressure in the lumen is increased from 0 to 70 mmHg, the concentration in the

vicinity of leaky cleft exit is increased by 60 %, while the concentration in the SI far removed from the leakage site is decreased by a factor of eight. Therefore, the average concentration in the SI, which is not shown to save space, is decreased by a factor of two. If the pressure in the lumen is continuously increased to 200 mmHg, the increase in the concentration in the vicinity of the leaky cleft is slowed down and the concentration in the SI far removed from the leakage site is continuously decreased, as shown in Fig.7. This behavior can be explained as follows. When the convection is introduced by applying a transmural pressure difference, the total macromolecular flux entering the wall is initially increased, and the concentration in the vicinity of leaky cleft exit rises rapidly. However, as shown in Figs.4 and 5, the dominant direction of convection in the SI at locations more than 3 cell radii removed from the leaky cleft exit arises from filtration through normal clefts and is normal to endothelium. The macromolecules in these regions are convected out of the SI and the concentration falls to a value that is lower than that expected if only diffusion was present. In addition, the radius of the periodic unit for $\phi = 0.0005$ is about 45 times the cell radius. For this value of ϕ, the increase in the concentration in the region surrounding the leaky cell is not large enough to offset the decrease in concentration at larger distances, and the average SI concentration for the purely diffusive case is greater than when convection is present.

The time-dependent laterally averaged concentration profile across the arterial wall is shown in Fig.8. As the time increases, the average concentration in planes parallel to the endothelial surface increases and changes from a concave to a convex profile in

the media. The average concentrations in the SI are represented by the short horizontal bars in Fig.8. In contrast to the lateral concentration distributions shown in Figs.6 and 7, the effect of ϕ_I, the fractional area of the fenestra, on the average concentration profile is insignificant. In addition, one can see from Fig.8 that at short times, t=0.01 (13.2 minutes), the average concentration in the SI is greater than in the media just under the IEL; however, at long times, the average concentration in the SI can be less than in the media. These results indicate that the IEL functions as a temporary barrier to macromolecular transport. The increase in the average concentration drop across the IEL at long times is due to the lateral transport of macromolecules in the media.

4.4.4 Total macromolecular flux across the arterial wall

The total macromolecular flux Q across the arterial wall in the present model is equal to the total macromolecular flux through the leaky cleft, since the normal endothelial junctions are assumed to be impermeable to macromolecules. When the frequency of the leaky cells in the endothelium $\phi \ll 1$, the steady state macromolecular flux is proportional to ϕ, as shown in Fig.9, because the interactions between the leaky cells can be neglected. Q_d in Fig.9 represents the pure diffusive flux across the de-endothelialized arterial wall. This flux is used to non-dimensionalize Q. As ϕ is increased, the interaction between the cells with leaky clefts becomes significant and leads to a rapid non-linear increase in Q/Q_d as shown in Fig.3(c) of Wen et al. (1988). The effect of lumen pressure p_L on the total macromolecular flux Q/Q_d is also shown in Fig.9. When $p_L > 70$ mmHg, Q/Q_d increases alomost linearly with p_L. This is because the

convection is the dominant mode of transport when $p_L > 70$ mmHg ($Pe_j = 1.5$) and the convective flux is proportional to p_L.

It was observed in Lin (1989) and Chuang et al. (1990) that ϕ in branching areas of rat aorta is roughly twice that of non-branching areas. These regions have been shown in other animal species to exhibit a typically twofold increase in macromolecular permeability (Bell et al., 1974a and 1974b; Packham et al., 1967; Schwartz,C.J. et al., 1983). Our theoretical predictions shown in Fig.9 are consistent with these experimental results, whether or not the convective transport is considered.

In the case of hypertension, say $p_L = 200$ mmHg, not only the pressure in the lumen is increased by a factor of three, but the frequency ϕ of the cells with the leaky junction is also increased by a factor of three (Wu et al., 1990). Therefore, the present model predicts that the total macromolecular flux entering the artery wall will be increased by an order of magnitude.

4.5 Discussion

The transport of LDL in the arterial wall involves the binding of the LDL to the cell membrane or the extracellular matrix of the arterial wall and the degradation of LDL by the endothelial cells and/or smooth muscle cells (Steinberg, 1983). The present model, which has neglected these two processes, is thus only a rough approximation for the LDL transport in the arterial wall. However, some of the key insights obtained in the chapter relating to the resistance of the IEL, the importance of convection in the different layers, the relative importance of fitltration in the leaky and normal clefts are also applicable to the problem of LDL transport.

These considerations govern the LDL delivery into the arterial wall for binding and degradation.

4.5.1 General features of macromolecular transport

In the present model we have assumed, based on experiments (Lin et al., 1988 and 1989; Lin, 1989; Chuang et al., 1990), that macromolecules can enter the arterial wall only through the leaky clefts. These open clefts occupy as little as 10^{-6} of the endothelial surface area (Lin et al., 1988). In addition, since the concentration at the edge of the periodic wall unit is very small, as shown in Fig.5 and 6, the interaction between the leaky cells is negligible. Therefore, the total flux across the arterial wall is proportional to the number of the leaky cells per unit endothelial surface area, as shown in Fig.9.

After crossing the leaky cleft, the macromolecules will either spread laterally or leak into the media through the fenestrae in the IEL. The convective flux through the leaky cleft rapidly fills the SI region around the leaky cell. After this rapid filling , the concentration profile in this SI region does not change substantially, as shown in Fig.6, since the diffusion in the vicinity of the leaky cleft is relatively unimportant and the convection is assumed to be steady. Therefore, the size of the leakage spot defined in the last section is limited to 3~4 cell diameters. In contrast, diffusion is important in the media and in the SI far from the leakage site. Thus, the average concentration in the SI as shown in Fig.8 will continue to increase on a longer time scale. In addition, the IEL is only a temporary barrier to macromolecular transport as discussed in the last section and shown in Fig.8.

4.5.2 Filtration across the endothelium

The filtration through the normal endothelial clefts of large arteries has been modeled in this chapter using the new theoretical approach developed in (Tsay et al., 1989; Tsay and Weinbaum, 1990). Whereas the ultrastructure of capillary endothelial junctions has been extensively studied (Tsay et al., 1989), there have been few studies of normal endothelial cleft structure in large arteries. In this chapter, we assumed that the basic model for endothelial cleft of a large artery is the same as for capillary endothelium as shown in Fig.2. The principal difference between the two clefts is the vast difference in the number frequency of missing proteins n_p predicted by the model in the endothelial junction strands of the two cells. n_p has a significant effect on the hydraulic conductivity of the endothelium. The relationship between the hydraulic conductivity of the endothelium and n_p as a function of cross-bridging fiber spacing Δ is shown in Fig.10, where the fiber radius a is 0.6 nm and the values of the other parameters for the normal endothelial cleft are the same as described in the last section.

As already discussed, there are no direct experimental measurements of $(\tilde{L}_p)_e$ in large arteries. Its value was obtained in this chapter by requiring that the average Peclet number in the media Pe_{zm} and pressure in the SI correspond to the measured values for the rabbit aorta, i.e. 4.4 and 0.5, respectively. The value of $(\tilde{L}_p)_e$ does not change significantly (< 3 %) between ϕ_I= 0.005 and 0.02, the average value for $(\tilde{L}_p)_e$ is 3.8×10^{-9} cm/sec-cmH_2O. The corresponding

value for n_p is 1725, if there are no cross-bridging fibers in the wide part of the normal cleft. However, it is shown in Fig.10 that, even if a fiber matrix is present, the number of missing proteins required to maintain this value of $(\tilde{L}_p)_e$ is decreased at most by a factor of two at the closest fiber spacing Δ = 6 nm. This prediction suggests that there is a dramatic change in endothelial junction strand structure as one proceeds from capillaries on the arterial side to large arteries. n_p for the normal endothelial junctions of large arteries is more than an order of magnitude smaller than predicted in Tsay et al. (1989) for muscle capillaries. The present analysis suggests that there are only a few missing proteins in an entire cell perimeter.

The leaky cleft was approximated in this chapter by an open channel without matrix components. This assumption can be justified by using Fig.10. It was observed in Lin et al. (1989) that the LDL molecules can enter the artery wall through leaky clefts. For this to occur the spacing between the cross-bridging fibers should be greater than 22 nm. If we assume that for a leaky cleft, $n_p \simeq 1$ or $2D \simeq 11$ nm, one concludes from Fig.10 that the hydraulic conductivity of the leaky cleft will be decreased by less than 20 %, if cross-bridging fibers with this value of Δ exist in the leaky cleft.

4.5.3 The resistance of the arterial wall to macromolecular transport

Based on the results of the present model, the major resistance to macromolecular transport resides in the endothelial layer. For albumin the present theory predicts that 99.6 % of the total decrease in the average albumin concentration at steady state in the rabbit aorta occurs across the endothelium when ϕ=0.0005 as shown in Fig.8.

The remaining 0.4 % of the total decrease in the average concentration occurs in the media. Because the size of the fenestra in the IEL are very large compared with the size of macromolecules, the IEL is only a temporary barrier to macromolecular transport, as shown in Fig.8.

4.5.4 The validity of 1-D transport models for the velocity field

The principal difficulty in formulating a simplified 1-D convective-diffusive transport model is the treatment of the interface matching conditions when there is a discontinuity in the area for filtration and macromolecular transport between layers. One needs to relate the local pressure and concentration at the exit of leaky cleft to the average pressure and concentration in the SI, respectively. These problem are critical, because the pressure and concentration differences across the leaky cleft control the total macromolecular flux entering the arterial wall. Pe_j in the present filtration model varies from 1.5 when the pressure in the lumen is 70 mmHg to 12.8 when the luminal pressure is 200 mmHg. Thus the diffusive flux in the leaky cleft is smaller than the convective flux. In addition, the present 2-D filtration model predicts from Fig.5 that the dimensionless pressure drop across the leaky cleft is 0.025, while the average pressure drop across the endothelium is 0.5. If one assumes that the pressure in the SI is uniform as required by a 1-D model, one finds that the total convective flux will be overestimated by a factor of twenty.

A second difficulty arises from the discontinuity in the velocity at the endothelial-SI interface when a 1-D model for the convective velocity is used. As mentioned in the Introduction, this simplified model for the velocity can lead to concentrations in the

SI which are greater than in the lumen even if a 2-D model is used for the concentration field. Typical results for the concentration profile in the SI using a model of this nature in last chapter are shown in Fig.11. Three curves are shown, one corresponding to no convection ($Pe_m = 0$) and two curves, $n_p = 255$ and 2160, corresponding to the same convective flux in the media ($Pe_m = 4.4$), but a different apportionment of the water flux through the normal and leaky clefts. In this simplified 2-D model the pressure in the SI is uniform and the water velocity in the leaky cleft increases as n_p decreases to maintain the same average Peclet number in the SI and media. As observed in Fig.11 the dimensionless cleft exit concentration in the SI can greatly exceed unity and give the appearence of molecular sieving in the SI when n_p is small at physiological values of Pe_m, whereas this is not possible when $Pe_m = 0$. The discontinuity in the average velocity in a 1-D model for the velocity field leads to SI concentration profiles which have the same qualitative shape as those shown in Fig.7, but completely erroneous SI concentration levels in the vicinity of the leaky cell. We shall next show that this spurious behaviour disappears if the velocity is continuous at the leaky cleft exit.

4.5.5 Effect of macromolecular sieving

Smith and Staples (1982) and Fry et al (1986) have observed that the macromolecular concentration in the SI can be higher than that in the lumen. The results in Figs.6,7 and 8 do not exhibit this behavior either locally or in an average sense. Moreover, we shall now show that the SI concentrations must be lower than that in the lumen,

unless a sieving structure is present either in the IEL or the SI itself.

In order to investigate the detailed transport behavior in the vicinity of the leaky cleft exit, simplified local models are proposed for filtration and macromolecular transport in the leaky cleft and SI, respectively, as shown in Fig.12 and described in Appendix D. The leaky cleft is approximated by an open channel and the SI tissue is assumed to be a radially symmetric porous media in which the velocity decays as 1/r with distance r from the cleft exit. Two parameters α and β are introduced to account for possible macromolecular sieving effects in the leaky cleft proper or at the level of the basement membrane at the cleft exit plane. $\alpha=f_j/f_i$ describes the retardation of solute in the leaky cleft due to wall or matrix components in the intercellular channel, whereas $\beta=C^2_{ji}/C^1_{ji}$ describes the discontinuity in concentration at the leaky cleft exit if the basement membrane were to function as a molecular sieve at this location.

There are two sets of curves in Fig.13 (dashed and solid). The dashed curves 1,2,3 are representative of solutions for $C_I<1$ in which there is no sieving structure in the IEL ($f_I= 1$ in the fenestra as assumed in our 2-D model results).

It can be shown mathematically from equations (D.4), (D.7), (D.11) and (D.12) that if $C_I< 1$, then C_i must be less than unity for all values of α and β, curves 1,2,3, although C_j can be greater than C_L in the lumen, as observed in curve 2, when $\beta < 1$ and the basement membrane functions as a molecular sieve. Thus, results of the type

shown in Fig.11, which are based on a 2-D model with a discontinuity in average water velocity at the enodthelial-SI interface, in which $C_I>1$, are artifacts. The solid curves 4,5,6 are representative of solutions for $C_I>1$, in which there exists a sieving structure in the IEL, the macromolecular concentration in the SI just above the IEL can be higher than that in the lumen whether or not α or β are less than unity. When $\alpha=\beta=1$ (curve 4), there is no additional sieving; when $\alpha=1$, $\beta=0.55$ (curve 5) there is additional sieving at the basement membrane and when $\beta=1$, $\alpha=0.1$ (curve 6) there is also sieving in the leaky cleft proper. Both curves 2 and 5 exhibit a sharp increase in concentration in the cleft and a sharp discontinuity at the level of the basement membrane. In general, the macromolecular concentration in the SI can not be higher than that in the lumen unless a sieving structure exists on the tissue side of the endothelial-SI interface. This sieving needs not occur in the IEL but could also be present in more superficial levels of the SI, e.g., if the basement membrane was not in the cleft exit plane, but a small distance beneath the endothelial-SI interface. The discontinuity in curves 2 and 5 would then be displaced to $r_i>r_1$ in Fig.13 but would have the same general shape.

4.6 Concluding remarks

The major conclusions of the new transport model in the intima proposed in this chapter are: (1) it is impossible for the macromolecular concentrations in the SI to be higher than in the lumen unless a sieving structure exists in the intima; (2) 1-D convective-diffusive models can lead to the concentrations in the SI that are higher than in the lumen, and overestimate the

macromolecular convective flux entering the artery wall by more than an order of magnitude; (3) the structure of the normal endothelial junction strand varies tremendously as one proceeds from the large arteries to capillaries; and (4) for rabbit aorta (200 μm wall thickness) the new model predicts, (i) 99 percent of the total arterial wall resistance to macromolecular transport resides in the endothelium, (ii) the macromolecular flux entering the artery wall is proportional to the frequency ϕ of the endothelial cells with leaky clefts when $\phi \leq 0.05$, and is proportional to the lumen pressure p_L when $p_L \geq 70$ mmHg, and (iii) the growth of the fluorescent leakage spot in the SI is confined to only several cell radii after 2 hrs of labeling.

Appendix A

This appendix contains the approximate model for estimating the hydraulic conductivity $(L_p)_I$ of the IEL. We assumed that $(L_p)_I$ depends only on the structure of the IEL and the interaction of the water jets through the fenestral pores in the underlying media. A local periodic wall unit was thus constructed as shown in Fig.3, which is similar in concept to the periodic wall unit shown in Fig.1. This periodic wall unit is a circular cylinder with a fenestra at the center of the top surface, and has a diameter equal to the average distance ξ_I between the fenestrae. The height of the cylinder is equal to $L_I + L_m$.

The governing equations and the boundary conditions at the center line and the peripheral and bottom surfaces of the periodic unit are similar to equations (15) through (19). The only difference is that the pressure (p_{ml}) and water velocities (U_{ml} and W_{ml}) in the media in this local model are non-dimensionalized by $\bar{p}_i$ and $(\bar{L}_p)_m \bar{p}_i$. The matching condition at the IEL-media interface for the water velocity is

$$\begin{cases} \frac{2}{\epsilon^2} \int_0^{\epsilon} W_{ml}\, r\,dr = W_f \\ W_{ml} = 0 \qquad\qquad \epsilon < r < \xi_I, \quad z_m = 1 \end{cases} \tag{A.1}$$

where ϵ is the radius of fenestra and W_f is the water velocity through the fenestra. It was also assumed that the interstitial space of the fenestra is the same tissue as in the media, and, therefore, that the intrinsic hydraulic conductivity of the fenestra is the same as the media. If we assume 1-D filtration in the fenestra, the normal velocity in the fenestra is given by

$$W_f = (L_p)_f[1 - P_{m1}(r=0, z_m=1)] \tag{A.2}$$

where

$$(L_p)_f = L_m/L_I \tag{A.3}$$

The hydraulic conductivity L_I of the IEL is defined as

$$(L_p)_I = \frac{\bar{W}_{m1}}{1 - \bar{p}_{m1}} \qquad \text{at } z_m = 1 \tag{A.4}$$

where the mean velocity and pressure are given by

$$\bar{W}_{m1} = \frac{1}{\xi_I^2}\int_0^{\xi_I} W_{m1} r dr \tag{A.5}$$

$$\bar{p}_{m1} = \frac{1}{\xi_I^2}\int_0^{\xi_I} p_{m1} r dr \tag{A.6}$$

The solution of the equations (15) through (19) and (A.1) through (A.6) leads to the following expressions,

$$\bar{W}_{m1} = \bar{p}_{m1} = W_f \phi_I \tag{A.7}$$

$$W_f = \frac{(L_p)_f}{1 + (L_p)_f G_0} \tag{A.8}$$

$$G_0 = \phi_I + \sum_{n=2}^{\infty} s_n, \qquad s_n = \frac{2\epsilon J_1(\mu_n \epsilon)}{\mu_n^2 \coth(\mu_n)\xi_I^2 J_0^2(\mu_n \xi_I)} \tag{A.9}$$

where $J_0(\ )$ and $J_1(\ )$ are the zeroth and the first order Bessel functions, and the $\mu_n (n=1,2,3,\ldots,\infty)$ are the roots of eigenvalue equation $J_1(\mu_n \xi_I)=0$. The result (A.9) for s_n is based on the center line pressure value as stated in the boundary condition (A.2).

Appendix B

This appendix contains the expressions for a_1, a_2, a_3 and A_n ($n=1,2,\ldots,\infty$) in the solutions for the filtration model.

By defining

$$\lambda_3 = \frac{(L_p)_e}{(L_p)_e + (L_p)_I}, \qquad \lambda_4 = 1 - \lambda_3, \qquad \lambda_5 = \frac{I_0(\lambda_1 R_1)}{K_0(\lambda_1 R_1)}$$

$$c_1 = 1 + \lambda_3 (L_p)_I, \qquad c_k = \mu_k \coth(\mu_k) + (L_p)_I \left[1 - \frac{(L_p)_I}{\eta(\mu_n^2 + \lambda_1^2)}\right] \qquad k>1$$

$$D_k = \lambda_1 \xi^2 J_0^2(\mu_k \xi) C_k / [2(L_p)_I] \qquad k\geq 1$$

$$E_1 = -\frac{2(L_p)_I}{\xi^2 \lambda_1^2 c_1} R_1 I_1(\lambda_1 R_1)$$

$$E_k = -\left[\int_0^{R_1} I_0(\lambda_1 r) J_0(\mu_k r)\, r\, dr\right] / D_k \qquad k>1$$

$$F_1 = -\frac{2(L_p)_I}{\xi^2 \lambda_1^2 c_1} [\xi K_1(\lambda_1 \xi) - R_1 K_1(\lambda_1 R_1)]$$

$$F_k = \left[\int_{R_1}^{\xi} K_0(\lambda_1 r) J_0(\mu_k r)\, r\, dr\right] / D_k \qquad k>1$$

$$G_1 = \sum_{n=2}^{\infty} \frac{J_0(\mu_n R_1)}{\mu_n^2 + \lambda_1^2} E_n, \qquad G_2 = \sum_{n=2}^{\infty} \frac{J_0(\mu_n R_1)}{\mu_n^2 + \lambda_1^2} F_n$$

$$\lambda_6 = \frac{\Delta R (L_p)_j}{[\lambda_5 K_1(\lambda_1 R_1) + I_1(\lambda_1 R_1)]\eta}$$

$$\lambda_7 = 1 - \lambda_3 [1 + \lambda_4 (L_p)_I / c_1]$$

$$\lambda_8 = I_0(\lambda_1 R_1)/\lambda_1 - \lambda_4 (E_1 - \lambda_5 F_1)$$

we obtained

$$a_1 = -\frac{\lambda_6 \lambda_7}{1 + \lambda_6 [\lambda_8 + \lambda_2 (\lambda_5 G_2 - G_1)]}, \qquad a_2 = -\lambda_5 a_1$$

$$A_1 = \lambda_3 (L_p)_I / c_1 + a_1 E_1 + a_2 F_1, \qquad A_k = a_1 E_k + a_2 F_k \qquad k>1$$

$$a_3 = \lambda_3 + \lambda_4 A_1$$

Appendix C

The governing transport equation can be written as

$$\frac{\partial C}{\partial t} = G[C] \qquad (C.1)$$

where G is a general convective-diffusive differential operator. If one uses a forward difference in time, (C.1) can be approximated by,

$$C_{nm}^{\ell+1} = C_{nm}^{\ell} + \Delta t\, G_h[C_{nm}^{\ell}] \qquad \text{for } n+m+\ell = \text{odd} \qquad (C.2)$$

$$C_{nm}^{\ell+1} = C_{nm}^{\ell} + \Delta t\, G_h[C_{nm}^{\ell+1}] \qquad \text{for } n+m+\ell = \text{even} \qquad (C.3)$$

where G_h is the conrresponding convective-diffusive difference operator, and C_{nm}^{ℓ} represents the concentration at $t = \ell\Delta t$, $r = n\Delta r$, and $z_m = m\Delta z$, where ℓ, n, and m = 1,2,..., respectively.

It can be shown easily from (C.2) and (C.3) that

$$C_{nm}^{\ell+2} = 2C_{nm}^{\ell+1} - C_{nm}^{\ell} \qquad \text{for } n+m+\ell+1 = \text{odd} \qquad (C.4)$$

This formula makes the Hopscotch Method more efficient and also independent of the operator G_h.

The procedure to solve the problem is the following:

(a) For $\ell = 1$, one uses (C.2) to obtain C_{nm}^{2} for n+m+1 = odd.

(b) At any position (n,m) and time interval ℓ, one uses (C.3) to obtain $C_{nm}^{\ell+1}$ for $n+m+\ell$ = even. The results can be printed out at this step.

(c) If n+m+ℓ+1 = odd, one uses the fast formula (C.4) to obtain the solution $C_{nm}^{\ell+2}$, and then goes on to step (b) to obtain $C_{nm}^{\ell+2}$ for n+m+ℓ+1 = even.

Repeating steps (b) and (c), one obtains the solution for C_{nm}^{ℓ} at any time interval ℓ and position (n,m).

In order to increase the resolution of the solutions in the vicinity of the leaky cleft exit, the coordinate system (r,z_m) is transformed to (x,y) according to

$$r = a_x x^3 + b_x x^2 + c_x x \qquad (C.5)$$

$$z_m = a_y[1 - \exp(-b_y y)] \qquad (C.6)$$

where the constants a_x, b_x, c_x, a_y and b_y are determined by requiring that

$r=R_1$ at x=0.1; $r=5R_1$ at x=0.5; and $r=\xi$ at x=1

and

z_m=0.7 at y=0.5; and z_m=1 at y=1.

Appendix D

This appendix contains two simplified 1-D steady state models for the filtration and macromolecular transport in a local region surrounding the leaky cleft, as shown in Fig.12. The purpose of these two models is to investigate possible macromolecular sieving mechanisms in the vicinity of the leaky cleft exit. The leaky cleft is approximated by a uniform open channel and the SI tissue is assumed to be a radially symmetric porous medium. From simple continuity arguments, one can shown that the water velocity in the leaky junction W_j is a constant and the velocity field W_i must decay

in the SI as 1/r. The Peclet number P_x and the macromolecular flux q_x in the region x are defined as

$$Pe_x = \frac{f_x L_x W_x}{\gamma_x D_x} \qquad x=i,j \qquad (D.1)$$

$$q_x = -\frac{\partial C_x}{\partial r_x} + Pe_x C_x \qquad x=i,j \qquad r_x = z_j,\ r_i \qquad (D.2)$$

where the subscripts i and j denote the SI and leaky cleft, respectively; f_x, L_x, γ_x, and D_x are the retardation coefficient, the thickness, the tissue-plasma partition coefficient and the diffusion coefficient in the region x, in that order; the coordinate r_x and the concentration C_x are non-dimensionalized by L_x and the lumen concentration, respectively. In this model the transport in the leaky cleft is described by a 1-D model similar to that in Tzeghai et al. (1986). The solution for the concentration and flux in the channel are

$$C_j = \frac{q_j}{Pe_j} + \left(1 - \frac{q_j}{Pe_j}\right) \exp(Pe_j z_j) \qquad (D.3)$$

$$q_j = d_1 - d_2 C^1_{ji},\ d_1 = Pe_j/[1-\exp(-Pe_j)],\ d_2 = d_1 \exp(-Pe_j) \qquad (D.4)$$

where the boundary conditions $C_j = 1$ at $r_j = 0$ and $C_j = C^1_{ji}$ at $r_j = 1$ have been satisfied. C^1_{ji} is unknown and will be determined by matching (D.3) and (D.4) with the solutions in the SI. In the SI, the 1-D radially symmetric transport must satisfy

$$\frac{\partial^2 C_i}{\partial r_i^2} + \left(\frac{1}{r_i} - Pe_i\right) \frac{\partial C_i}{\partial r_i} = 0 \qquad (D.5)$$

if no solute crosses the membranes of either the normal or lealy cell.

The matching conditions at the leaky cleft-SI interface are

$$W_i = \frac{2}{\pi} W_j, \qquad q_i = \frac{2}{\pi} H_q q_j, \qquad H_q = \frac{\gamma_j D_j L_i}{\gamma_i D_i L_j} \tag{D.6}$$

where $2/\pi$ is introduced by considering the change in geometry from an open channel to a radially symmetric porous media.

From (D.5) and (D.6), we obtained

$$C_i = \alpha \frac{q_j}{Pe_j} + (C^2_{ji} - \alpha \frac{q_j}{Pe_j})(\frac{r_i}{r_1})^B \tag{D.7}$$

$$B = \frac{2H_q r_1}{\pi \alpha} Pe_j, \qquad \alpha = f_j/f_i \tag{D.8}$$

where r is the half-width of the leaky cleft, C^2 is concentration in the SI at $r=r_1$. Fry et al. (1986) observed that the superficial layers of the intima (e.g. the basement membrane) exhibit molecular selectivity for macromolecules. This behavior is easily accounted for, in this model, by introducing a reflection coefficient σ in the boundary condition at the leaky cleft-SI interface. However, for convenience, we define a new parameter β, which is equivalent to σ.

$$\beta = C^2_{ji}/C^1_{ji} \qquad 0 \leq \beta \leq 1 \tag{D.9}$$

Therefore, $\beta=0$ and 1 correspond to $\sigma=1$ and 0, respectively. Generally, $f_j \leq f_i$, hence $0 \leq \alpha \leq 1$.

The boundary condition far from the leaky cleft in the SI at $r_i = 1$ is

$$C_i = C_I \tag{D.10}$$

where C_I in this model is taken as a free parameter.

Substituting (D.4) and (D.10) into (D.7), one obtains

$$C_{ji}^{1} = \frac{C_I r_1^B Pe_{jo} + (1 - r_1^B) d_1}{\beta Pe_{jo} + (1 - r_1^B) d_2} \tag{D.11}$$

where $Pe_{jo} = Pe_j/\alpha$. Substituting (D.11) into (D.9), one obtains

$$C_{ji}^{2} = \frac{C_I r_1^B Pe_{jo} + (1 - r_1^B) d_1}{Pe_{jo} + (1 - r_1^B) d_2/\beta} \tag{D.12}$$

Similar to the previous model Wen et al. (1988), we shall assume that $L_i = 1$ μm, $L_j = 2$ μm, $D_j/D_i = 1.4$, $\gamma_j = 1.0$, $\gamma_i = 0.16$, and $r_1 = 10$ nm. The Peclet number in the leaky junction for $\alpha = 1$, i.e. Pe_{jo}, is assumed to be 1.5. This corresponds to $p_L = 70$ mmHg in the 2-D filtration model proposed in this chapter.

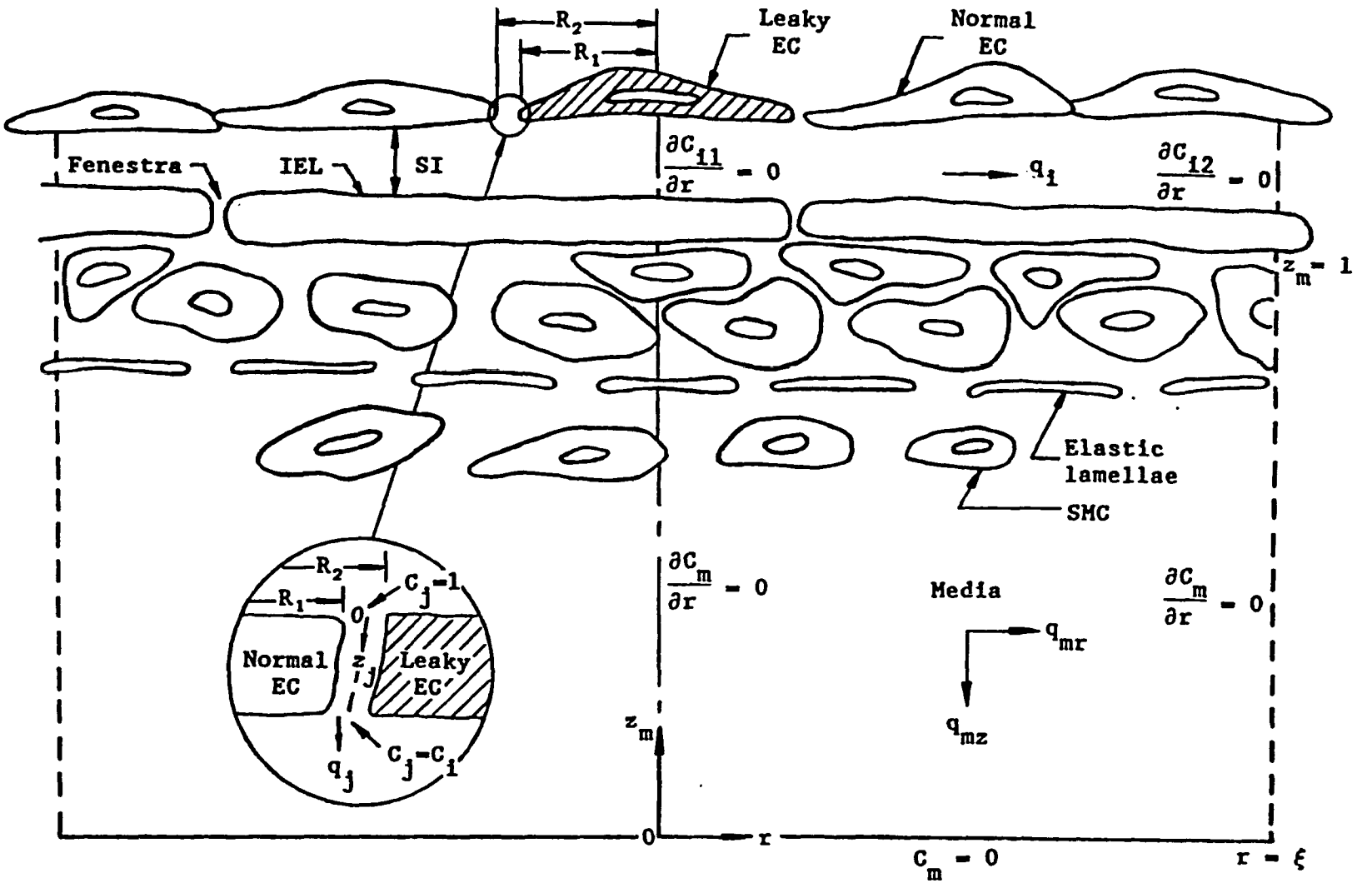
R_2
R_1
Leaky EC
Normal EC
Fenestra
IEL
SI
$\frac{\partial C_{i1}}{\partial r} = 0$
q_i
$\frac{\partial C_{i2}}{\partial r} = 0$
$z_m = 1$
Elastic lamellae
SMC
$\frac{\partial C_m}{\partial r} = 0$
Media
q_{mr}
q_{mz}
$\frac{\partial C_m}{\partial r} = 0$
R_2
R_1
$C_j = 1$
0
Normal EC
z_j
Leaky EC
q_j
$C_j - C_i$
z_m
0
r
$C_m = 0$
$r = \xi$

Figure 1

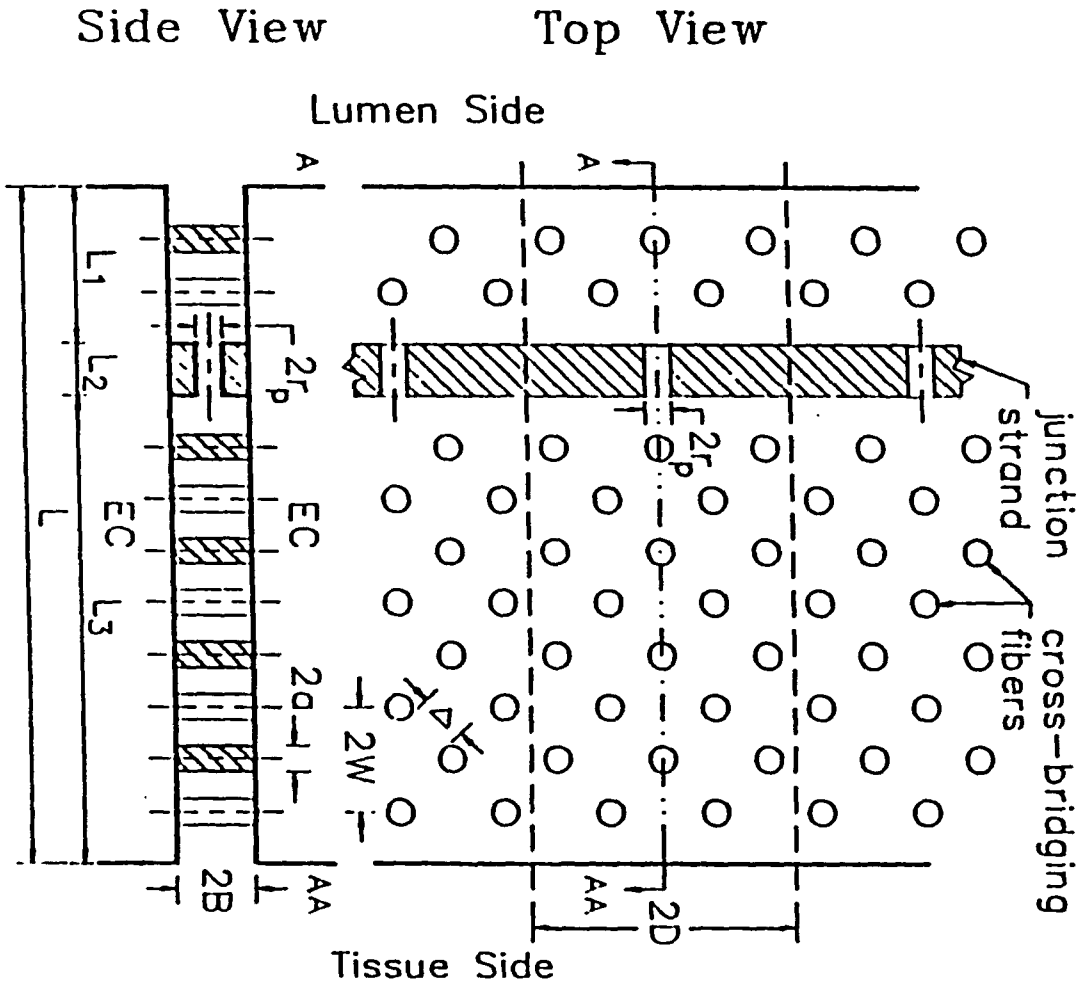
Side View
Top View
Lumen Side
Tissue Side
junction strand
cross-bridging fibers
L
L1
L2
L3
EC
2rp
2a
2W
2B
2D
A
AA
T

Figure 2

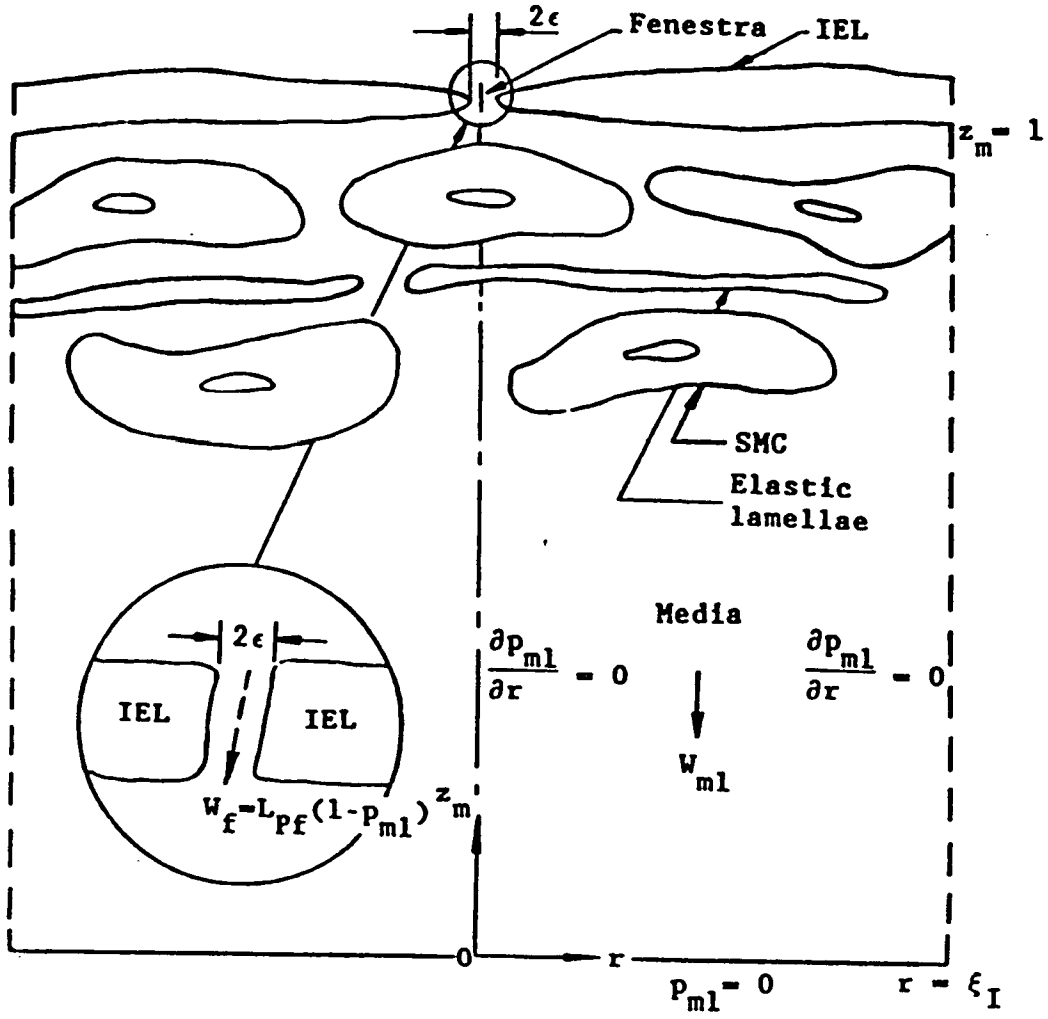
2ϵ
Fenestra
IEL
$z_m = 1$
SMC
Elastic lamellae
Media
2ϵ
IEL
IEL
$\frac{\partial p_{ml}}{\partial r} = 0$
$\frac{\partial p_{ml}}{\partial r} = 0$
W_{ml}
$W_f = L_{pf}(1-p_{ml})^{z_m}$
0
r
$p_{ml} = 0$
$r = \xi_I$

Figure 3

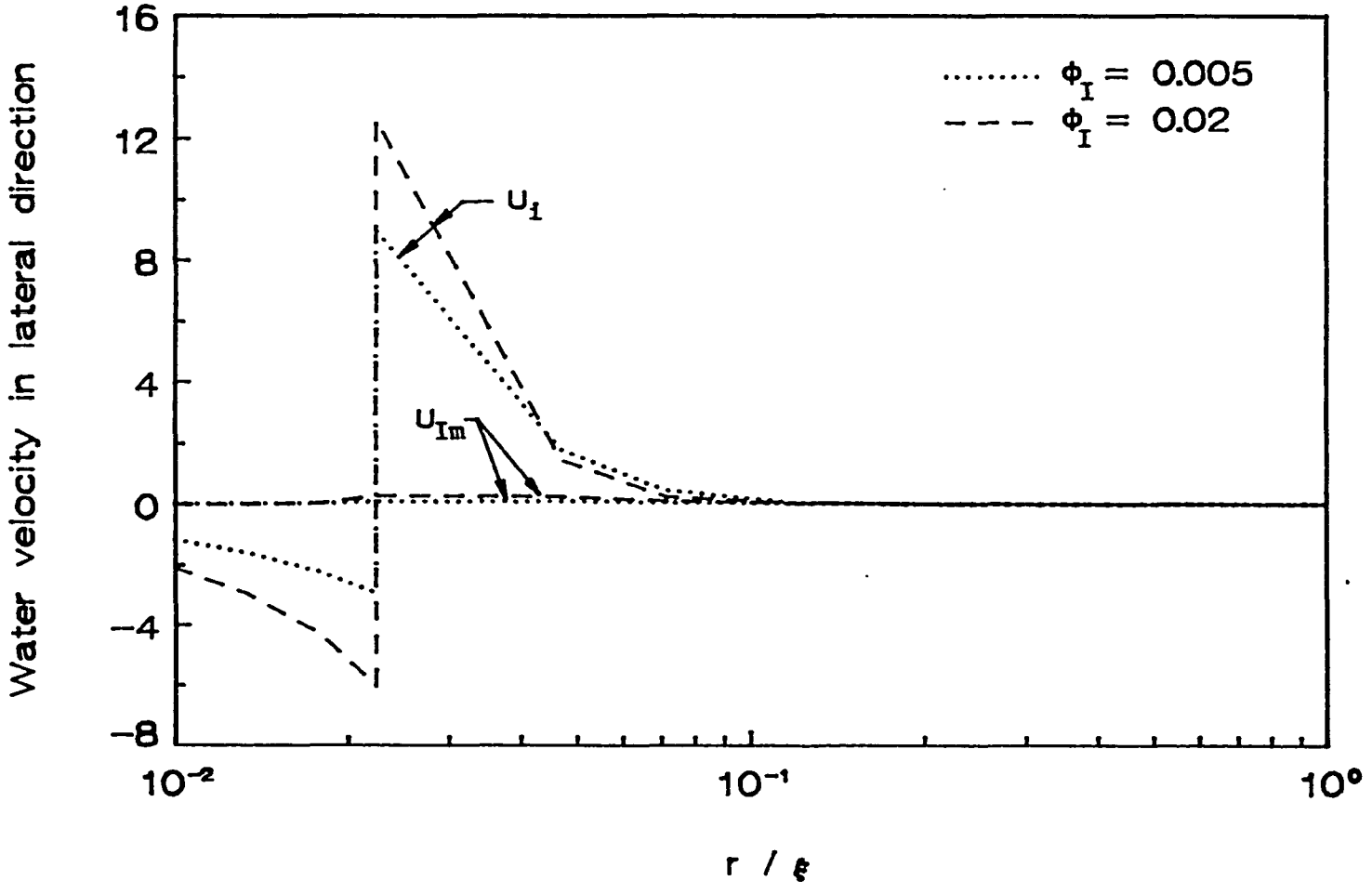
16
12
8
4
0
−4
−8
Water velocity in lateral direction
10^{-2}
10^{-1}
10^{0}
r / ξ
ϕ_I = 0.005
ϕ_I = 0.02
U_i
U_{Im}

Figure 4

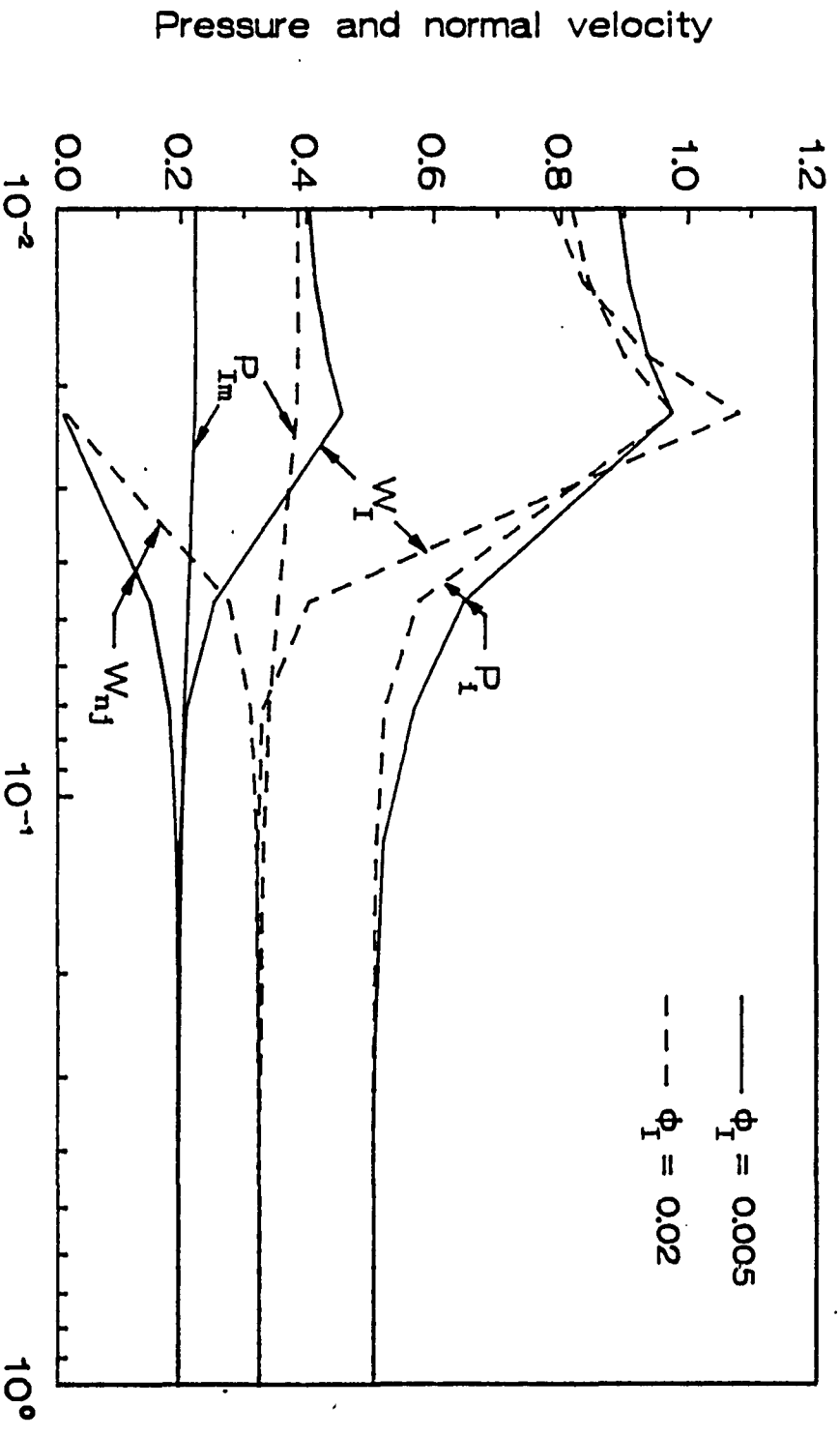
Pressure and normal velocity
1.2
1.0
0.8
0.6
0.4
0.2
0.0
10^{-2}
10^{-1}
10^{0}
r / ε
P_{Im}
W_I
P_I
W_{nj}
$\Phi_I = 0.005$
$\Phi_I = 0.02$

Figure 5

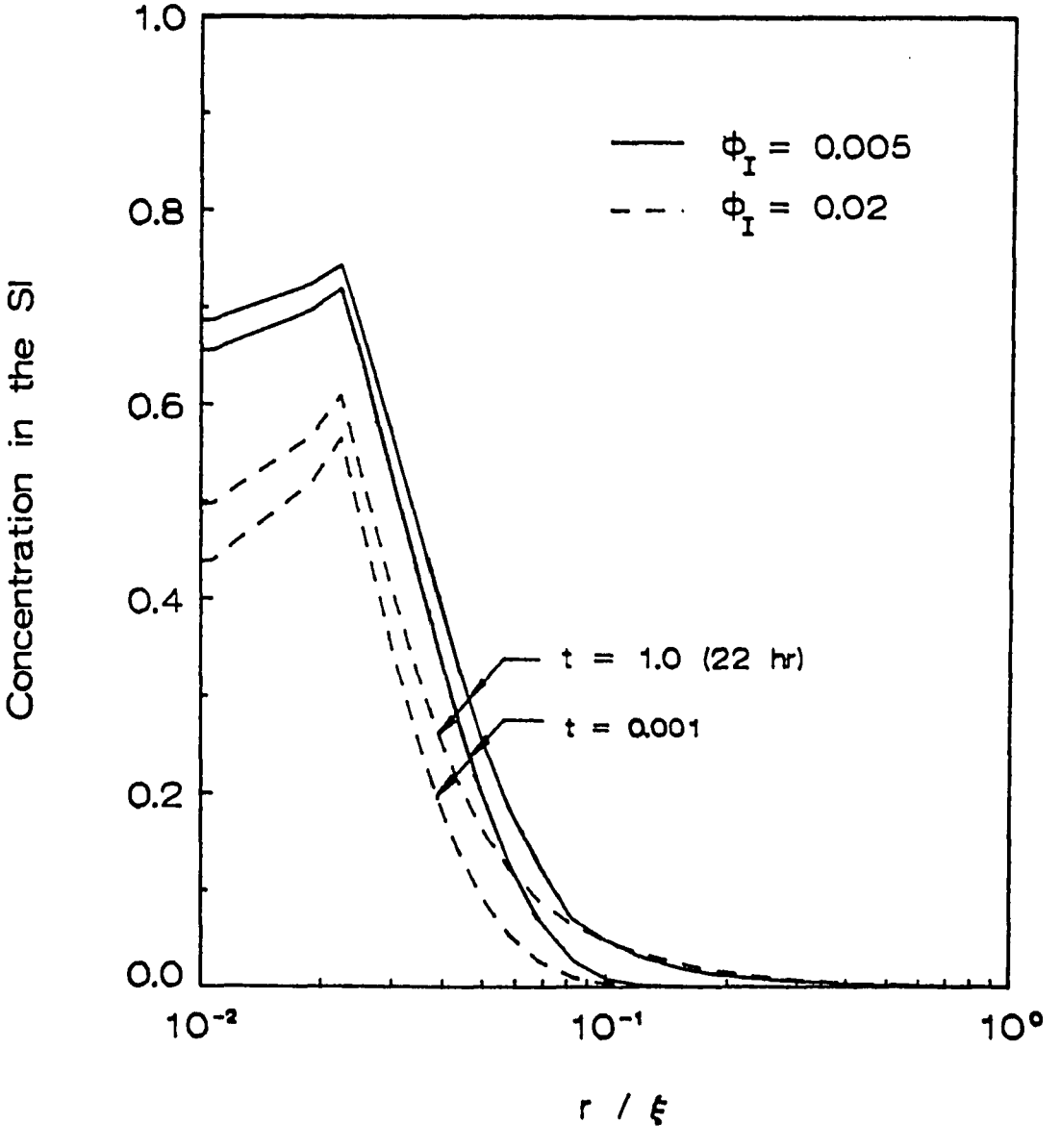
1.0
0.8
0.6
0.4
0.2
0.0
Concentration in the SI
Φ_I = 0.005
Φ_I = 0.02
t = 1.0 (22 hr)
t = 0.001
10^{-2}
10^{-1}
10^{0}
r / ξ

Figure 6

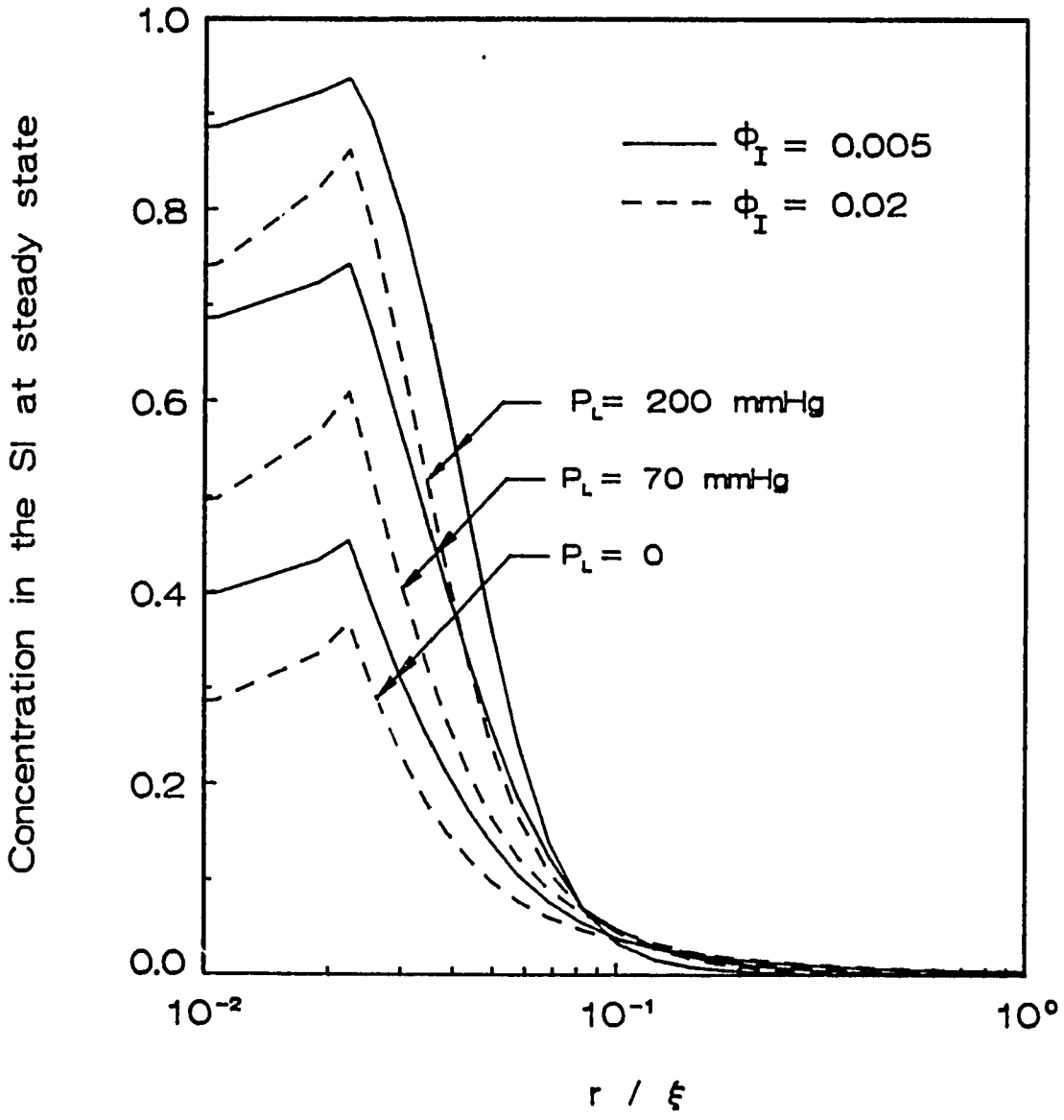
1.0
0.8
0.6
0.4
0.2
0.0
Concentration in the SI at steady state
Φ_I = 0.005
Φ_I = 0.02
P_L= 200 mmHg
P_L = 70 mmHg
P_L = 0
10^{-2}
10^{-1}
10^{0}
r / ξ

Figure 7

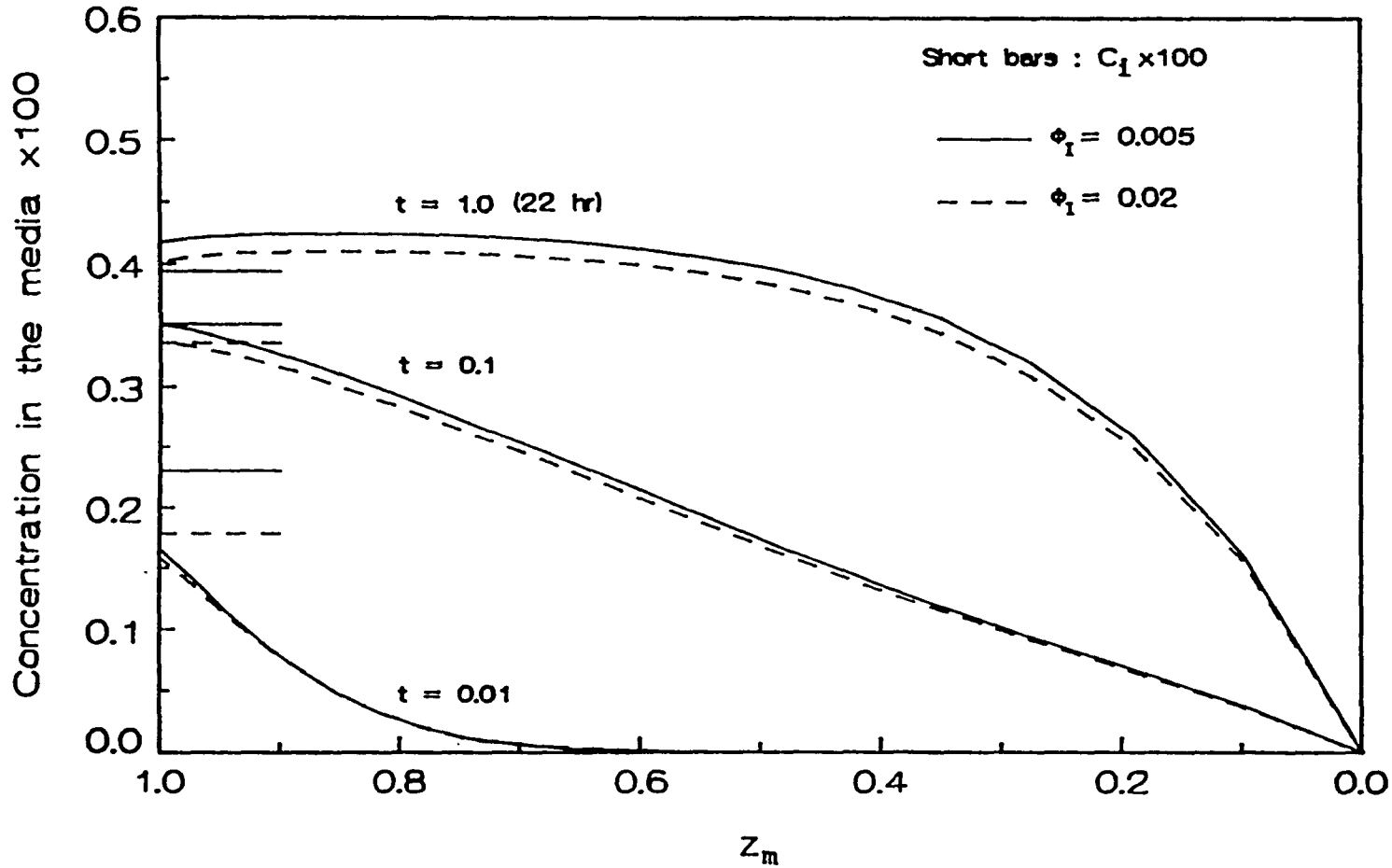
Concentration in the media x100
0.6
0.5
0.4
0.3
0.2
0.1
0.0
Short bars : C_I x100
Φ_I = 0.005
Φ_I = 0.02
t = 1.0 (22 hr)
t = 0.1
t = 0.01
1.0
0.8
0.6
0.4
0.2
0.0
Z_m

Figure 8

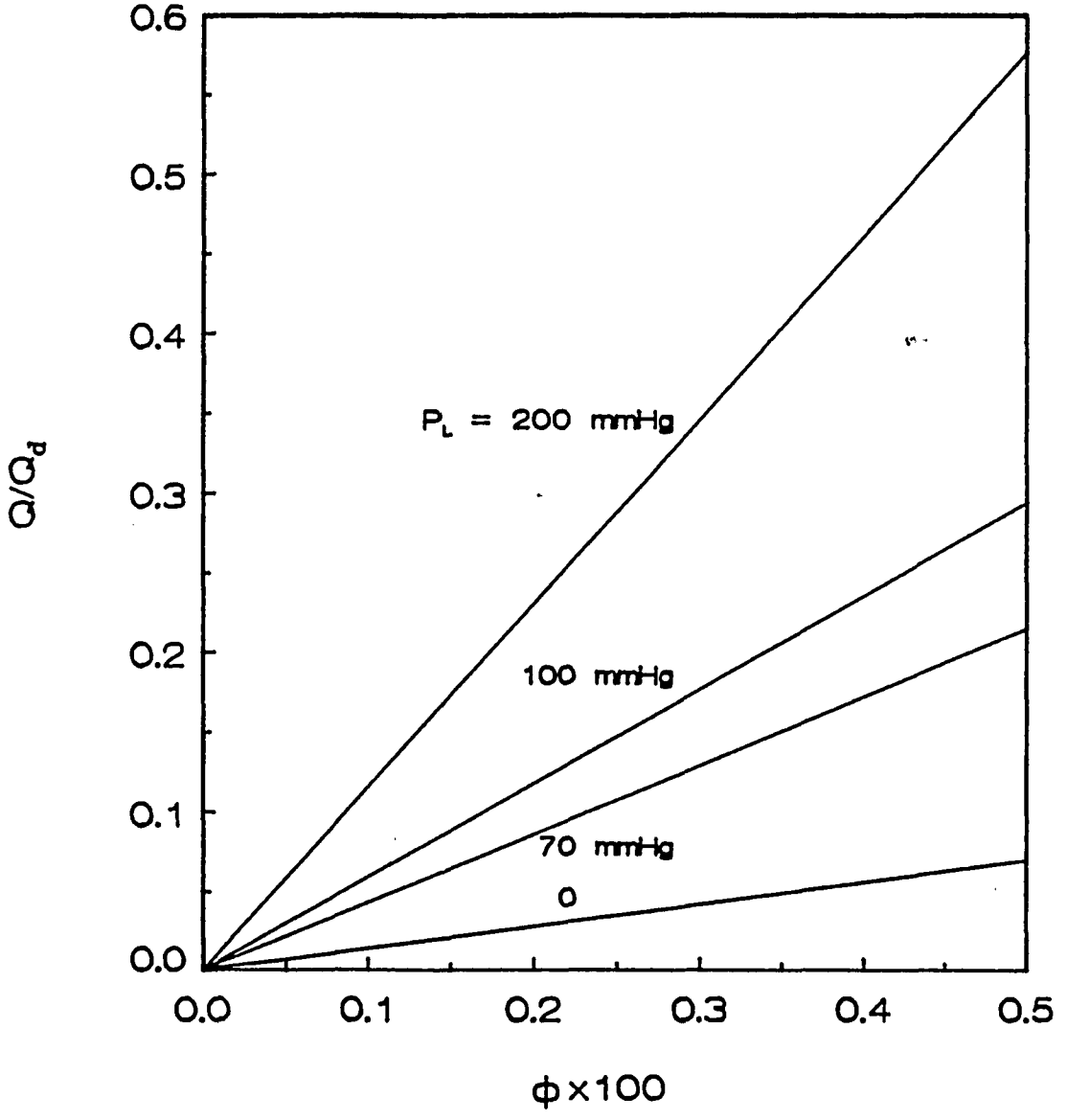
0.6
0.5
0.4
0.3
0.2
0.1
0.0
Q/Q_d
P_L = 200 mmHg
100 mmHg
70 mmHg
0
0.0
0.1
0.2
0.3
0.4
0.5
φ×100

Figure 9

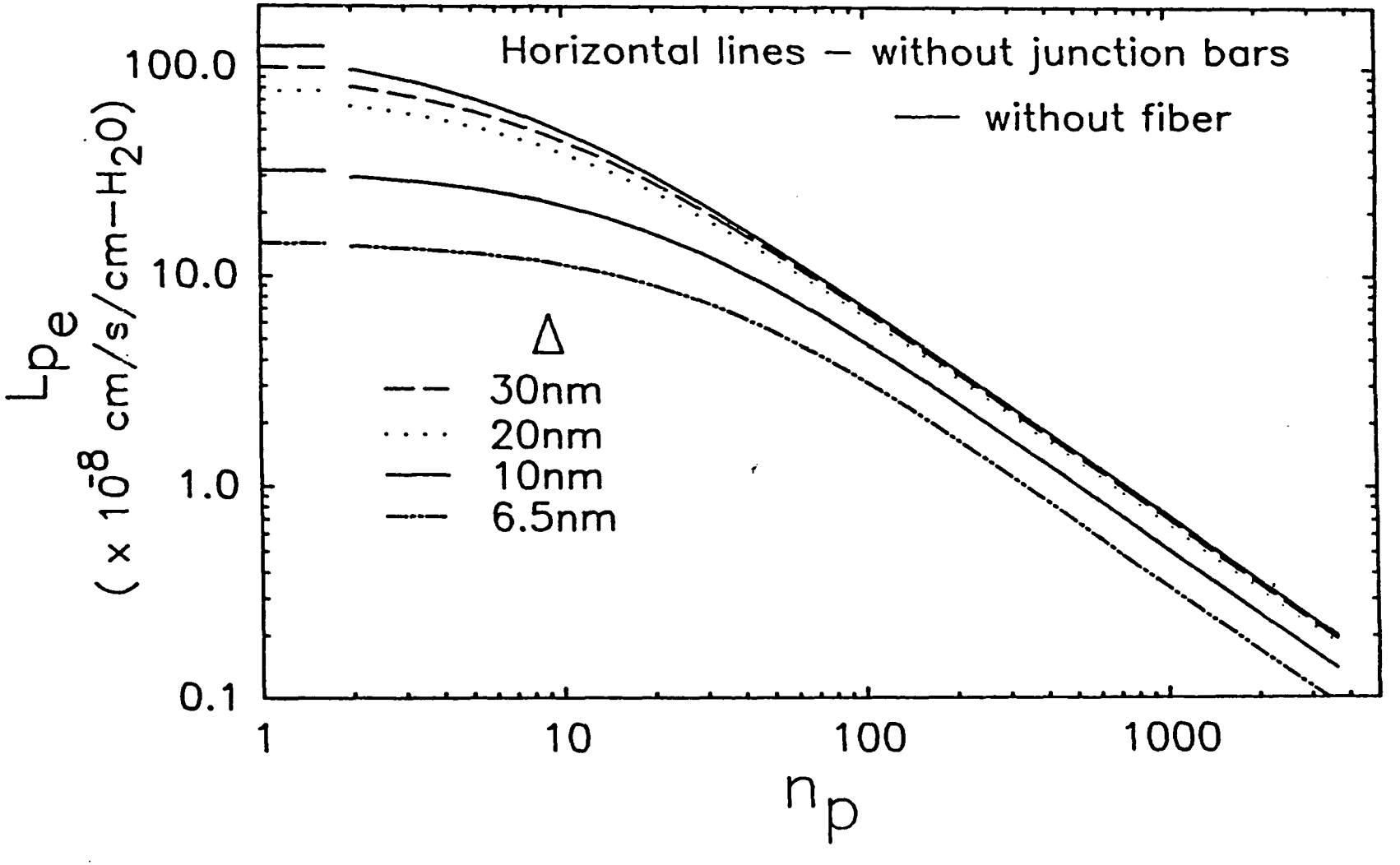
Horizontal lines – without junction bars
without fiber
Δ
30nm
20nm
10nm
6.5nm
100.0
10.0
1.0
0.1
1
10
100
1000
L_{p_e}
(x 10^{-8} cm/s/cm−H_2O)
n_p

Figure 10

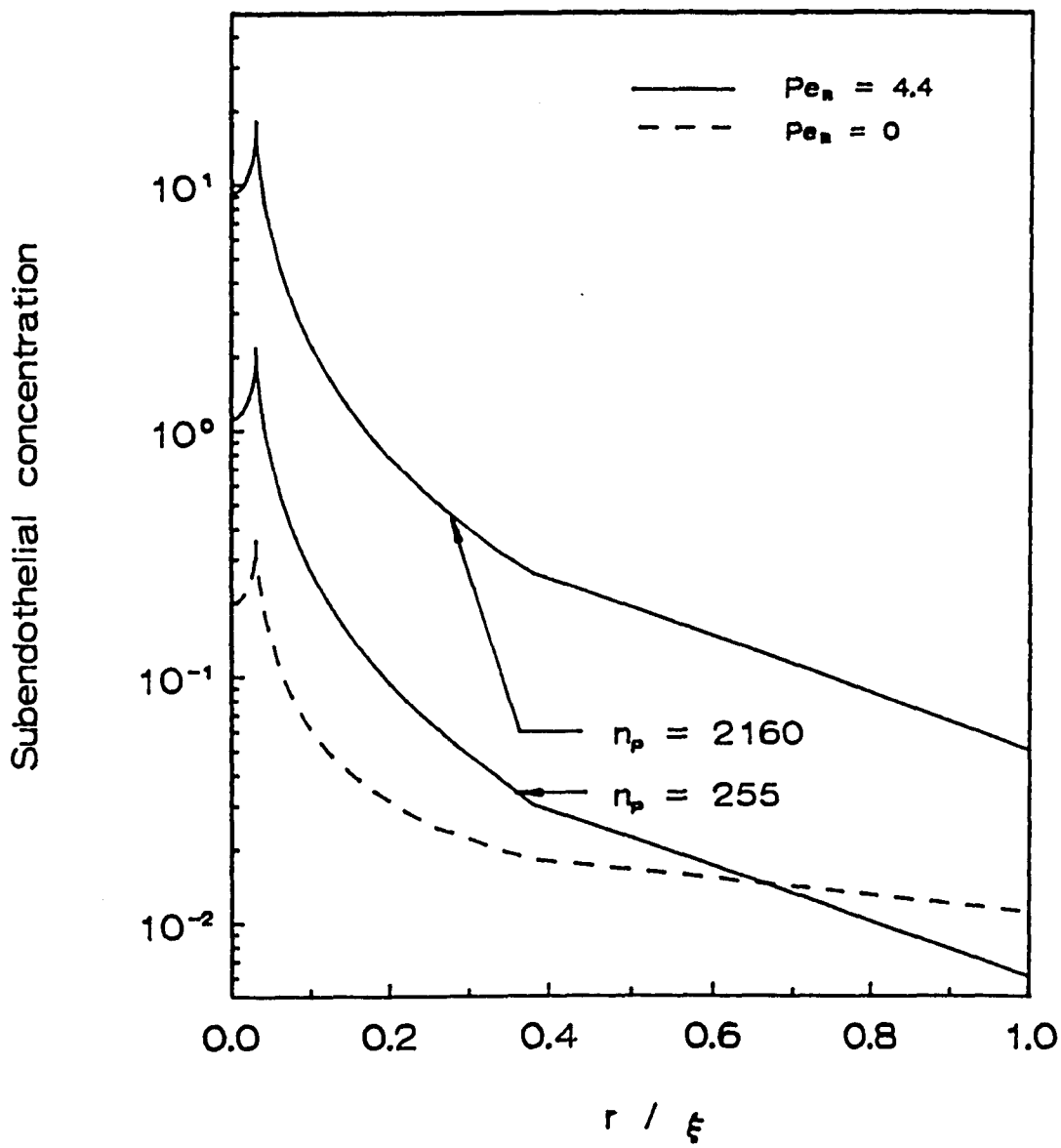
Pe$_R$ = 4.4
Pe$_R$ = 0
10^1
10^0
10^{-1}
10^{-2}
Subendothelial concentration
n_p = 2160
n_p = 255
0.0
0.2
0.4
0.6
0.8
1.0
r / ξ

Figure 11

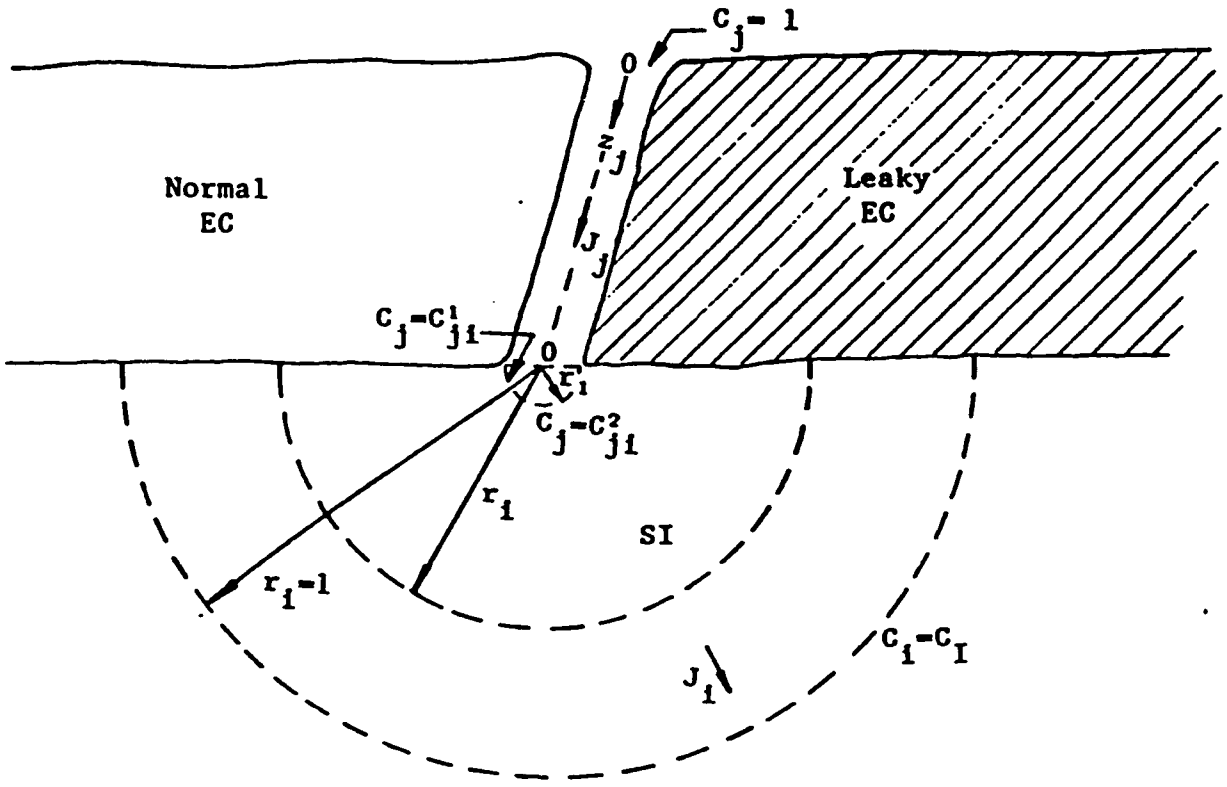
$C_j = 1$
0
z_j
J_j
Normal
EC
Leaky
EC
$C_j = C^1_{ji}$
0
$\bar{r}_1$
$\bar{C}_j = C^2_{ji}$
r_i
SI
$r_i = 1$
$C_i = C_I$
J_i

Figure 12

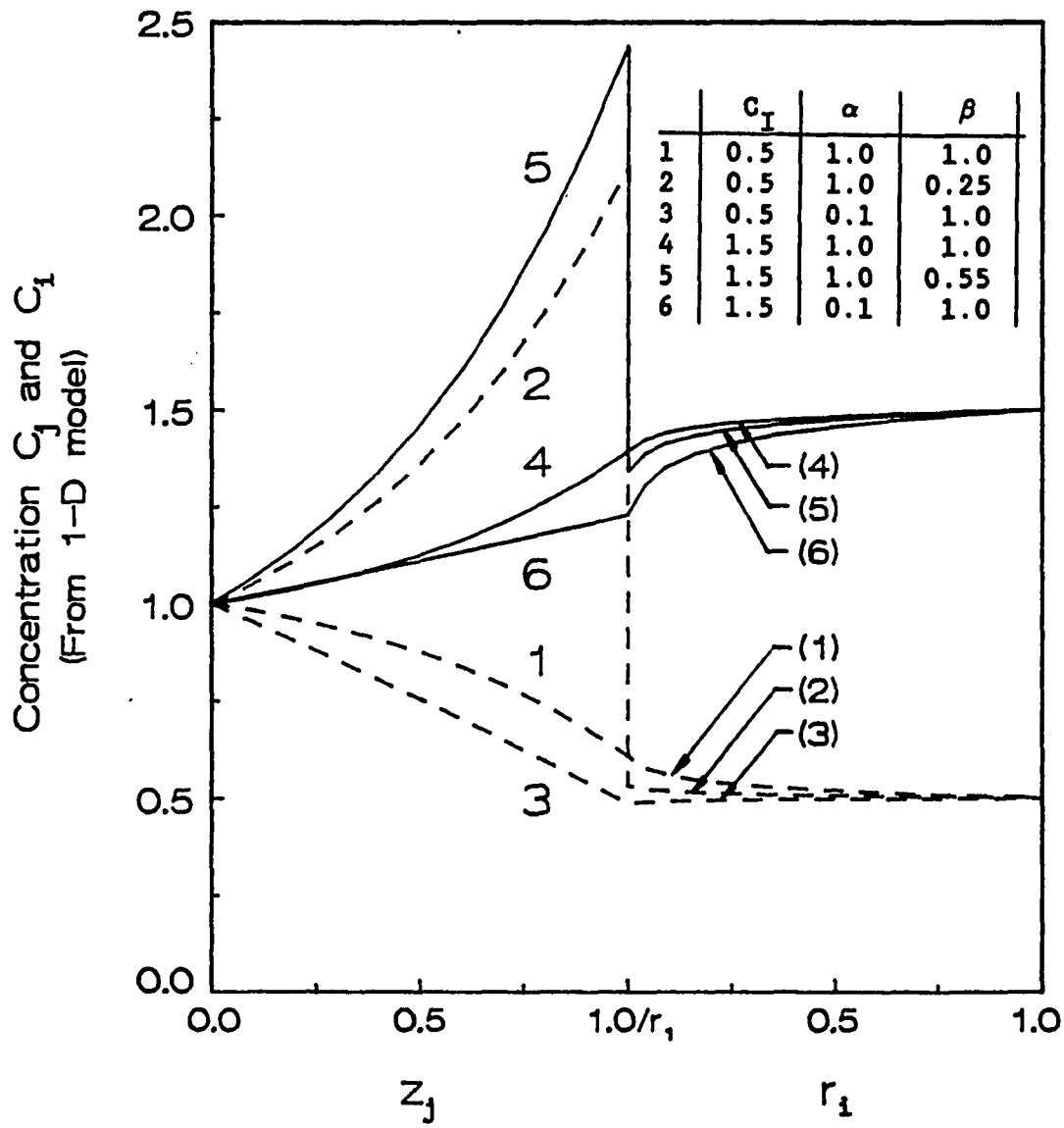
Concentration C_j and C_i
(From 1-D model)
2.5
2.0
1.5
1.0
0.5
0.0
0.0
0.5
1.0/r_1
0.5
1.0
z_j
r_i
5
2
4
6
1
3
(4)
(5)
(6)
(1)
(2)
(3)
	C_I	α	β
1	0.5	1.0	1.0
2	0.5	1.0	0.25
3	0.5	0.1	1.0
4	1.5	1.0	1.0
5	1.5	1.0	0.55
6	1.5	0.1	1.0

Figure 13

CHAPTER 5

Summary and Future Studies

In this dissertation, three mathematical models have been proposed. The model in chapter 2 examines the LDL receptor-mediated pathway in non-hepatic cells, and the models in chapters 3 and 4 investigate the macromolecular transport across the arterial wall. These models attempt to provide new insights into the most important initial feature of atherogenesis, the accumulation of lipid in the intima of the arterial wall.

5.1 LDL receptor-mediated pathway

The LDL receptor-mediated pathway is a self-adaptive regulation system. It will let the non-hepatic cells obtain enough cholesterol from the extracellular medium and yet prevent the excessive accumulation of cholesterol in cells.

Several kinetic models have been proposed for different aspects of the LDL receptor-mediated pathway (Keizer et al., 1985; Peacock-Lopez and Ramirez,1986; Truskey et al.,1984; Phillips et al.,1987). Howover, there is, to our knowledge, no overall mathematical model for the intracellular regulation of the LDL pathway. The LDL receptor-mediated pathway is a very complex system involving at least six primary processes and many chemical reactions. In addition, some of the detailed mechanisms for the primary processes have not been determined, and there is inadequate experimental data to formulate a general kinetic model. In order to analyze the essential features of such a complex system quantitatively, and yet reflect the framework of the system, simplified models were formulated for the six primary

processes in the LDL receptor-mediated pathway. These models describe: (1) the synthesis and hydrolysis of LDL receptors in the cell, (2) the binding and the internalization of LDL by its receptors on the cell membrane, (3) the hydrolysis of LDL in the lysosome of the cell, (4) the storage of cholesteryl esters, (5) the regulation of de novo synthesis of cholesterol, and (6) the efflux of free cholesterol to the external medium.

Most of the experimental data, used in obtaining the values of the parameters in the model, are based on the experimental results for fibroblasts [see summary in Brown and Goldstein (1979)], because the data for fibroblasts is the most complete of any cell type, and fibroblasts behave in a manner that is representative of most nonhepatic cells (e.g. ECs and SMCs).

Using these parameter values, the validity of the model is tested by showing that it can quantitatively predict many additional experimental results obtained for human fibroblasts in tissue culture studies, as shown in the figures of Chapter 2.

The main purpose of the overall model is to determine how the free cholesterol level in the cell is related to the external LDL concentration and to predict the regulatory capacity of the cells to adapt to a changing LDL environment. The relation between the rate of intracellular LDL degradation and the LDL concentration in the extracellalar medium in this model can be used in future models to study the degradation of LDL in the arterial wall as will be discussed shortly. When the model is applied to SMCs, it reveals that, for slowly increasing LDL concentration in the extracellular medium, the rate of intracellular degradation of LDL will first increase and then become saturated, although the number of LDL

receptors on the cell membrane, in this case, decreases monotonically. This theoretical prediction is consistant with the in vivo experimental studies of Schwenke and Carew (1986b) for the rabbit aorta.

It is proposed based on these results that the saturation of LDL degradation by SMCs and the subsequent increase in subendothelial LDL levels in regions of high macromolecular permeability might play a vital role in the formation of the early foam cell lesion.

5.2 Macromolecular transport across the artery wall

Macromolecular transport across the arterial wall has been the subject of numerous mathematical models (Fry,1987; Weinbaum et al.,1985; Wen et al.,1988). However, no previous model has adequately treated the convective transport processes in the intima, the wall layer of greatest interest in the disease process.

In general, macromolecular transport across the artery wall is three-dimensional. However, if the interaction between the cells in turnover is not very strong, the wall can be divided into axisymmetric periodic units surrounding each leakage site. For a normal aorta, this assumption is true, because the frequency of the cells in the normal endothelium whose junctions are leaky to macromolecules is less than one in a thousand (Lin et al.,1988). For this spacing between leakage sites, the normal endothelium and the IEL can be treated as a continuum.

In the proposed new models for filtration and solute transport, the arterial wall is divided into four discrete layers: the endothelium, the SI, the IEL, and the media as shown in Fig.1 of Chapter 4. The loose connective tissue of the adventitia layer is not considered since it is not a significant transport barrier. The model

for filtration is treated as steady and 2-D. It is obtained by replacing the concentration (C) and the solute flux (q) by the corresponding pressure (p) and water velocity in the lateral and normal directions (U and W), respectively, in Fig.1 of Chapter 4. The tissue space in the SI and media is treated as a porous media, and is assumed to obey Darcy's law. The hydraulic conductivity of the normal endothelial cleft is determined from a new 3-D model for the intercellular cleft proposed in Tsay et al.(1989) and the hydraulic conductivity of the IEL is found from a new periodic unit model for the fenestra proposed in this paper. In the latter model, the geometric structure of the IEL is based on the measurements of Song and Roach (1983) for the size and spacing of the fenestra in major mammalian arteries. The model for convective-diffusive transport is time-dependent and 2-D as shown in Fig.1 of Chapter 4. The expressions for the water velocities in the convection terms of the transport equations in each layer are obtained from analytic solutions for the 2-D steady state boundary value problem for filtration. The leaky cleft in both the filtration and convective-diffusive transport model is approximated by a circular ring-source, wherein the driving force (concentration drop or pressure drop across the leaky cleft) is related to the unknown flux or velocity using an open channel model for the leaky cleft.

The new models for filtration and convective-diffusive transport described above have led to several important and in some cases unexpected new findings that are summarized below:

(1) The model for filtration assumes that the measured average pressure drop across the normal endothelium is about one half of the total transmural pressure drop when the arterial wall is 200 μm in

thickness (Vargas et al.,1979). The Peclet number in the media for this wall thickness is 4.4 (Tedgui and Lever,1985). Using these values and the new model for the intercellular cleft proposed in Tsay et al.(1989), the model predicts that the number of missing proteins in a normal endothelial junction strand of the rabbit aorta is only 1 in 1700 proteins. This result is nearly two orders of magnitude less than that predicted for muscle capillaries. This unexpected result reveals that there is a tremendous variation in junction strand structure as one proceeds from the large arteries to capillaries. Experiments are now being designed to confirm this new view of normal arterial interendothelial cleft structure.

(2) The major resistance to macromolecular transport across the artery wall resides in the endothelium. For albumin the model predicts that the average macromolecular concentration in the SI at steady state decreases to less than one percent of its luminal value for a 200 μm thick rabbit aorta in which there is filtration at in vivo pressures.

(3) Although the model asssumes that all the macromolecules enter the artery wall through the leaky cleft, the model predicts that the fractional water flux across the endothelium through the leaky cleft is less than 0.5 percent of the total water flux when the frequency of cells with clefts leaky to macromolecules is five in ten thousand.

(4) In the vicinity of the leaky cleft exit, the dominant macromolecular transport mode is convection. This convection occurs in a direction that is primarily parallel to the endothelial surface. The lateral convection decreases rapidly at a distance of approximately 50 μm from the cell with the leaky cleft where the

transport in the lateral direction becomes nearly purely diffusive. However, the average Peclet number in the normal direction in the media is 4.4 as noted before. Thus convection in the media in the normal direction is still at least as important as diffusion.

(5) If the SI location, where the concentration of fluorescent-labeled macromolecules (e.g. EBA) falls to 10 percent of its value at the center of the leaky cell, is defined as the margin of a fluorescent spot for this molecule, the theory predicts that the radius of the fluorescent spot will be roughly 3~4 times as large as that of the endothelial cell as shown in Fig.6 of Chapter 4. This result confirms the unexpected experimental observations by Chuang et al. (1990), where the growth of the fluorescent leakage spot in the SI was confined to only several cell radii after 2 hrs. of labeling.

(6) The pressure distribution in the direction parallel to the endothelium in the SI is non-uniform as shown in Fig.5 of Chapter 4. However, this horizontal pressure distribution becomes much more uniform on the media side of the IEL. This indicates that the IEL functions as a pressure equalizer. In addition, the IEL is only a temporary barrier to macromolecular transport across the artery wall.

(7) Because the cells with leaky clefts are widely dispersed over the endothelial surface (Lin et al.,1988), the total macromolecular flux entering the artery wall is linearly proportional to the number of leaky cells per unit endothelial surface area.

(8) In view of the above results, the most serious limitations of 1-D convective-diffusive models were investigated. The major difficulties that make the 1-D model inappropriate in describing the macromolecular transport across the artery wall are as follows:

(a) The average pressure drop across the normal endothelium is roughly 20 times greater than that across the leaky cleft as shown in Fig.5 of Chapter 4. Thus, the convective flux can not be estimated correctly using existing 1-D models, e.g. Fry (1987) and the one in Chapter 3 of this dissertation. Since convection is the dominant macromolecular transport mechanism across the leaky cleft, the total macromolecular flux entering the artery wall will be overestimated by more than an order of magnitude using previous 1-D models which assume a uniform pressure in the SI.

(b) The water velocity is discontinuous across the leaky cleft-SI interface in the 1-D model, due to the abrupt change in cross-sectional area available for transport in each layer. This discontinuity in velocity will lead to a concentration in the vicinity of the leaky cleft exit which is greater than that in the lumen (Chapter 3 of this dissertation).

(9) Smith and Staples (1982) and Fry et al.(1986) have observed that the concentration of macromolecules in the SI could be higher than that in the lumen. In order to investigate whether it is possible to have such a concentration distribution in the subendothelial space, a simplified local 1-D model was also developed. The conclusion of this model is that the concentration in the SI can not be higher than that in the lumen unless a sieving structure exists in the IEL or the SI.

5.3 Future studies

Based on the studies in this dissertation, several future research directions are suggested as follows:

(1) In the model for receptor-mediated pathway of LDL metabolism in non-hepatic cells, the rate of mRNA transcription for LDL receptor

synthesis and the activity of HMG-CoA reductase for cholesterol synthesis in the cells were assumed to be dependent on the LDL concentration in the extracellular medium. This assumption is qualitatively correct at steady state, but the quantitative results in theoretical predictions for time-dependent process may differ from the experimental data, see discussion in Chapter 2. This is because the regulation of mRNA synthesis in the cell's nucleus and the activity of HMG-CoA reductase are controlled by the intracellular content of free cholesterol rather than the LDL concentration in the extracellular medium. Therefore, the manner, in which the intracellular content of free cholesterol controls the transcription of mRNA for LDL receptor synthesis, requires further study. When the LDL concentration in the external medium is high, the de novo synthesis of free cholesterol contributes insignificantly to the intracellular cholesterol pool. Thus the error in the model for this process can be neglected, if one studies the LDL degradation in atherogenesis, where the LDL concentration is generally high enough for de novo synthesis to be negligible.

(2) We have assumed in Chapter 2 that the rate constant K_2 in the model for cellular lysosomal degradation of LDL depends on the degree of confluency of cell monolayer. This assumption needs to be verified experimentally, and the quantitative relationship between K_2 and the degree of confluency of cell monolayer needs to be determined.

(3) The ultrathin serial sectioning of the endothelium from different arteries is suggested by the present theoretical research, because the present model reveals that the structure of the

endothelial junction varies tremendously as one proceeds from the large arteries to the arterial capillaries.

(4) In order to explain the macromolecular sieving in the arterial intima observed in Smith and Staples (1982) and Fry et al. (1986), the sieving structures of the basement membrane and/or the IEL should be studied further, both theoretically and experimentally.

(5) The estimation of the macromolecular permeability of the IEL used in this dissertation needs to be improved. In future studies, it should consider the interaction between macromolecular fluxes in the media through the different fenestrae in the IEL, which is similar to the estimation of the hydraulic conductivity of the IEL.

(6) Finally, in order to formulate a model for atherogenesis, which combines the LDL transport and degradation in the arterial wall, the mathematical model for the LDL pathway (both receptor-mediated and non-receptor-mediated pathways) has to be incorporated into the mathematical model for macromolecular transport. This is the most important future study suggested by the present dissertation.

BIBLIOGRAPHY

1. Attie,A.D.,Pittman,R.C.and Steinberg,D.(1982) Hepatology 2, 269
2. Baker,D.P., van Lenten,B.J., Fogelman,A.M., Edwards,P.A., Kean,C. and Berliner,J.A. (1984) Arteriosclerosis 4, 248.
3. Barr,D.P., Russ,E.M. and Eder,H.A. (1951) Am.J.Med 11, 480.
4. Barrett,T.B., Gajdusek,C.M., Schwartz,S.M. et al. (1984) Proc. Natl.Acad.Sci.USA 81, 6772.
5. Bell,F.P., Adamson,I.L. and Schwartz,C. (1974a) Expl.Molec. Pathol 20, 57.
6. Bell,F.P., Gallus,A.S. and Schwartz,C. (1974b) Expl.Molec.Pathol 20, 281.
7. Benditt,E.P. and Benditt,J.M. (1973) Proc.Natl.Acad.Sci.USA 70, 1753.
8. Berliner,J.A., Territo,M., Almada,L., Carter,A., Shafonsky,E. and Fogelman,A.M. (1986) Arteriosclerosis 6, 254.
9. Bevilacqua,M.P., Pober,J.S, Cotran.R.S. and Gimbrone,M.A.Jr. (1985) J.Cell Biochem Suppl 9A, 148. (Abstract)
10. Booyse,F.M., Bell,S., Sedlak,B.J. and Rafelson,M.E. (1975) Artery 1, 518.
11. Bratzler,R.L., Chisolm,G.M., Colton,C.K., Smith,K.A. and Lees,R.S. (1977) Atherosclerosis 28, 289.
12. Bray,H.G.and White,K.(1966) "Kinetics and Thermodynamics in Biochemistry" 2nd edition. New York:Academic Press Inc. pp 208-215.
13. Breslow,J.L.,Lothrop,D.A.,Spaulding,D.R.,and Kandutsch,A.A. (1975) Biochim Biophys Acta 398, 10.

14. Brown,M.S.,Faust,J.R.and Goldstein,J.L.(1975) J.Clin.Invest. 55, 783.

15. Brown,M.S.and Goldstein,J.L.(1975) Cell 6, 307.

16. Brown,M.S.and Goldstein,J.L.(1976) Science 191, 150.

17. Brown,M.S.and Goldstein,J.L.(1979) Proc.Natl.Acad.Sci.USA 76, 3330.

18 Brown,M.S.and Goldstein,J.L.(1983) Ann.Rev.Biochem 52, 223.

19. Bruckdorfer,K.R. and Graham,J.M. (1976) In: Biological Membranes (Chapman,D. and Wallach,D.F.H. eds), vol.3. London:Academic Press, pp103-152.

20. Bundgaard,M. (1984) J.Ultrastructure Res 88, 1.

21. Bundgaard,M. and Frokjaer-Jensen,J. (1982) Microvasc.Res 23, 1

22. Bundgaard,M., Frokjaer-Jenson,J. and Crone,C. (1979) Proc.Natl. Acad.Sci.USA 276, 6439.

23. Bundgaard,M., Hagman,P. and Crone,C. (1983) Microvasc.Res 25, 358.

24. Campbell,G.J. and Roach,M.R. (1981) Stroke 12, 489.

25. Caplan,B.A. and Schwartz,C.J. (1973) Atherosclerosis 17, 401.

26. Carew,T.E., Schwenke,D.C. and Steinberg,D. (1987) Proc.Natl.Acad.Sci.USA 84, 7725.

27. Chait,A.,Ross,R.,Albers,J.J.and Bierman,E.L.(1980) Proc.Natl. Acad.Sci.USA 77, 4084.

28. Chen,H.W.,Cavenee,W.K.and Kandutsch,A.A.(1979) J.Biol.Chem. 254, 715.

29. Chien,S., Laufer,L. and Handley,D.A. (1982) J.Ultrastruct.Res 79, 198.

30. Chien,S., Lin,S.J., Weinbaum,S., Lee,M.M.L. and Jan,K.M. (1988) Adv.Exper.Med.Biol 242, 59.

31 Chuang,P., Cheng,H., Lin,S., Jan,K. and Chien,S. (1990) "Macromolecular Transport across Arterial and Venous Endothelium in Rats: Study with Evans Blue-Albumin and Horseradish Peroxidase". Arteriosclerosis (in press).

32. Crone,C. (1984) In:"Recent Advances in Physiology". London: Churchill-Livingston, p125

33. Crone,C. and Levitt,D.G. (1984). In Handbook of Physiology (Renkin,E.M. and Michel,C.C. eds), sect.2, The Cardiovascular System, vol.4, Microcirculation. Bethesda, Md, American Physiological Society, p441.

34. Curry,F.E. (1986) Circ.Res 59, 367.

35. Curry,F.E. and Michel,C.C. (1980) Microvasc.Res 20, 96.

36. Daniels,R.J.,Guertler,L.S.,Parker,T.S.and Steinberg,D. (1981) J.Biol.Chem. 256, 4978.

37. Davies,P.F.and Kerr,C. (1982) Biochim.Biophys.Acta 712, 26.

38. Davies,P.F., Truskey,G.A., Warren,H.B., O'Connor,S.E.and Eisenhaure,B.H. (1985) J.Cell.Biol. 101, 871.

39. Deuel,T.F., Senior, R.M., Huang,J.S. and Griffin,G.L. (1982) J. Clin.Invest. 69, 1046.

40. DiCorleto,P.E. and Bowen-Pope,D.F. (1983) Proc.Natl.Acad.Sci.USA 80, 1919.

41. Faggiotto,A., Ross,R. and Harker,L. (1984) Arteriosclerosis 4, 323.

42. Faggiotto,A. and Ross,R. (1984) Arteriosclerosis 4, 341.

43. Ferrans,V.J. (1980) "Vascular structure". In: Basic Hemodynamics and Its Role In Disease Processes (Patel,D.J. and Vaishnav,R.N.eds). Baltimore: University Park Press, pp 105-154.

44. Fielding,C.J.and Fielding,P.E.(1985)"Metabolism of cholesterol and lipoproteins". In: Biochemistry of Lipids and Membranes (Vance,D.E.and Vance,J.E.ed). Menlo Park,California:The Benjamin/Cummings Publishing Company,Inc. pp404-474.

45. Fielding,P.E.,Vlodavsky,I.,Gospodarowicz,D., and Fielding,C.J. (1979) J.Biol.Chem. 254, 749.

46. Firth,J.A., Bauman,K.F. and Sibley,C.P. (1983) J.Ultrastructure Res 85, 45.

47. Floren,C.,Albers,J.J.and Bierman,E.L.(1981) Biochim Biophys Acta 663, 336.

48. Fowler,S.D., Mayer,E.P. and Greenspan,P. (1985) "Foam cells and Atherogenesis". Ann.NY Acad.Sci 454, 79.

49. Fry,D.L. (1983) Am.J.Physiol 245, H977.

50. Fry,D.L. (1985) Am.J.Physiol 248, H240.

51. Fry,D.L. (1987) Arteriosclerosis 7, 88.

52. Fry,D.L., Cornhill,J.F., Sharma,H., Pap,J.M. and Mitschelen,J. (1986) Arteriosclerosis 6, 475.

53. Ganatos,P., Weinbaum,S. and Pfeffer,R. (1982) J.Fluid Mech 124, 27.

54. Gerrity,R.G., Goss,J.A. and Soby,L. (1985) Arteriosclerosis 5, 55.

55. Glomset,J.A. (1968) J.Lipid Res 9, 155.

56. Goldstein,J.L.,Basu,S.K.,Brunschede,G.Y.and Brown,M.S.(1976a) Cell 1, 85.

57. Goldstein,J.L.and Brown,M.S.(1974) J.Biol.Chem. 249, 5153.

58. Goldstein,J.L.and Brown,M.S.(1977) Ann.Rev.Biochem. 46, 897.

59. Goldstein,J.L.,Dana,S.E.and Brown,M.S.(1974) Proc.Natl.Acad. Sci.USA 71, 4288

60. Goldstein,J.L.,Dana,S.E.,Faust,J.R.,Beaudet,A.L.and Brown,M.S. (1975) J.Biol.Chem. 250, 8487.

61. Goldstein,J.L.,Sobhani,M.K.,Faust,J.R.and Brown,M.S.(1976b) Cell 9, 195.

62. Gourlay,A.R. (1970) J.Inst.Maths.Applics. 6, 375.

63. Gresham,G.A. (1987) "Natural History of Atherosclerosis". In: Atherosclerosis--Biology and Clinical Science (Olsson,A.G. ed.). New York:Churchill Livingstone, pp 51-56.

64. Grotendorst,G.R., Chang,T., Seppa,H.E.J., et al. (1982) J.Cell Physiol 113, 261.

65. Gupta,A, Sexton,R.C.and Rudney,H.(1986) J.Biol.Chem. 261, 8348.

66. Hansson,G.K. and Schwartz,S.M. (1983) Am.J.Path 112, 278.

67. Haust,M.D. (1987) "Pathogenesis of Atherosclerosis--Current Status". In:Expanding Horizons in Atherosclerosis Research (Schlierf,G. and Morl,H. ed.). Berlin:Springer-Verlag, pp 3-12.

68. Henriksen,T. Mahoney,E.M. and Steinberg,D. (1981) Proc.Natl.Acad.Sci.USA 78, 6499.

69. Jan,K.M. (184) Anatomical Record 210, 11.

70. Jauchem,J.R., Lopez,M., Sprague,E.A. and Schwartz,C.J. (1982) Exp. Mol.Pathol. 37, 166.

71. Kandutsch,A.A.(1986)"Apo B-dependent and -Independent Cellular Cholesterol Homeostasis". In: Biochemistry and Biology of Plasma Lipoproteins(Scanu,A.M.and Spector,A.A.ed). New York:Marcel Dekker,Inc. pp281-300.

72. Kandutsch,A.A.and Chen,H.W.(1977) J.Biol.Chem. 252, 409.

73. Karlin,J.B., Johnson,W.J., Benedict,C.R., Chacko,G.K., Phillips,M.C. and Rothblat,G.H. (1987) J.Biol.Chem 262, 12557.

74. Keizer,J.,Ramirez,J.and Peacock-Lopez,E.(1985) Biophys.J 47, 79.

75. Ku,D.N., Giddens,D.P., Zarins,C.K. and Glagov,S. (1985) Arteriosclerosis 5, 293.

76. Lin,S.J. (1989) "Effects of Cell Turnover And Leaky Junctions On Arterial Macromolecular Permeability -- Relation to Atherogenesis". Doctoral dissertation, Columbia University, New York, N.Y.

77. Lin,S.J., Jan,K.M., Schuessler,G., Weinbaum,S. and Chien,S. (1988) Atherosclerosis 73, 223.

78. Lin,S.J., Jan,K.M., Weinbaum,S. and Chien,S. (1989) Arteriosclerosis 9, 230.

79. Martin,T.R., Altman,L.C., Albert,R.K., Henderson,W.R. (1984) Am. Rev.Respir.Dis 129, 106.

80. Minick,C.R., Stemerman,M.B. and Insull,W.Jr. (1977) Proc.Natl. Acad.Sci.USA 74, 1724.

81. Nerem,R.M., and Levesque, M.T. (1983) "The Case for Fluid Dynamics as a Localizing Factor in Atherogenesis". In: Fluid Dynamics as a Localizing Factor for Atherosclerosis (Schettler et al. eds.). Berlin: Springer-Verlag, 1983, pp. 26-37.

82. Nerem,R.M., Levesque,M.J. and Cornhill,J.F. (1981) J.Biomech. Engng 103, 172.

83. Packham,M.A., Roswell,H.C., Jorgensen,L. and Mustard,J.F. (1967) Expl.Molec.Pathol 7, 214.

84. Palade,G.E. (1960) Anat.Rec 136, 245.

85. Peacock-Lopez,E.and Ramirez,J.(1986) Biophys.Chem 25, 117.

86. Phillips,M.C.,Johnson,W.J.and Rothblat,G.H.(1987) Biochim. Biophys.Acta 906, 223.

87. Quinn,M.T. (1987) Proc.Natl.Acad.Sci USA 84, 2995.

88. Reidy,M.A. and Schwartz,S.M. (1981) Lab.Invest 44, 301.

89. Rinninger,F.and Pittman,R.C. (1988) J.Lipid.Res. 29, 1179.

90. Rizzo,F.J. and Shippy,D.J. (1970) AIAA Journal 8, 2004.

91. Robert,L. (1987) "The Extracellular Matrix of the Vessel Wall, Its Role and Modification During the Atherosclerotic Process". In:Expanding Horizons in Atherosclerosis Research (Schlierf,G. and Morl,H. ed.). Berlin:Springer-Verlag, pp 3-12.

92. Ross,R. (1986) N.Engl.J.Med 314, 488.

93. Ross,R. and Glomset,J.A. (1976) N.Engl.J.Med 295, 420.

94. Ross,R., Glomset,J.A., Kariya,B. and Harker,L.A. (1974) Proc.Natl.Acad.Sci USA 71, 1207.

95. Schwartz,C.J., Sprague,E.A., Fowler,S.R. and Kelley,J.L. (1983). In: Fluid Dynamics as a Localizing Factor for Atherogenesis (Schettler,G. et al.eds). Berlin: Springer-Verlag, pp200-207.

96. Schwartz,S.M., Reidy,M.A. and Hansson,G.K. (1983) "Injury at the Vascular Surface". In:Fluid Dynamics as a Localizing Factor for Atherosclerosis (Schettler,G. et al. eds.). Berlin:Springer-Verlag, pp188-199.

97. Schwenke,D.C.and Carew,T.E. (1988) Circ.Res. 62, 699.

98. Schwenke,D.C. and Carew,T.E. (1989a) Arteriosclerosis 9, 895.

99. Schwenke,D.C. and Carew,T.E. (1989b) Arteriosclerosis 9, 908.

100. Simionescu,M., Simionescu,N. and Palade,G.E. (1975) J.Cell Biol 67, 863.

101. Smith,E.B. and Staples,M.E. (1982) Proc.R.Soc B 217, 59.

102. Song,S.H. and Roach,M.R. (1983) Blood Vessels 20, 145.

103. Stein,Y., Glangeaud,M.C., Fainaru,M. and Stein,O. (1975) Biochem.Biophys.Acta 380, 106.

104. Steinberg,D. (1983) Arteriosclerosis 3, 283.

105. Steinberg,D. (1987) "Current Theories of the Pathogenesis of Atherosclerosis". In:Hypercholesterolemia and Atherosclerosis -- Pathogenesis and Prevention (Steinberg,D. and Olefsky,J.M. eds.). New York:Churchill Livingstone, pp 5-24.

106. Stemerman,M.B., Morrell,E.M., Burke,K.R., Colton,C.K., Smith,K.A. and Lees,R.S. (1986) Arteriosclerosis 6, 64.

107. Stryer,L (1988) Biochemistry(textbook). New York:W.H.Freeman and Company. pp555-559

108. Tedgui,A. and Lever,M.J. (1984) Am.J.Physiol 247, H784.

109. Tedgui,A. and Lever,M.J. (1985) Circ.Res 57, 856.

110. Thurn,A.L. (1982) "Effect of Endothelial Injury on Macromolecular Transport in The Arterial Wall". Doctor dissertation, Columbia University, New York, N.Y.

111. Truskey,G.A.,Colton,C.K.and Davies,P.F.(1984) Ann. NY Acad.Sci 435, 349.

112. Tsay,R. and Weinbaum,S. (1990) "Viscous Flow in a Channel with Periodic Cross-Bridging Fibers of Arbitrary Aspect Ratio" (submitted to JFM)

113. Tsay,R., Weinbaum,S. and Pfeffer,R. (1989) Chem.Eng.Comm 82, 67.

114. Tzeghai,G., Ganatos,P., Pfeffer,R., Weinbaum,S. and Nir,A. (1986) J.Theor.Biol 121, 141.

115. Tzeghai,G., Weinbaum,S. and Pfeffer,R. (1985) J.Biomech.Eng 107, 123.

116. Vargas,B.C., Vargas,F.F., Pribyl,J.G. and Blackshear,P.L. (1979) Am.J.Physiol 236, H53.

117. von Rokitansky,K. (1852) "A Manual of Pathological Anatomy", vol.4. Sydenham Society, London, pp261-273.

118. Walker,L.N., Bowen-Pope,D.F., Ross,R. and Reidy,M.A. (1985) Proceedings of FASEB, 44, 737.

119. Weinbaum,S. and Caro,C.G. (1976) J.Fluid Mech 74, 611.

120. Weinbaum,S., Pfeffer,R. and Chien,S. (1988a) PCH PhysicoChemical Hydrodynamics 10, 705.

121. Weinbaum,S., Tzeghai,G., Ganatos,P., Pfeffer,R. and Chien,S. (1985) Am.J.Physiol 248, H945.

122. Weinbaum,S., Wen,G.B., Ganatos,P., Pfeffer,R., Lee,M. and Chien,S. (1988b) J.Theor.Biol 135, 1.

123. Wen,G.B., Weinbaum,S., Ganatos,P., Pfeffer,R. and Chien,S. (1988) J.Theor.Biol 135, 219.

124. Wissig,S.L. (1979) Acta Physiol.Scand.Suppl 463, 33.

125. Wissler,R.W., Vesselinovitch,D. and Davis,H.R. (1987) "Cellular Components of the Progressive Atherosclerotic Process". In:Atherosclerosis--Biology and Clinical Science (Olsson,A.G. ed.). New York:Churchill Livingstone, pp 57-74.

126. Wu,C., Chi,J., Jerng,J., Lin, S., Jan,K., Wang,D., and Chien,S. (1990) "Transendothelial Macromolecular Transport in the Aorta of Spontaneously Hypertensive Rats". (submitted to Hypertension).